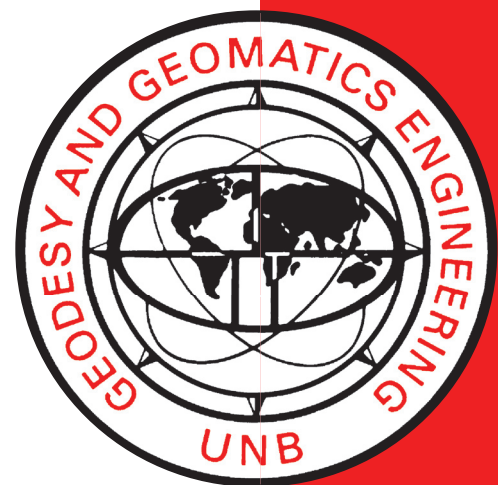


THE EFFECT OF PHYSICAL CORRELATIONS ON THE AMBIGUITY RESOLUTION AND ACCURACY ESTIMATION IN GPS DIFFERENTIAL POSITIONING

A. E-S. EL RABBANY

May 1994



**TECHNICAL REPORT
NO. 170**

PREFACE

In order to make our extensive series of technical reports more readily available, we have scanned the old master copies and produced electronic versions in Portable Document Format. The quality of the images varies depending on the quality of the originals. The images have not been converted to searchable text.

**THE EFFECT OF PHYSICAL
CORRELATIONS ON THE AMBIGUITY
RESOLUTION AND ACCURACY
ESTIMATION IN GPS DIFFERENTIAL
POSITIONING**

Ahmed El-Sayed El-Rabbany

Department of Geodesy and Geomatics Engineering
University of New Brunswick
P.O. Box 4400
Fredericton, N.B.
Canada
E3B 5A3

May 1994
Latest Reprinting December 1997

© Ahmed El-Sayed El-Rabbany, 1994

PREFACE

This technical report is a reproduction of a dissertation submitted in partial fulfillment of the requirements for the degree of Doctor of Philosophy in the Department of Geodesy and Geomatics Engineering, April 1994. The research was supervised by Dr. Alfred Kleusberg and funding was provided partially by the Natural Sciences and Engineering Research Council of Canada, and the University of New Brunswick. Data were provided by the Geological Survey of Canada, the Geodetic Survey of Canada, and the Scripps Institute of Oceanography.

As with any copyrighted material, permission to reprint or quote extensively from this report must be received from the author. The citation to this work should appear as follows:

El-Rabbany, A. E-S. (1994). *The Effect of Physical Correlations on the Ambiguity Resolution and Accuracy Estimation in GPS Differential Positioning*. Ph.D. dissertation, Department of Geodesy and Geomatics Engineering Technical Report No. 170, University of New Brunswick, Fredericton, New Brunswick, Canada, 161 pp.

ABSTRACT

High accuracy GPS carrier phase differential positioning requires complete modelling of the GPS measurement errors. Generally, in GPS positioning, the mathematical model does not describe the observations perfectly. The main reason for this is the lack of information about the physical phenomena associated with the GPS observations. Therefore, a residual error component remains unmodelled.

The analysis of many data series representing baselines of different lengths shows that, in GPS carrier phase double difference positioning, the residual model errors are positively correlated over a time period of about 20 minutes. Not accounting for this correlation, known as physical correlation, usually leads to an overestimation of the accuracy of both the observations and the resulting positions.

A simple way of accounting for these correlated residual errors is to model them stochastically through the modification of the observations' covariance matrix. As the true covariance function is not known, the stochastic modelling of the GPS measurement errors must be achieved by using an empirical covariance function. It is shown that the exponential function is the best approximation for the covariance function of the GPS carrier phase errors in the least squares sense. Although this way of accounting for the unmodelled errors yields a fully populated covariance matrix for the GPS carrier phase

double difference observations, its inverse takes the simple form of a block diagonal matrix.

A modified least squares adjustment algorithm incorporating the newly developed, fully populated covariance matrix is derived. The covariance matrix of the ambiguity parameters is used to form a confidence region of a hyperellipsoid around the estimated real values which is then used for searching the likely integer values of the ambiguity parameters. To speed up the searching time, the covariance matrix for the ambiguities is decomposed using Cholesky decomposition.

The software DIFGPS is developed to verify the validity of the technique. Real data of several baselines of different lengths observed under different ionospheric activities are used. It is shown that including the physical correlations requires more observations to obtain a unique solution for the ambiguity parameters than when they are neglected. However, for all tested baselines, neglecting the physical correlations leads to an overly optimistic covariance matrix for the estimated parameters. Additionally, the use of a scale factor to scale the optimistic covariance matrix was found to be inappropriate. However, without physical correlations, a more realistic covariance matrix is obtained by using data with large sampling interval.

TABLE OF CONTENTS

ABSTRACT	i
TABLE OF CONTENTS	iii
LIST OF FIGURES	vi
LIST OF TABLES	viii
ACKNOWLEDGMENTS	ix
Chapter 1: INTRODUCTION	1
1.1 Motivation.....	1
1.2 Previous Studies.....	3
1.2.1 Physical Correlations	3
1.2.2 Ambiguity Resolution.....	3
1.3 Methodology.....	6
1.4 Outline of the Dissertation.....	7
1.5 Contributions of the Research	8
Chapter 2: GPS MEASUREMENT ERRORS	10
2.1 GPS Errors and Biases.....	12
2.1.1 Errors and Biases Originating at the Satellites	12
2.1.2 Atmospheric Errors and Biases.....	13
2.1.3 Errors and Biases Originating at the Receiver.....	16
2.2 Geometric Effects	17
2.2.1 Satellite Configuration Geometry Effect.....	17
2.2.2 Ambiguity Resolution Effect.....	18

2.3	Mathematical Correlations in GPS Differential Positioning	19
2.4	Physical Correlations in GPS Differential Positioning.....	20
2.5	Covariance Functions of GPS Residual Errors.....	22
Chapter 3:	EMPIRICAL MODELLING OF PHYSICAL CORRELATIONS IN GPS DIFFERENTIAL POSITIONING.....	26
3.1	Analytical Covariance Function.....	26
3.1.1	Removing the Trend	27
3.1.2	The Autocovariance Function.....	28
3.1.3	The Crosscovariance Function.....	29
3.1.4	Assessment of Errors in the Estimated Covariance Function	30
3.2	Results for Empirical Covariance Functions	33
3.2.1	Results for the Autocovariance Function	34
3.2.2	Results for the Crosscovariance Function.....	38
3.3	Forming the Covariance Matrix.....	40
Chapter 4:	ALGORITHM FOR THE INVERSE OF THE FULLY POPULATED COVARIANCE MATRIX.....	43
4.1	The Covariance Matrix of Carrier Phase Double Differences	43
4.2	Inverting the Covariance Matrix	45
4.2.1	Ideal Case: The Same Satellites are Tracked Over Time	45
4.2.2	Real Case: Different Satellites are Tracked Over Time	47
4.3	Storage Requirements.....	51
Chapter 5:	MODIFIED LEAST SQUARES ADJUSTMENT FOR THE DETERMINATION OF POSITIONS AND AMBIGUITIES....	53
5.1	Modified Sequential Least Squares Adjustment	53
5.2	Updating the Inverse of the Normal Equation Matrix.....	56
5.3	Ambiguity Resolution Technique.....	58
5.4	Solution with Ambiguities as Functional Constraints.....	61

5.5	Storage Requirements.....	62
Chapter 6:	SOFTWARE DEVELOPMENT AND DISCUSSION OF THE RESULTS.....	64
6.1	Description of the Software	64
6.2	Discussion of the Results.....	66
6.2.1	Results for TI 4100 Data	67
6.2.2	Results for Other Data Sets.....	73
6.3	Effect of Sampling Interval.....	79
6.4	Effect of Correlation Time.....	82
6.5	Effect of Scaling the Covariance Matrix	83
Chapter 7:	CONCLUSIONS AND RECOMMENDATIONS.....	86
7.1	Summary and Conclusions.....	86
7.1.1	Modelling the Physical Correlations	86
7.1.2	The Effect of the Physical Correlations.....	88
7.2	Recommended Future Work	90
	REFERENCES	92
APPENDIX I:	ESTIMATED AUTOCOVARANCE FUNCTIONS DUE TO RESIDUAL TROPOSPHERIC DELAYS	100
APPENDIX II:	ESTIMATED AUTOCOVARANCE FUNCTIONS DUE TO IONOSPHERIC DELAYS.....	104
APPENDIX III:	ESTIMATED AUTOCOVARANCE FUNCTIONS FOR THE ADJUSTMENT RESIDUALS	110
APPENDIX IV:	DERIVATION OF THE INVERSE OF THE FULLY POPULATED COVARIANCE MATRIX.....	157

LIST OF FIGURES

Figure 2.1.	Effect of the Physical Correlation on the Incoming Signals.....	21
Figure 2.2.	Estimated Autocovariance Function of the Nonlinear Tropospheric Delay for a 29 km Baseline.....	23
Figure 2.3.	Estimated Autocovariance Function of the Nonlinear Ionospheric Delay for a 29 km Baseline	24
Figure 3.1a.	Autocovariance Function for 7 Minutes Data Series	31
Figure 3.1b.	Autocovariance Function for Two Hours Data Series	31
Figure 3.2a.	Spectrum for 7 Minutes Data Series.....	32
Figure 3.2b.	Spectrum for Two Hours Data Series.....	32
Figure 3.3.	Effect of the Finiteness of the Data on the Estimated Autocovariance Function	32
Figure 3.4.	The Empirical Autocovariance Function for L1 Data and its Approximation.....	37
Figure 3.5.	The Empirical Autocovariance Function for L2 Data and its Approximation.....	37
Figure 3.6.	The Empirical Autocovariance Function for L3 Data and its Approximation.....	38
Figure 3.7a.	Crosscovariance Function for Simulated Data with Statistically Independent Noise	40
Figure 3.7b.	Crosscovariance Function for Simulated Data with Coloured Noise ($\beta =$ $1/270$).....	40

Figure 5.1.	Required Storage for the Weight Matrix When Tracking Different Groups of Satellites Between Epochs j and k	63
Figure 6.1.	Effect of Physical Correlations on the Accuracy Estimation for a 20 km Baseline.....	72
Figure 6.2.	Effect of Physical Correlations on the Accuracy Estimation for a 60 km Baseline.....	73
Figure 6.3.	Effect of Physical Correlations on the Accuracy Estimation for a 13 km Baseline.....	78
Figure 6.4.	Effect of Physical Correlations on the Accuracy Estimation for a 55 km Baseline.....	79
Figure 6.5.	Effect of Sampling Interval on the Accuracy Estimation for a 13 km Baseline.....	80
Figure 6.6.	Effect of Sampling Interval on the Ratio Between the Second Smallest a posteriori Variance Factor and the Smallest a posteriori Variance Factor for a 13 km Baseline	81
Figure 6.7.	Effect of Varying the Correlation Time on the Accuracy Estimation for a 13 km Baseline	83
Figure 6.8.	The Resulting Standard Deviations from Two Software Packages for a 13 km Baseline	84
Figure 6.9.	The Resulting Standard Deviations from Two Software Packages for a 55 km Baseline	85

LIST OF TABLES

Table 3.1	Results of the L1 data.....	35
Table 3.2	Results of the L2 data.....	35
Table 3.3	Results of the L3 data.....	36
Table 3.4	Results for General Autocovariance Function	36
Table 6.1	Estimated Real Ambiguities and the Search Ranges for a 20 km Baseline ..	68
Table 6.2	Estimated Real Ambiguities and the Search Ranges for a 60 km Baseline ..	69
Table 6.3	Estimated Real Ambiguities and the Search Ranges for an 81 km Baseline.....	69
Table 6.4	Effect of Physical correlations on a 20 km Baseline	70
Table 6.5	Effect of Physical correlations on a 60 km Baseline	71
Table 6.6	Effect of Physical correlations on an 81 km Baseline.....	72
Table 6.7	Estimated Real Ambiguities and the Search Ranges for a 13 km Baseline ..	74
Table 6.8	Estimated Real Ambiguities and the Search Ranges for a 55 km Baseline ..	75
Table 6.9	Estimated Real Ambiguities and the Search Ranges for a 90 km Baseline ..	75
Table 6.10	Effect of Physical correlations on a 13 km Baseline	76
Table 6.11	Effect of Physical correlations on a 55 km Baseline	77
Table 6.12	Effect of Physical correlations on a 90 km Baseline	78

ACKNOWLEDGMENT

This research was supported by the University of New Brunswick and the Natural Science and Engineering Council (NSERC) operating grants. The data used in this research was provided by the Geological Survey of Canada, the Geodetic Survey of Canada and the Scripps Institute of Oceanography.

I wish to express my sincere gratitude and warmest thanks to Dr. Alfred Kleusberg for his supervision, valuable advice and continuous guidance and support during the achievement of this research.

I also would like to express my appreciation to the members of the Examining Board for their constructive recommendations. The Examining Board consisted of Prof. A. Kleusberg (Supervisor), Prof. D. Wells (Geodesy and Geomatics Engineering), Prof. J. Horton (Computer Science), Prof. B. Colpitts (Electrical Engineering) and Dr. D. Delikaraoglou (Trilogy Hellas Ltd.).

Finally I dedicate this thesis to my father for his immeasurable support and continuous encouragement; my wife for her special help and understanding; and to my sons, Mohamed and Moathe.

وقضى ربك ألا تعبدوا إلا إياه وبالوالدين إحسانا أما يبلغن عندك
الكبر أحدهما أو كلاهما فلا تقل لهما أف ولا تنهرهما وقل لهما قولا كريما .
واخفض لهما جناح الذل من الرحمة وقل رب ارحمهما كما ربياني صغيرا .

Thy Lord hath decreed that ye worship none but Him, and that ye be kind to parents.
Whether one or both of them attain old age in thy life, say not to them a word of
contempt, nor repel them, but address them in terms of honour. And, out of kindness,
lower to them the wing of humility, and say: "My Lord! bestow on them thy Mercy even
as they cherished me in childhood."
(Qur'an; 17:23-24)

Chapter 1

INTRODUCTION

1.1 Motivation

GPS carrier phase double difference observations are used for high accuracy relative positioning. The double differencing reduces or eliminates many common errors and biases. Unfortunately, the carrier phase observables are ambiguous by an integer number of full cycles called an “ambiguity parameter”. Although they are nuisance parameters, the ambiguity parameters play a very important role in obtaining high accuracy positioning. This comes from the integer nature of these parameters. Once the ambiguity parameters are correctly resolved and fixed to integer values, the estimated standard deviations of the unknown coordinates decrease dramatically due to the improvement in the geometry and the increase in the number of redundant observations.

GPS double difference carrier phase observations are subject to two types of correlations, namely mathematical correlation and physical correlation. Mathematical correlation results from differencing the original phase observations. This type of correlation depends on how the double differences are formed. Physical correlation results from the improper modelling of partially correlated measurement errors. It can be of a temporal and/or a spatial nature. The mathematical correlation yields a block diagonal structure for the covariance matrix of the double difference observations since there is no differencing between epochs. Physical correlations can yield a fully populated covariance matrix.

Previous studies consider the covariance matrix of the observations to be either diagonal (i.e. no correlation is considered) or block diagonal (i.e. only the mathematical correlation is considered). Physical correlation has not been taken into account. For this reason, the accuracy obtained from the GPS is questionable (Hollmann et al., 1990).

The goal of the present investigation can be separated into two parts. The first one is to model the temporal physical correlations in GPS carrier phase double difference observations to obtain a more realistic covariance matrix. The second goal is to find a reliable and efficient way for the ambiguity resolution as well as a reliable accuracy estimation. It should be pointed out that the word reliable, mentioned here and throughout the dissertation, means trustworthy. A reliable solution requires consideration of both the mathematical and the physical correlations among the observations. An efficient solution results from using the covariance matrix of the unknown parameters for searching the likely integer values of the ambiguity parameters in the neighbourhood of the estimated real values. In the past, the simultaneous occurrence of the ambiguity parameters was not considered. Therefore, the search window was treated as a hyperbox.

Usually in the least squares estimation, the covariance matrix of the estimated parameters is used to assess the accuracy of the parameters by forming a confidence region around their estimates. At a certain probability level, the expected values of any of these parameters fall somewhere inside this region. However, in the case of ambiguity resolution, the covariance matrix is used to form a confidence region for searching the likely integer values of the ambiguity parameters. Since the covariance matrix is the primary tool for defining the search area for the ambiguity parameters, it is of utmost importance that it is computed correctly. This requires taking into account both the mathematical and the physical correlations among the observations, assuming that all other tasks of the adjustment are done correctly.

1.2 Previous Studies

This section reviews the previous investigations concerning both the physical correlations and the ambiguity resolution.

1.2.1 Physical Correlations

The problem of physical correlations in GPS carrier phase differential positioning is usually neglected (Hofmann-Wellenhof et al., 1992). In fact, very few publications were found that deal with this subject at all. Vanicek et al. (1985) proposed a way of modelling the physical correlations, but no results are reported. Wells et al. (1987) emphasize the difficulty of handling the physical correlations. Abidin (1992) assumed that the required corrections are received from external sources such as the wide area differential GPS system.

1.2.2 Ambiguity Resolution

Procedures for ambiguity resolution have been investigated by several researchers. A brief discussion for the main methods used for static and kinematic positioning is given below.

Brown and Hwang (1983) have presented an approach to resolve the ambiguity parameters using a bank of parallel Kalman filters. Each filter in the bank is based on an assumed value for each of the ambiguity parameters. For each tested ambiguity parameter, they compute an associated probability. After some time, the probability of the correct ambiguity parameter will approach unity while the others approach zero.

Langley et al. (1984) presented three different strategies for resolving the ambiguity parameters. The first strategy consists of rounding the estimated real values of the

ambiguity parameters to the nearest integer. The second strategy is based on the estimated standard deviation σ for any of the ambiguity parameters. To find a solution, a search within a band that equals the estimated ambiguity parameter $\pm 3\sigma$ is performed. In this strategy, only one ambiguity parameter is fixed and the other parameters are determined to minimize the sum of the squared residuals. The last strategy checks every linear combination of the integer ambiguity parameters in the vicinity of the estimated values. As a result, the best choice of an integer set is the one that gives the smallest sum of the squared residuals.

Recently, Frei and Beutler (1989; 1990) realized the usefulness of using all available information from the resulting covariance matrix of the unknown ambiguity parameters in reducing the search space. However, instead of searching within the confidence hyperellipsoid corresponding to the resulting covariance matrix of the ambiguities, one-dimensional search ranges for both the individual ambiguities and the differences between the ambiguities are used. The first search range is used to select the individual ambiguities which fall within the confidence interval of the estimated ambiguities at a certain confidence level. The second search range is used to reject those ambiguity pairs whose differences do not fall within the confidence interval of the corresponding differences of the estimated values. This criteria was found effective in reducing the searching time (Erickson, 1992). Each admissible integer combination for the ambiguities is introduced as fixed values into another least squares adjustment and a unique solution is selected to be the one with the smallest a posteriori variance factor and does not have any other compatible solutions.

The least squares search technique is an approach presented recently by Hatch (1990). He separates the available satellites into two groups. The first group consists of the observations from four satellites and is used to obtain a set of potential solutions. The second group consists of observations from the remaining satellites and is used to reject

any potential solution which is not compatible with the second group of observations. A unique solution is selected to be the one with the smallest a posteriori variance factor and less than a prespecified threshold.

In 1990, Mader applied the ambiguity mapping function (AMF) technique (Counselman and Gourevitch, 1981). The AMF is an exponential function of the difference between the double difference observed phase and a calculated double difference phase based on a trial position. The correct position is that which minimizes the phase residual (i.e. makes the AMF maximum).

Euler and Landau (1992) use the ordinary least squares adjustment to obtain a preliminary solution for the unknown ambiguity parameters. The resulting standard deviations for the ambiguities are used to form a search window. The novelty of their technique is the use of Cholesky decomposition to modify the resulting covariance matrix of the ambiguity parameters. This modification proved to be very efficient in speeding up the search operation. However, they did not fully exploit the covariance matrix of the ambiguity parameters in specifying the search window.

Another technique was presented by Wubbena (1989) and Seeber and Wubbena (1989) is called the extrawidelaning technique. This technique uses several linear combinations of the carrier phase observations of L1 and L2 as well as the P-code observations on both L1 and L2. From these linear combinations, one can get three different artificial signals: a wide-lane signal, a narrow-lane signal, and an ionospheric signal. The wide lane signal has a relatively long wavelength of 86.2 cm. Therefore, the a priori wide-lane ambiguity parameters can be determined rather easily. The narrow-lane ambiguity parameters are then determined with the help of the ionospheric signal. Using the so-called even/odd relation (Abidin, 1992), the wide-lane can have its ambiguity parameters fixed. Following this, the narrow-lane ambiguity parameters can be fixed. This technique

usually combines with one or more of the previously described techniques (Abidin, 1992).

Combinations of some of the above techniques have been also investigated by Abidin (1992). He combines the least squares search technique with the ambiguity mapping function (AMF) technique. This results in a strategy that combines the fast processing of the least squares search technique with the reliable rejection criteria based on the ambiguity mapping function (AMF) technique. Whenever the P-code is available on both L1 and L2, he takes advantage of the widelaning technique to reduce the searching size of the ambiguity parameters.

1.3 Methodology

The first step in reaching the goal of this investigation is to model the physical correlations in GPS carrier phase double difference observations. A simple way of modelling the physical correlation may be done empirically using the adjustment residuals obtained with only the mathematical correlation included. In this case, the adjustment residuals reflect the presence of the unmodelled measurements errors. A number of data series representing baselines of different lengths is required for this purpose. Once a general empirical covariance function, representing the physical correlation, is obtained, it can be used to modify the observation covariance matrix. This leads to a more realistic covariance matrix.

In general, including both the physical and mathematical correlations yields a fully populated covariance matrix for the GPS carrier phase double difference observations. Implementing this fully populated covariance matrix into a software package usually slows down the numerical computations. To overcome this, an efficient algorithm for the inverse of a particular choice of the fully populated covariance matrix is developed.

A modified least squares adjustment algorithm for position parameters and the ambiguities is introduced incorporating the newly developed fully populated covariance matrix. Following this, an efficient algorithm for the ambiguity resolution is given. In the ambiguity resolution technique, the resulting covariance matrix of the ambiguity parameters forms a confidence region of a hyperellipsoid which is then used as a searching area. The searching time is optimized by using Cholesky roots for the covariance matrix of the ambiguity parameters. Data from several baselines of different lengths are analyzed to verify the validity of the technique.

1.4 Outline of the Dissertation

Chapter 2 starts with a short introduction to GPS. The main errors and biases affecting the GPS carrier phase measurements are discussed. The mathematical and the physical correlations, and the ways of handling them are also discussed. Finally, the expected covariance functions from different sources of the unmodelled errors are given.

Chapter 3 describes in detail how the empirical covariance function is developed. Results of the empirical covariance functions for L1, L2, and L3 (ionosphere free) data are given. Finally, the way of building the observations' covariance matrix using both the mathematical and the empirically modelled physical correlation is given.

Chapter 4 contains description of the developed algorithm for the inverse of the fully populated covariance matrix. Firstly, an ideal case of tracking the same satellites continuously is presented. Secondly, a general case of tracking different satellites over time is given. This chapter ends with a discussion of the reduction of the required memory when using this algorithm.

In chapter 5, a modified sequential least squares adjustment algorithm for positions and ambiguities is developed which incorporates the newly developed, fully populated

covariance matrix. The technique used for ambiguity resolution is also given. The final constraint solution after fixing the ambiguities is then described. Finally, the storage requirements are again discussed.

Chapter 6 describes the computer software and discusses the results. In this chapter, the effect of neglecting/including the physical correlations on the ambiguity resolution and accuracy estimation is given and discussed.

Chapter 7 summarizes the obtained results, gives conclusions and recommends future investigations.

1.5 Contributions of the Research

The contributions of this research can be summarized as follows:

- to develop an empirical covariance model for the temporal physical correlations of the unmodelled errors in GPS carrier phase double difference positioning as a function of the baselines length;
- to develop a general empirical covariance model for the temporal physical correlations of the unmodelled errors in GPS carrier phase double difference positioning which is valid for any baseline of length up to 100 km;
- to develop a realistic fully populated covariance matrix for the GPS carrier phase double difference observations;
- to develop an efficient algorithm for the inverse of a particular choice of the fully populated covariance matrix;

- to develop a modified sequential least squares adjustment algorithm incorporating the new developed fully populated covariance matrix for positions and ambiguities;
- to develop an efficient ambiguity resolution technique based on the stochastic modelling of the GPS residual errors, hyperellipsoid search space and Cholesky decomposition of the resulting covariance matrix for the unknown ambiguities;
- to develop a GPS processing software which takes into account the physical correlation, including automatic ambiguity resolution; and
- to improve the accuracy estimation of the estimated parameters.

Chapter 2

GPS MEASUREMENT ERRORS

The Global Positioning System (GPS) currently being developed by the US Department of Defense is a worldwide, all weather navigation and timing system. For security reasons as well as serving a large number of users, GPS is a passive system, i.e., users can only receive the satellite signals (Langley, 1990). The full GPS constellation will consist of 24 operational satellites (Montgomery, 1993a). To ensure continuous worldwide coverage, four satellites are arranged in each of six orbital planes. The GPS satellite orbits are nearly circular (maximum eccentricity is about 0.01), with an inclination of about 55° to the equator, and a semi-major axis of about 26560 km (Langley, 1991b). The GPS system has achieved the initial operational capability at the end of 1993.

Each GPS satellite transmits a signal which has a number of components: two carriers generated at 1575.42 MHz (L1) and 1227.60 MHz (L2), pseudorandom noise (PRN) codes added to the carriers as binary biphase modulations at chipping rates of 10.23 MHz (P-code) and 1.023 MHz (C/A-code), and a 1500 bit long navigation message added to the carriers as binary biphase modulations at 50 Hz. The L1 carrier is modulated with both the P-code and the C/A-code, whereas the L2 carrier is modulated with the P-code only. The navigation message contains, along with other information, the coordinates of the satellites as a function of time and is modulated onto both carriers.

The PRN codes are used for real-time navigation. A replica of the PRN code transmitted from the satellite is generated by the receiver. The time offset between the arrival of the

transmitted code and its replica is the signal travel time. Multiplying the travel time by the speed of light gives the range between the satellite and the receiver antenna. This range, however, is contaminated, along with other biases, by the mis-synchronization between the satellite and receiver clocks. For this reason, this quantity is referred to as pseudorange (Langley, 1991c). The measured pseudorange can be expressed as follows (Wells et al., 1987)

$$P = \rho + c (dt - dT) + d_{ion} + d_{trop} + \epsilon_P \quad (2.1)$$

where P is the measured pseudorange, ρ is the geometric range between the receiver and the GPS satellite, c is the speed of light, dt and dT are the offsets of the satellite and the receiver clocks from the GPS time, d_{ion} and d_{trop} are the ionospheric and tropospheric delays, and ϵ_P represents the multipath error and the system noise in the measured pseudorange. The system noise represents the contribution of the receiver and antenna/preamplifier components (Nolan et al., 1992).

GPS was designed so that real-time navigation with the civilian C/A code receivers would be less precise than military P-code receivers. Surprisingly, the obtained accuracy was almost the same from both receivers (Georgiadou and Doucet, 1990). To ensure national security, the US Department of Defense implemented the so-called selective availability (SA) on the new generation GPS satellites to deny accurate real-time positioning to unauthorized users. With SA, nominal horizontal and vertical errors can be up to 100 m and 150 m respectively, at a 95% probability level. A remedy for that is to use Differential GPS (DGPS) instead of point positioning. DGPS provides better accuracy than the stand-alone P-code receiver due to the elimination or the reduction of the common errors including SA.

In surveying applications, where more precise positioning is required, the GPS carrier phase measurements are generally used. Carrier phases are also subject to several kinds

of errors and biases such as clock errors, ephemeris errors, atmospheric errors, multipath and receiver noise. The phase measurement is also biased by an unknown integer, called ambiguity. The GPS receiver assigns an arbitrary integer number for the ambiguity when it first locks on (Langley, 1991a). It should be noted, however, that the initial unknown ambiguity remains constant over time as long as no loss of phase lock occurs. The carrier phase observation equation can be written as (Wells et al., 1987)

$$\Phi = \rho + c (dt - dT) + \lambda N - d_{\text{ion}} + d_{\text{trop}} + \epsilon_{\Phi} \quad (2.2)$$

where Φ is the observed carrier phase multiplied by the carrier wavelength λ , N is the initial integer ambiguity parameter and ϵ_{Φ} represents the multipath error and the system noise in the observed carrier phase. The remaining parameters are defined as before. To obtain the highest possible accuracy, the effect of errors and biases must be kept as minimal as possible, and the unknown integer ambiguities must be determined correctly.

2.1 GPS Errors and Biases

In this section, the main errors and biases affecting the GPS carrier phase measurements are discussed. GPS error sources may be classified as errors originating at the satellite, errors due to signal propagation and errors originating in the receiver. Other effects such as satellite configuration geometry and ambiguity resolution are also discussed.

2.1.1 Errors and Biases Originating at the Satellites

The errors originating at the satellites include orbital errors (satellite ephemeris errors), clock errors, and selective availability. Satellite positions as a function of time are predicted from previous GPS observations at ground control stations (Kleusberg and Langley, 1990). However, due to the improper modelling of the forces acting on the GPS satellites, ephemeris errors are usually expected. Although an ephemeris error is identical

to all users, its effect on the range measurement is different and cannot be totally removed through differencing. This occurs because different users see the same satellite at different view angles. However, the range error due to the ephemeris error is highly correlated between users of short separations and is roughly proportional to user separation (Loomis et al., 1991). Nominal ephemeris error is usually of the order of 5 to 10 m and can reach from 50 to 100 m under selective availability (Kleusberg, 1992). Post-mission precise orbital service is available at the 5 m accuracy level or better (Lachapelle, 1990). However, it cannot be used for real-time or near real-time GPS positioning.

The GPS satellite clocks, although highly accurate, are not perfect. This causes additional errors to GPS measurements. These errors are also common to all users observing the same satellite and can be removed through differencing between the receivers. After applying the broadcast correction, satellite clock error can be of the order of several nanoseconds (Kleusberg, 1992).

Selective availability introduces two additional errors. The first one, called δ -error, results from dithering the satellite clock and is common to all users. The second one, called ϵ -error, is an additional slowly varying orbital error (Georgiadou and Doucet, 1990). Like the range error due to ephemeris error, the range error due to ϵ -error is highly correlated between users of short separations.

2.1.2 Atmospheric Errors and Biases

At the uppermost part of the atmosphere, ultraviolet radiation from the sun interacts with the gas molecules. Gas ionization results in a large number of free electrons affecting GPS signals (Klobuchar, 1991). This region of the atmosphere, which extends from a height of approximately 50 to 1000 km, is called the ionosphere. The ionosphere is a

dispersive medium which speeds up the propagation of the carrier phase beyond the speed of light while it slows down the propagation of the pseudorange the same amount (Langley, 1993). This occurs because the carrier phase is subject to phase advance while the pseudorange is subject to group delay. The ionospheric delay is proportional to the number of free electrons along the signal path or the total electron content (TEC). TEC, on the other hand depends on the time of the day (highest at 2:00 pm local), time of the year (highest at spring equinox), the 11-year solar cycle, and geographic location. Also, ionospheric delay is frequency dependent, the lower the frequency the greater the delay. Nonetheless, the ionosphere reflects signals of frequencies below 30 MHz (Klobuchar, 1991). Generally, ionospheric delay is of the order of 5 to 15 m but can reach over 100 m (Kleusberg, 1992).

The ionospheric delay was found to be correlated over distance from about 200 km under disturbed ionospheric conditions to about 1000 km under normal conditions. On the other hand, it is temporally correlated over time periods of 2 to 50 minutes under disturbed and normal conditions respectively (Wild et al., 1990). This means that differencing the GPS observations between users of short separation can remove the major part of the ionospheric delay.

Ionospheric delay or TEC can be best determined by combining P-code pseudoranges observed on L1 and L2. Dual frequency carrier phase measurements can also be combined to generate ionosphere free observations. However, this linear combination is noisier than the single frequency observation and is not recommended for short baselines where the errors are highly correlated over distance and cancel sufficiently through differencing (Langley, 1993). Single frequency users can correct up to 60% of the delay using ionospheric correction models (Klobuchar, 1991). It was found, however, that these models are suitable for mid latitude locations only (Loomis et al., 1991).

The troposphere is the electrically neutral atmospheric region which extends up to about 50 km from the surface of the earth (Brunner and Welsch, 1993; Jong, 1991). It is a nondispersive medium for radio frequencies below 30 GHz. As a result, it delays the GPS carriers and codes identically. Signals from satellites at low elevation angles travel a longer path through the troposphere than those at higher elevation angles. Therefore the tropospheric delay is minimized at zenith and maximized near the horizon. According to Brunner and Welsh (1993), tropospheric delay results in values of about 2.4 m at zenith and about 9.3 m for 15° elevation angle. Tropospheric delay may be broken into two components, dry and wet. Dry component represents about 90% of the delay and can be predicted to a high degree of accuracy using empirical models (Wells et al., 1987). However, the wet component is not easy to predict. Wet component can be measured accurately as a function of elevation and azimuth angle using water vapor radiometers (WVR). Unfortunately, WVR are very expensive and cannot be considered as a standard technique for GPS positioning (Brunner and Welsch, 1993).

Several empirical models use surface meteorological measurements to compute the wet component. However, the wet component is weakly correlated with surface meteorological data. It was found that, in most cases, a default tropospheric data gives better results than tropospheric models using surface meteorological data (Brunner and Welsch, 1993). However, both ways lead to a biased value of the tropospheric correction. A residual component should be added to reach the actual value of tropospheric correction. One way of computing this residual value is to include it as an additional unknown parameter in the least squares adjustment (Rothacher et al., 1990). Alternatively, it can be dealt with stochastically as a time-varying parameter (Tralli and Lichten, 1990). Unfortunately, the precision of the height determination in comparison to the horizontal component was found to be worse by a factor of 3 when using the first method and by a factor of 6 when using the second method (Brunner and Welsch, 1993). These factors are related to the an elevation mask angle of 15°.

2.1.3 Errors and Biases Originating at the Receiver

The errors originating in the receiver include clock errors and receiver noise. The receiver clock error is much larger than that of the GPS satellite (Kleusberg and Langley, 1990), but can be removed through differencing between the satellites or it can be treated as an additional unknown parameter.

The receiver measurement noise results from the limitations of the receiver's electronics. The receiver noise and the antenna/preamplifier noise are usually combined together to form the system noise (Nolan et al., 1992). The system noise is uncorrelated. Typical reported values of the system noise for the Ashtech P-12 are about 0.4% of the signal wavelength for the carrier phase and about 0.8% for the pseudorange (Nolan et al., 1992).

There are two other errors which occur at the receiver antenna, multipath and phase center variation of the antenna. Multipath error occurs when a signal arrives at the receiver antenna through different paths (Wells et al., 1987). These different paths can be the direct line of sight and reflected signals from obstacles in the vicinity of the receiver antenna. Multipath distorts the original signal through interference with the reflected signals with a maximum value of a quarter of a cycle in case of carrier phase (Georgiadou and Kleusberg, 1988). The pseudorange multipath takes the value for up to one chip length of the code pseudorange (Wells et al., 1987). Multipath is totally uncorrelated between stations, i.e., it cannot be removed by differencing the GPS observations. An important fact about multipath is that, under the same environment, its signature repeats every sidereal day because of the repeated geometry of the satellite-antenna (Evans, 1986). This means, multipath can be detected by observing the high correlation of the GPS adjustment residuals over two consecutive days.

Additional range error occurs as a result of the antenna phase center variation. The antenna phase center variation depends on the direction angle of the observed signal. It is

very difficult to model this error and care has to be taken when selecting the antenna type (Kleusberg and Langley, 1990). It should be pointed out that phase center errors can be different on L1 and L2 carrier phase observations (Rothacher et al., 1990). This can affect the accuracy of the ionosphere free linear combination particularly when observing short baselines. As mentioned before, for short baselines, the errors are highly correlated over distance and cancel sufficiently through differencing. Therefore, using a single frequency might be more appropriate for short baselines.

2.2 Geometric Effects

In this section, the geometric effects on the GPS positioning accuracy are discussed. These include the effects of the satellite configuration geometry and the ambiguity resolution.

2.2.1 Satellite Configuration Geometry Effect

Satellite configuration geometry represents the geometric locations of the GPS satellites as seen by the receiver(s). Satellite configuration geometry plays a very important role in the obtained accuracy. Even under the full constellation of 24 GPS satellites, shadow areas where no satellites can be observed will exist. The shadow area will move from the horizon to the zenith as we move from the equator towards the pole (Santerre, 1989). This means that the satellite coverage is not uniform. On the other hand, satellite geometry has a direct effect on the formation of the design matrix, which in turn affects the resulting covariance matrix of the station coordinates. It is recommended, therefore, that a suitable observation time be selected. GPS satellite configuration geometry changes slowly with time. For this reason, it is sometimes better to take observations for several minutes and then revisit the same station after a few hours.

Satellite configuration geometry effect can be measured by a single number called the dilution of precision (DOP). The lower the value of DOP, the better the geometric strength. Unfortunately, DOP describes the geometrical configuration at only one epoch and not the whole observation time (Santerre, 1989).

2.2.2 Ambiguity Resolution Effect

As mentioned before, the carrier phase observation equation contains an unknown integer number, the carrier phase ambiguity. The determination of this integer number is known as ambiguity resolution. Usually the least squares technique is applied first to obtain a preliminary solution for the unknown station coordinates along with real values for the ambiguity parameters. Based on the preliminary solution and its covariance matrix, the integer ambiguity parameters may be determined. It is therefore very important to obtain a reliable covariance matrix. The resulting covariance matrix is a function of the design matrix, which contains the geometry and the covariance matrix of the observations.

Correctly determined ambiguity parameters lead to increased precision in GPS positioning. This results from the improvement in the geometry once the ambiguities are correctly resolved and fixed at integer values. A comparison between the fixed-ambiguity solution and the float-ambiguity solution as a function of observation time span and the elevation mask angle was presented by Santerre et al. (1990). They found that, with the float solution, the size of the confidence ellipsoid for the unknown coordinates changes significantly as a function of the observation time span. For short observation time span, the size of the confidence ellipsoid is very large and it tends to stabilize for an observation time span of more than 3 hours. In contrast, with the fixed solution, the size of the confidence ellipsoid remains more or less constant.

2.3 Mathematical Correlations in GPS Differential Positioning

For the purpose of removing common errors and reducing partially correlated errors, GPS double difference observations are widely used in surveying applications. A very important advantage of using the double difference observations is that the ambiguity parameters remain integers. However, it has the disadvantage that the double difference observations are mathematically correlated as a result of differencing the observed phases. The mathematical correlation depends on how the double differences are formed (Beutler et al., 1989). For example, if a, b and c are three uncorrelated "between-receiver" single differences, then forming the double differences (a-b) and (b-c) results in a mathematical correlation of -0.5 between the two double differences. However, if the double differences are formed in the sequence (a-b) and (a-c), then a mathematical correlation of +0.5 is obtained.

The carrier phase double difference observations for one epoch may be written as (Beutler et al., 1984)

$$\nabla\Delta\Phi = \mathbf{a} \Phi \quad (2.3)$$

where $\nabla\Delta$ represents the double difference operator, \mathbf{a} is a differencing operator matrix and Φ is the vector of the observed phase values. Applying the law of covariance propagation to (2.3) yields the covariance matrix for the carrier phase double difference observations M at this particular epoch

$$M = \mathbf{a} \mathbf{C}_\Phi \mathbf{a}^T \quad (2.4)$$

where \mathbf{C}_Φ is the covariance matrix of the undifferenced observations and is usually assumed to be an identity matrix scaled by a common variance factor (Hofmann-Wellenhof et al., 1992). Note that the matrix (2.4) above remains unchanged from epoch to epoch as long as the same satellites are observed and the double differences are formed

in the same sequence. If the double differences are formed in the sequence (a-b), (b-c), (c-d), etc., the covariance matrix (2.4) takes the form

$$\mathbf{M} = \begin{bmatrix} 2 & -1 & 0 & \cdots & 0 & 0 \\ -1 & 2 & -1 & \cdots & 0 & 0 \\ \cdots & \cdots & \cdots & \cdots & \cdots & \cdots \\ 0 & 0 & 0 & \cdots & 2 & -1 \\ 0 & 0 & 0 & \cdots & -1 & 2 \end{bmatrix} \quad (2.5)$$

If, however, the double differences are formed in the sequence (a-b), (a-c), (a-d), etc., the covariance matrix (2.4) takes the form (Biacs et al., 1990)

$$\mathbf{M} = \begin{bmatrix} 2 & 1 & 1 & \cdots & 1 \\ 1 & 2 & 1 & \cdots & 1 \\ \cdots & \cdots & \cdots & \cdots & \cdots \\ 1 & 1 & 1 & \cdots & 2 \end{bmatrix} \quad (2.6)$$

Note that the common variance factor is removed from (2.5) and (2.6) above. For data of more than one epoch, the covariance matrix of the double difference observations will be a block diagonal matrix.

2.4 Physical Correlations in GPS Differential Positioning

As discussed earlier, GPS observations are affected by several kinds of errors and biases. When forming the observation double differences, the satellite and the receiver clock errors are eliminated. The residual effect of the orbital errors, the residual ionospheric and tropospheric delays, the multipath error and the system noise remain. The orbital errors or ephemeris errors result from improperly modelling the forces acting on the GPS satellites. The atmospheric delays, on the other hand, represent the physical phenomena that affect the GPS signal propagation. Due to insufficient knowledge of these physical phenomena, modelling the above errors cannot, in general, be done rigorously.

Therefore, a residual error component is expected to remain unmodelled. Usually, the effect of the remaining unmodelled errors increases as the baseline length increases. Because the environments associated with the GPS observations are similar to a certain degree, it is expected that the residual errors show a certain degree of temporal and/or spatial correlation which is known as physical correlation. Figure 2.1 describes both kinds of correlations for the undifferenced observations.

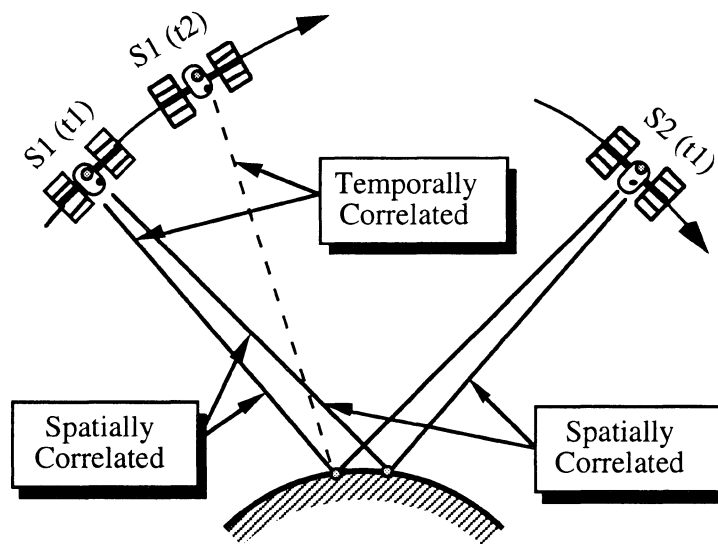


Figure 2.1. Effect of the Physical Correlation on the Incoming Signals

If the physical correlation is not accounted for, an overestimation of the accuracy of the estimated parameters can be expected. One way of modelling the physical correlation may be done through examining the adjustment residuals obtained with only the mathematical correlation included. In this case, the adjustment residuals exhibit the presence of unmodelled errors. The next step is to generate a series of autocovariance functions for each double difference series and also crosscovariance functions among the double differences. This has to be done for a sufficient number of baselines of different lengths to model the temporal physical correlation as a function of baseline length.

However, as shown later, the covariance function has to be interpreted carefully to avoid any distortion. The resulting estimated covariance functions represent the effect of the correlations among the unmodelled errors, the effect of the so-called artificial correlations which result from the adjustment process, the distortions due to the finiteness of the data series and the effect of the mathematical correlations. It is only the first type of correlation that we are interested in. The remaining effects must be removed. After removing the undesired effects, the estimated covariances are used to generate an empirical covariance function which can be used to form a more appropriate covariance matrix for the double difference observation.

2.5 Covariance Functions of GPS Residual Errors

Each one of the residual error components exhibits a certain degree of correlation. The effects of orbital errors are highly correlated. Therefore, for short baselines, a relatively long correlation length is expected for the double difference adjustment residuals. If the linear trend is removed from the adjustment residuals, the effect of unmodelled orbital errors may disappear.

To test the significance of the unmodelled tropospheric and ionospheric errors on the estimated covariance functions, dual frequency data of two baselines were used. Their lengths were 12 and 29 km, respectively. They were observed twice on two consecutive days and were found to be free of multipath errors. First the L1 and L2 data were processed separately to determine the integer ambiguity parameters on L1 and L2. Then the ambiguity parameters were subtracted from the data. In this case, the mathematical model for the carrier phase double difference is given by

$$\nabla\Delta\Phi = \nabla\Delta\rho + \nabla\Delta d_{\text{trop}} - \nabla\Delta d_{\text{ion}} + \nabla\Delta\varepsilon_{\Phi} \quad (2.5)$$

where $\nabla\Delta$ represents the double difference operator and the remaining terms are defined as shown before. If the ionosphere free linear combination is processed, then the resulting adjustment residuals with the linear trend removed will exhibit the effect of the unmodelled nonlinear tropospheric delays. Figure (2.2) shows a sample of the estimated covariance function from the unmodelled nonlinear differential tropospheric delays. Appendix I shows the estimated covariance functions as a result of the unmodelled nonlinear differential tropospheric errors for the above mentioned baselines. It should be noted that the Hopfield model for the empirical modelling of the troposphere was applied using surface meteorological data when processing these baselines.

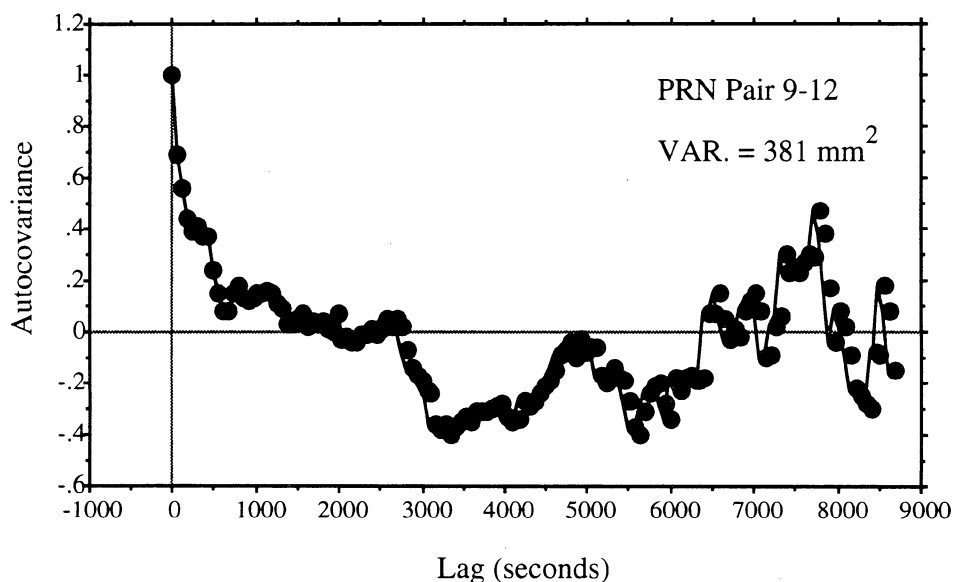


Figure 2.2. Estimated Autocovariance Function of the Nonlinear Tropospheric Delay for a 29 km Baseline

Figure 2.2 and Appendix I show that a correlation length of over about 20 minutes can be expected from the residual differential tropospheric delays.

Based on equation (2.7) and neglecting the measurement noise, the differential ionospheric delay on L1 can be derived as (Webster, 1992)

$$\nabla\Delta d_{\text{ion}1} = \frac{f_2^2}{f_1^2 - f_2^2} (\nabla\Delta\Phi_1 - \nabla\Delta\Phi_2) \quad (2.8)$$

where f_1 and f_2 are the frequencies of the L1 and L2 signals, respectively. Three baselines of lengths 12, 29 and 81 km were used to create the differential ionospheric delay data series (2.8). Figure (2.3) shows a sample of the estimated covariance function from the nonlinear differential ionospheric delays. Appendix II shows the estimated covariance functions as a result of the nonlinear differential ionospheric delays for the above mentioned baselines.

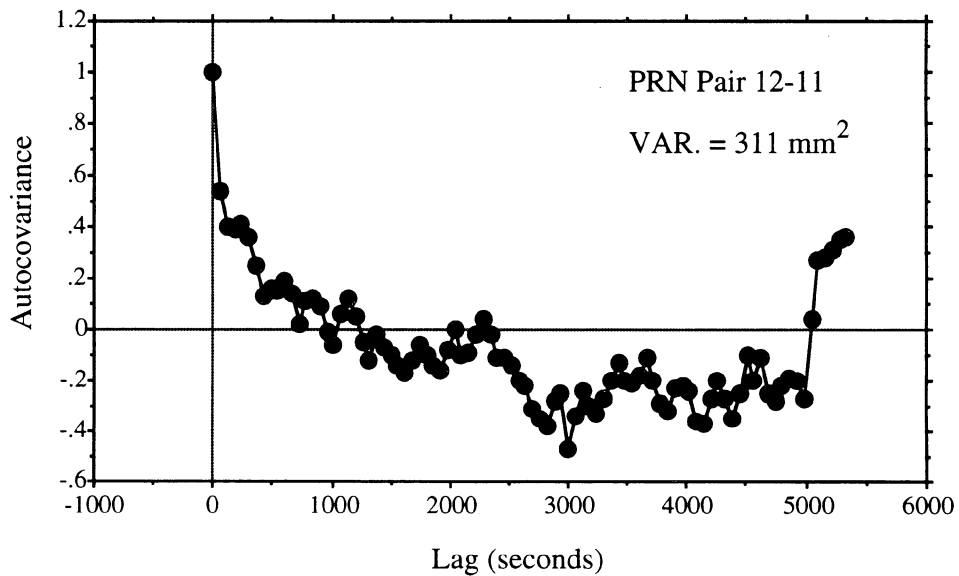


Figure 2.3. Estimated Autocovariance Function of the Nonlinear Ionospheric Delay for an 81 km Baseline

Like the tropospheric delays, the differential ionospheric delays show a high degree of correlation. It should be noted that the relatively small variance factors of the differential

ionospheric delays in Figure (2.3) and Appendix II come from the fact that the tested baselines were observed in 1986, a year of minimal ionospheric activities.

EMPIRICAL MODELLING OF PHYSICAL CORRELATIONS IN GPS DIFFERENTIAL POSITIONING

As stated before, the effect of the temporal physical correlation can be accounted for through the modification of the covariance matrix of the double difference observations. This may be done by developing a general empirical covariance function based on the analysis of sufficient data series representing baselines of different lengths. The adjustment residuals of these baselines obtained without physical correlation included are used for this purpose. A total of 47 baselines observed in North and South America were processed using DIPOP, the UNB GPS processing software (Vanicek et al., 1985). The observation time spanned between 4 to 5 hours in most cases. The resulting adjustment residuals, obtained with only mathematical correlations included, were then used to estimate the covariance functions. An empirical covariance function was then determined through a least squares fit to the estimated covariance functions.

3.1 Analytical Covariance Function

This section reviews the method of estimating and assessing the covariance function. We will restrict the discussion to discrete random processes.

3.1.1 Removing the Trend

Removing the trend from the data is necessary because otherwise a large distortion in the correlation function can be expected. However this has to be done only if the trends are physically expected or if they clearly appear in the data (Bendat and Piersol, 1986). One way of removing the trend is by fitting the data with a low order polynomial in the least squares sense. In our case a linear trend is removed from all the data. The general form of the trend $t(t_i)$ is given by Vanicek and Krakiwsky (1986) as

$$t(t_i) = r(t_i) + r'(t_i) = \varphi^T(t_i) \Lambda \quad (3.1)$$

where $r(t_i)$ is the observation component (in our case, the GPS double difference residual) at epoch t_i , $r'(t_i)$ is the residual component after removing the trend, $\varphi^T = [\phi_1, \phi_2, \dots, \phi_u]$ are u base functions selected beforehand, and $\Lambda = [\lambda_1, \lambda_2, \dots, \lambda_u]^T$ are u unknown coefficients which may be determined through the least squares regression. Over the whole data span equation (3.1) can be written as

$$\mathcal{V}^T(\mathcal{J}) \Lambda = \mathbf{r} + \mathbf{r}', \quad \mathcal{J} \equiv \{t_1, t_2, \dots, t_n\} \quad (3.2)$$

where $\mathcal{V}^T(\mathcal{J})$ is the Vandermonde's matrix and n is the number of sampling points. The least squares solution of this mathematical model is given by Vanicek and Krakiwsky (1986) as

$$\hat{\Lambda} = (\mathcal{V}^T \mathbf{P} \mathcal{V}^T)^{-1} \mathcal{V}^T \mathbf{P} \mathbf{r}. \quad (3.3)$$

The terms in (3.3) are defined as

$$\mathcal{V}^T \mathbf{P} \mathcal{V}^T = \begin{bmatrix} \langle \phi_1, \phi_1 \rangle & \langle \phi_1, \phi_2 \rangle & \cdots & \langle \phi_1, \phi_u \rangle \\ \langle \phi_2, \phi_1 \rangle & \langle \phi_2, \phi_2 \rangle & \cdots & \langle \phi_2, \phi_u \rangle \\ \cdots & \cdots & \cdots & \cdots \\ \langle \phi_u, \phi_1 \rangle & \langle \phi_u, \phi_2 \rangle & \cdots & \langle \phi_u, \phi_u \rangle \end{bmatrix}, \quad (3.4)$$

$$\Psi \mathbf{P} \mathbf{r} = \begin{bmatrix} \langle \varphi_1, \mathbf{r} \rangle \\ \langle \varphi_2, \mathbf{r} \rangle \\ \dots \\ \langle \varphi_u, \mathbf{r} \rangle \end{bmatrix}, \quad (3.5)$$

where $\langle \varphi_i, \varphi_j \rangle = \varphi_i^T(\mathcal{J}) \mathbf{P} \varphi_j(\mathcal{J})$.

Once the estimated coefficients for the trend are obtained, the trend $t(\tau_i)$ can be obtained from (3.1) and subtracted from the data.

3.1.2 The Autocovariance Function

The autocovariance function defines the degree of similarity between a random process and itself at different shifts or lags. Assuming that the data represents a stationary random process, an unbiased estimate of the autocovariance function is given by

$$\hat{C}_{xx}(\tau) = \frac{1}{N - |\tau|} \sum_{i=0}^{N-|\tau|-1} x'(i) x'(i + \tau), \quad (3.6)$$

where $\tau = -L, \dots, -1, 0, 1, \dots, L$, $x'(j)$, $j = 0, 1, \dots, N-1$ is the data sequence with the mean removed and L is the maximum lag to be considered (Marple, 1987). The normalized autocovariance function $\hat{\rho}_{xx}(\tau)$ at lag τ is defined as the ratio between the autocovariances at lag τ and zero lag. As we deal with single baseline solutions, the normalized covariance function is used. For simplicity, in the sequel the normalized autocovariance function is referred to as the autocovariance function.

The computation of the variance of the autocovariance function may be done through the following derivation. For a stationary random process the variance of the biased autocovariance function is given by Box and Jenkins (1970) as

$$\text{var}\{\hat{\rho}'_{xx}(\tau)\} \approx \frac{1}{N} \sum_{i=-\infty}^{+\infty} \{\rho^2(i) + \rho(i+\tau)\rho(i-\tau) - 4\rho(i)\rho(\tau)\rho(i-\tau) + 2\rho^2(i)\rho^2(\tau)\} \quad (3.7)$$

where $\rho(i)$ is the “true” or “population” autocovariance function, and $\hat{\rho}'_{xx}(\tau)$ is the biased estimated autocovariance function. The biased estimated autocovariance function is related to the unbiased one by

$$\hat{\rho}'_{xx}(\tau) = \frac{N-|\tau|}{N} \hat{\rho}_{xx}(\tau). \quad (3.8)$$

Equation (3.7) can be simplified by assuming that the true autocovariances are all essentially zero beyond some hypothesized lag $\tau = q$. That is

$$\text{var}\{\hat{\rho}'_{xx}(\tau)\} \approx \frac{1}{N} \{1 + 2 \sum_{i=1}^q \rho^2(i)\}, \quad \tau > q. \quad (3.9)$$

This expression can be simplified further using the estimated, instead of the true, autocovariance function. To get an expression for the variance of the unbiased autocovariance function we use the relation

$$\text{var}\{\hat{\rho}'_{xx}(\tau)\} = \frac{N-|\tau|}{N} \text{var}\{\hat{\rho}_{xx}(\tau)\}. \quad (3.10)$$

Therefore the variance of the unbiased autocovariance function can be written as (Pankratz, 1983)

$$\text{var}\{\hat{\rho}_{xx}(\tau)\} \approx \frac{1}{N-|\tau|} \{1 + 2 \sum_{i=1}^{\tau-1} \hat{\rho}_{xx}^2(i)\}. \quad (3.11)$$

3.1.3 The Crosscovariance Function

The crosscovariance function defines the degree of similarity between two random processes at different shifts or lags. In a similar way to the autocovariance function, we can write the expressions for the crosscovariance function as

$$\hat{C}_{xy}(\tau) = \frac{1}{N-|\tau|} \sum_{i=0}^{N-|\tau|-1} x'(i) y'(i + \tau) \quad (3.12)$$

where $x'(i)$, $i = 0, 1, \dots, N-1$ is the first data sequence with the mean removed, $y'(i)$ is the second data sequence with the mean removed and L is the maximum lag to be considered. The normalized crosscovariance function $\hat{\rho}_{xy}(\tau)$ at lag τ , sometimes called the sample correlation, is defined as

$$\hat{\rho}_{xy}(\tau) = \frac{\hat{C}_{xy}(\tau)}{\hat{C}_{xx}(0) \hat{C}_{yy}(0)}. \quad (3.13)$$

The variance of the normalized crosscovariance function may be defined as

$$\text{var}\{\hat{\rho}_{xy}(\tau)\} \approx \frac{1}{N-\tau} \sum_{i=-\infty}^{+\infty} \rho_{xx}(i) \rho_{yy}(i) \quad (3.14)$$

assuming that the true normalized crosscovariance function $\rho_{xy}(\tau)$ is non zero only in a certain range $R_1 \leq i \leq R_2$ and τ is not included in this range. If the two processes are not cross-correlated then equation (3.14) applies for all lags (Box and Jenkins, 1970).

3.1.4 Assessment of Errors in the Estimated Covariance Function

Rigorous steps have been taken to check the validity of the observation covariance function estimated from the adjustment residuals. The effect of the artificial correlation of the residuals introduced by the adjustment process was first checked. It is known that this artificial correlation tends to be significant if the number of observations is small (Vanicek et al., 1985). Statistically independent normally distributed random noise was added to a simulated GPS data set to assess the effect of the adjustment process on the correlation of the resulting residuals. Several data series of different length and satellite distribution have been processed. It was found that the correlation resulting from the adjustment process is very pronounced for short data sets. However, it is negligible for

data series of lengths longer than two hours. Figures 3.1a and 3.1b show examples of the estimated autocovariance functions for two data series of 7 minutes and two hours length, respectively. It is clear that, because its estimated autocovariance function has significant values for non-zero lags, the first data series is contaminated by the artificial correlation while the second data series is not.

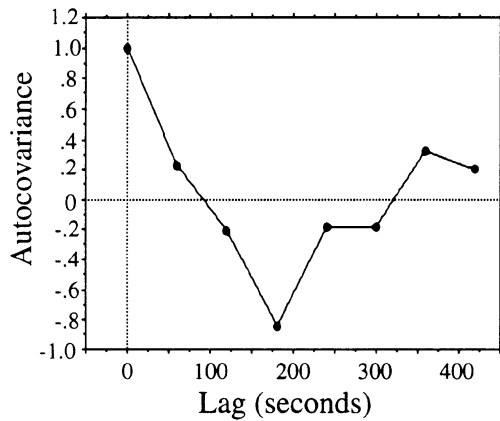


Figure 3.1a. Autocovariance Function for 7 Minutes Data Series

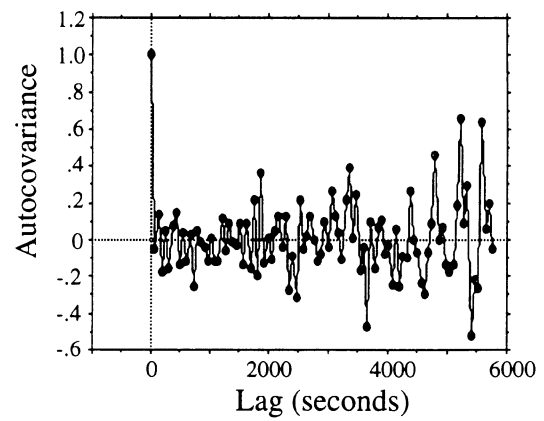


Figure 3.1b. Autocovariance Function for Two Hours Data Series

The least squares spectrum (Wells et al., 1985) was constructed for these residual data series. Figure 3.2a and 3.2b show the spectrum of the above two data series. The low frequency peak in the spectrum of the first data series indicates the existence of the artificial correlation. On the contrary, there are no obvious peaks in the two hour residual data series, indicating that the artificial correlation in this data is negligible. Other data series shorter than two hours were also processed and found to be contaminated by the artificial correlation. For this reason, it is more appropriate to use data series of two hours minimum.

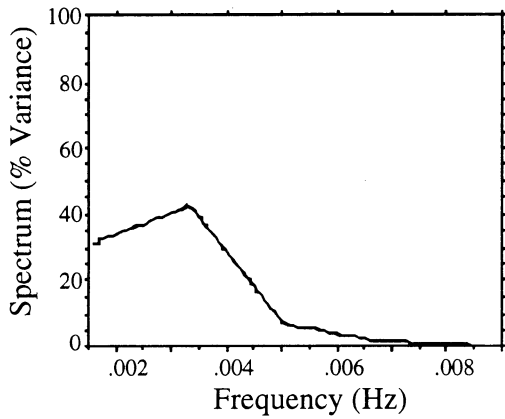


Figure 3.2a. Spectrum for 7 Minutes Data Series

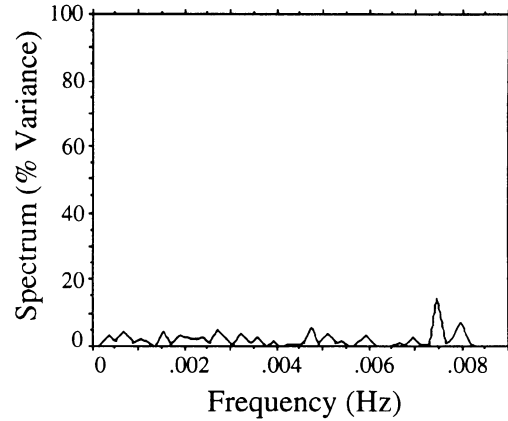


Figure 3.2b. Spectrum for Two Hours Data Series

The finiteness of the data series distorts the estimated covariance function. As the number of lags increases, the number of terms used to estimate the covariance function decreases and the reliability in the estimated covariance function is reduced. Figure 3.3 shows the autocovariance function for a data series with statistically independent values. The data series has a one second sampling interval. It is obvious that the variation of the autocovariance function increases with large lags.

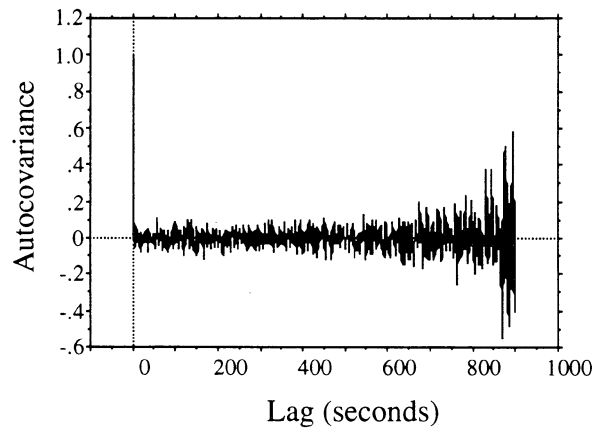


Figure 3.3. Effect of the Finiteness of the Data on the Estimated Autocovariance Function

To avoid this problem, several authors suggested a certain maximum length of the useful estimate of the covariance function. Box and Jenkins (1970) suggested a maximum lag of 25% of the data record, whereas Otens and Enochson (1978) mentioned that for a useful estimate of the covariance function the maximum lag seldom exceeds 10% of the data length. Another way of assessing the reliability of the covariance function is to compute the variances of the covariance function at different lags and then to assess the covariance function through the statistical testing. It is shown by Box and Jenkins (1970) and Pankratz (1983) that for moderate sample size the estimated autocovariances will be approximately normally distributed when the true autocovariances are essentially zero. Following Pankratz (1983), we test the null hypothesis $H_0: \rho(\tau) = 0$. The standard deviations can be obtained from (3.11) and (3.14). Since we use the estimated covariances in obtaining the variances we have to use the tau-distribution. In practice, using any of tau, student t or the standard normal distribution will not affect the result if the sample size is not small. In our analysis, the first 25% of the data records of the covariance function were considered useful estimates while statistical testing was applied for the remaining records.

3.2 Results for Empirical Covariance Functions

A total of 47 baselines were analyzed to develop the empirical covariance function. The baselines were located in various areas in North and South America. The data were separated into three sets. The first set had a 15 seconds sampling interval; the second, 20 seconds; and the third, 60 seconds. The results shown below are based on the analysis of baselines of lengths up to 100 km for L₁ data. The results for L₂ and L₃ (ionosphere free) are based on the analysis of baselines of lengths up to 60 km only. Appendix (III) shows a sample of the resulting estimated covariances.

3.2.1 Results for the Autocovariance Function

To obtain a general empirical autocovariance function, three different empirical functions have been tested. The first one is an exponential cosine model given by

$$f(\tau) = \exp(-|\tau| / T1) \cos (\tau T2) \quad (3.15)$$

where f is the empirical covariance function, τ is the time shift (lag) in seconds, $T1$ and $T2$ are unknown parameters to be determined, say, from a least squares fit. The second one is an exponential function given by

$$f(\tau) = \exp(-|\tau| / T) \quad (3.16)$$

where τ is the time shift (lag) in seconds and T is the unknown correlation time (the $1/e$ point). The last empirical function is a quadratic form given by

$$f(\tau) = \lambda_1 + \lambda_2 \tau + \lambda_3 \tau^2 \quad (3.17)$$

where λ_1 , λ_2 and λ_3 are the unknown parameters.

The least squares technique was used to test which one of these functions best fits the estimated autocovariances. The exponential cosine function always gives the worst least squares fit (the largest a posteriori variance factor) and is not further discussed here. The exponential function always gives the best fit for the L3 (ionosphere free) data. For L1 and L2 data, the exponential function gives the best fit for the majority of the baselines. Tables 3.1, 3.2 and 3.3 show the final results for the L1, L2 and L3 data. The baselines have been grouped into classes based on their lengths. The first column represents the baseline range. The second column represents the number of baselines used in each class. The resulting average variances are presented in the third column. The remainder of the columns represent the estimated parameters for both the exponential function and the

quadratic model. The final column shows which of the exponential function or the quadratic model fits the actual results better.

Table 3.1 Results of the L1 data

Baseline Range	# B/Ls used	Av. Variance	Exp. Model	Quadratic Model			Best Fit
				λ_1	λ_2	λ_3	
km		mm^2	T				
< 10	1	61	256	1.000	-1.8662E-03	0.7070E-06	EXP.
10 - 20	7	132	341	1.000	-2.1284E-03	1.2159E-06	EXP.
20 - 30	14	142	283	1.000	-2.3224E-03	1.3376E-06	EXP.
30 - 40	4	154	266	1.000	-2.2969E-03	1.2069E-06	QUAD.
40 - 50	3	181	368	1.000	-1.9639E-03	0.9949E-06	EXP.
50 - 60	3	316	247	1.000	-2.5995E-03	1.4852E-06	QUAD.
60 - 70	1	172	242	1.000	-3.2582E-03	2.0220E-06	QUAD.
70 - 80	1	3131	314	1.000	-2.5567E-03	1.3025E-06	QUAD.
80 - 90	2	21406	341	1.000	-2.1358E-03	0.9703E-06	QUAD.
90 - 100	1	3197	351	1.000	-2.0753E-03	0.8881E-06	QUAD.

Table 3.2 Results of the L2 data

Baseline Range	# B/Ls used	Av. Variance	Exp. Model	Quadratic Model			Best Fit
				λ_1	λ_2	λ_3	
km		mm^2	T				
10 - 20	7	151	302	1.000	-2.2703E-03	1.3066E-06	EXP.
20 - 30	14	200	273	1.000	-2.2799E-03	1.2575E-06	EXP.
30 - 40	4	294	272	1.000	-2.3891E-03	1.2723E-06	QUAD.
40 - 50	3	365	415	1.000	-1.8995E-03	0.9543E-06	EXP.
50 - 60	3	814	264	1.000	-2.4282E-03	1.3117E-06	QUAD.

Table 3.3 Results of the L3 data

Baseline Range	# B/Ls used	Av. Variance	Exp. Model	Quadratic Model			Best Fit
				λ_1	λ_2	λ_3	
km		mm ²	T				
10 - 20	7	342	210	1.000	-2.7170E-03	1.7538E-06	EXP.
20 - 30	14	362	166	1.000	-2.4339E-03	1.3299E-06	EXP.
30 - 40	4	312	190	1.000	-2.6329E-03	1.6265E-06	EXP.
40 - 50	3	424	77	1.000	-1.8693E-03	1.7190E-06	EXP.
50 - 60	3	341	140	1.000	-2.9108E-03	1.8137E-06	EXP.

Tables 3.1 through 3.3 show that the correlation time for the covariance functions for different baseline lengths indicates little variations. Therefore, a general autocovariance function which is valid for the range up to 100 km can be developed. Table 3.4 summarizes the results obtained for each of the L1, L2 and L3 data sets.

Table 3.4 Results for General Autocovariance Function

Baseline Range used	# B/Ls used	Zero crossing	Corr. time, T	Quadratic Model			Best Fit
				λ_1	λ_2	λ_3	
km		min.	sec.				
< 100/L1	37	20	263	1.000	-2.2391E-03	1.4020E-06	EXP.
10 - 60 /L2	31	17	270	1.000	-2.3269E-03	1.3220E-06	EXP.
10 - 60/ L3	31	19	169	1.000	-2.7513E-03	1.7220E-06	EXP.

It can be seen from Table 3.4 that the GPS double difference observations are positively correlated over a time period of about 20 minutes. Also, it is shown that the empirical exponential function given by (3.16) gives the best fit for the estimated autocovariance function. Figures 3.4 through 3.6 show the resulting exponential function for L1, L2 and L3 data. It should be pointed out that a better fit for L3 data may be obtained if a smaller number of points is used in the least squares fit.

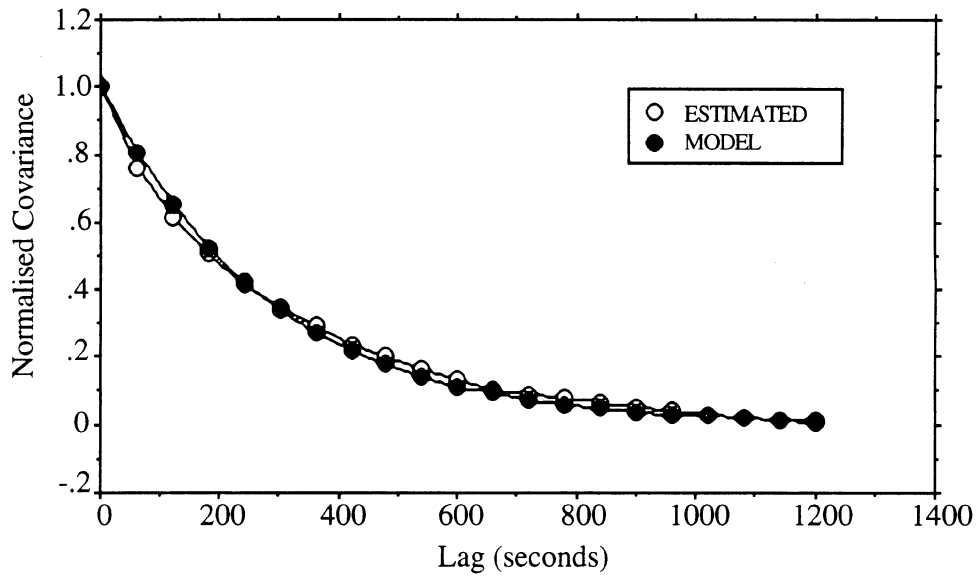


Figure 3.4. The Empirical Autocovariance Function for L1 Data and its Approximation

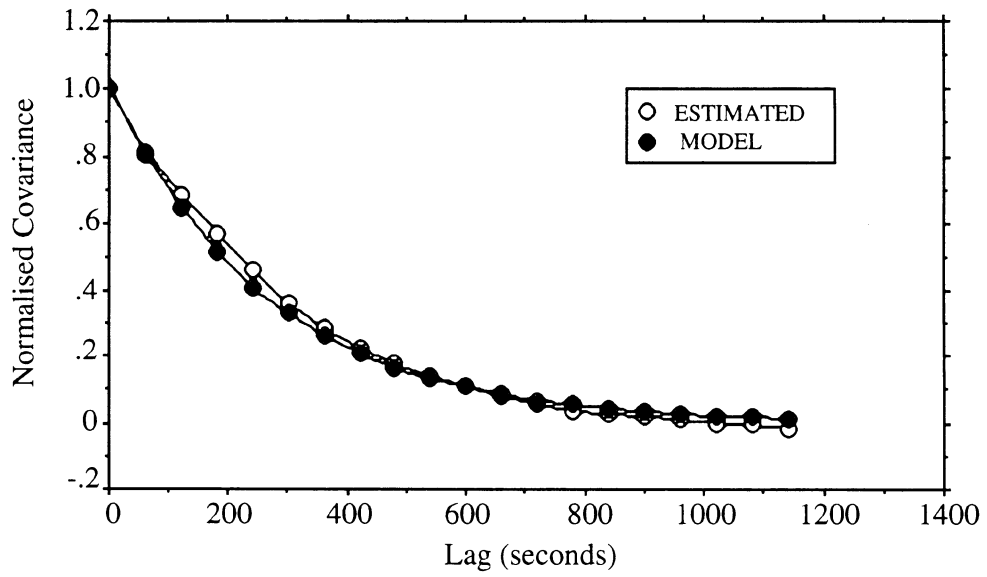


Figure 3.5. The Empirical Autocovariance Function for L2 Data and its Approximation

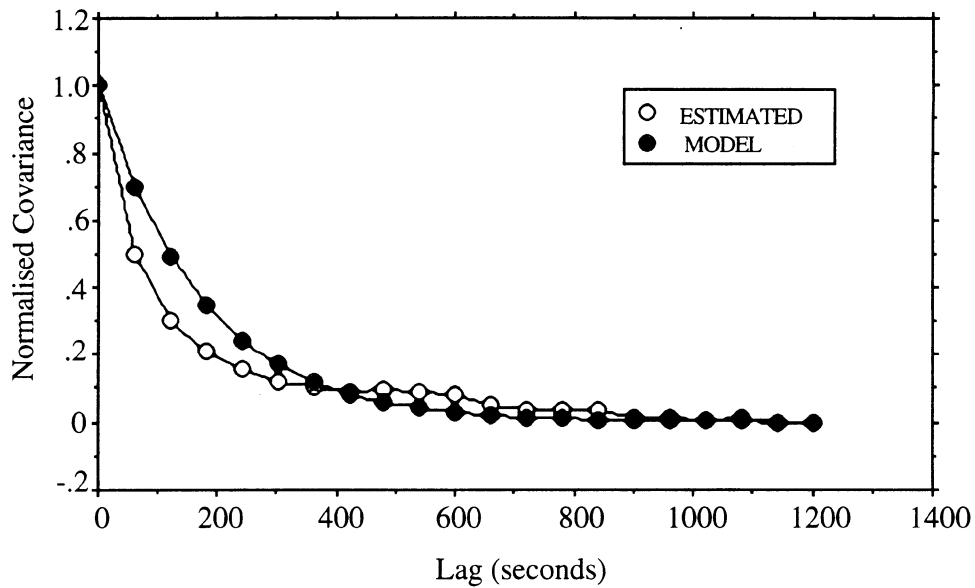


Figure 3.6. The Empirical Autocovariance Function for L3 Data and its Approximation

3.2.2 Results for the Crosscovariance Function

The adjustment residuals for every baseline contain several subsets of double difference residuals pertaining to different pairs of satellites. The crosscovariance functions among the double difference residual subsets for each baseline were evaluated. They were divided into two groups. The first group represents the crosscovariance functions in which the two subsets have a common satellite, i.e., have a common single difference. It should be mentioned that the way the DIPOP software forms the double differences results in a mathematical correlation of -0.5. The second group contained data without a common satellite. It was found that the crosscovariance functions for the first group generally starts with a value of about -0.5 resulting from the mathematical correlation. However, they do not drop to zero after the zero lag. A certain correlation length was found in each one of them. The crosscovariance functions of the second group were found to fluctuate around the zero value with negligible magnitudes.

It was expected that the long correlation length in the crosscovariance functions of the first group were coming from the “coloured” common single difference residuals, i.e., the autocovariance of the common single difference. To confirm this, a simulated data set with added coloured noise was analyzed. An exponentially correlated coloured noise was generated by passing a statistically independent sample of random noise through a simple filter. The resulting random variable x_{k+1} at time τ_{k+1} is given by

$$x_{k+1} = e^{-\beta (\tau_{k+1} - \tau_k)} x_k + w_k \quad (3.18)$$

where $1/\beta$ is the correlation time and w_k is the statistically independent random noise at time τ_k (Gelb, 1974).

Several independent coloured random noise data series were generated and added to the simulated phase measurements for individual satellites. It was found that, although the coloured noises were originally uncorrelated with each other, the crosscovariance function of any two double difference residual subsets which have a common satellite was found to have a certain correlation length. This indicates that it is actually the effect of the coloured noise in the common single difference. In other words, the autocovariance function is mapped into the crosscovariance function. Figures 3.7a and 3.7b show the crosscovariance function between two double difference residual subsets with a common satellite. Figure 3.7a shows the case of simulated data with statistically independent random noise and Figure 3.7b, the case of simulated data with coloured noise.

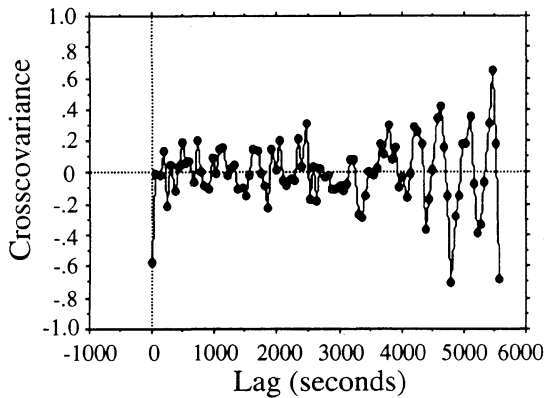


Figure 3.7a. Crosscovariance Function for Simulated Data with Statistically Independent Noise

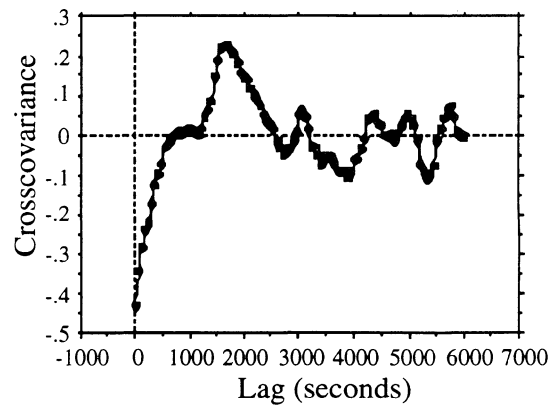


Figure 3.7b. Crosscovariance Function for Simulated Data with Coloured Noise ($b = 1/270$)

3.3 Forming the Covariance Matrix

Let us start with the simple case of tracking the same satellites over time. The carrier phase double difference observations for n epochs may be written as

$$\boldsymbol{\ell} = \begin{bmatrix} \Delta\nabla\Phi_1 \\ \Delta\nabla\Phi_2 \\ \vdots \\ \Delta\nabla\Phi_n \end{bmatrix} = \begin{bmatrix} \mathbf{a} \Phi_1 \\ \mathbf{a} \Phi_2 \\ \vdots \\ \mathbf{a} \Phi_n \end{bmatrix} \quad (3.19)$$

where $\Delta\nabla\Phi_i$ is the vector of carrier phase double differences at epoch i , \mathbf{a} is a differencing operator matrix and Φ_i is the vector of the observed phases at epoch i . Applying the law of covariance propagation to (3.19) yields the covariance matrix of the double difference observations as

$$\mathbf{C}_\ell = \begin{bmatrix} \mathbf{a} \mathbf{c}_{\Phi_1} \mathbf{a}^T & \mathbf{a} \mathbf{c}_{\Phi_1\Phi_2} \mathbf{a}^T & \cdots & \mathbf{a} \mathbf{c}_{\Phi_1\Phi_n} \mathbf{a}^T \\ \mathbf{a} \mathbf{c}_{\Phi_2\Phi_1} \mathbf{a}^T & \mathbf{a} \mathbf{c}_{\Phi_2} \mathbf{a}^T & \cdots & \mathbf{a} \mathbf{c}_{\Phi_2\Phi_n} \mathbf{a}^T \\ \vdots & \vdots & \vdots & \vdots \\ \mathbf{a} \mathbf{c}_{\Phi_n\Phi_1} \mathbf{a}^T & \mathbf{a} \mathbf{c}_{\Phi_n\Phi_2} \mathbf{a}^T & \cdots & \mathbf{a} \mathbf{c}_{\Phi_n} \mathbf{a}^T \end{bmatrix}. \quad (3.20)$$

If the off-diagonal submatrices are neglected, i.e., the measurement errors are assumed to be uncorrelated over time, a block diagonal covariance matrix representing the effect of the mathematical correlation is obtained. The term \mathbf{c}_{ϕ_i} is the covariance matrix of the undifferenced observations and is a diagonal matrix for uncorrelated phase measurements. The matrix $\mathbf{c}_{\phi_i\phi_j}$ represents the crosscovariances between the undifferenced observations of the i -th and the j -th epochs. If we assume stationarity and equi-spaced epochs, then $\mathbf{c}_{\phi_i} = \mathbf{c}_{\phi_{i+1}}$ and $\mathbf{c}_{\phi_i\phi_{i+1}} = \mathbf{c}_{\phi_j\phi_{j+1}}$. Therefore, the covariance matrix (3.20) can be simplified to

$$\mathbf{C}_\ell = \begin{bmatrix} C(\tau_0) & C(\tau_1) & C(\tau_2) & \cdots & C(\tau_n) \\ C(\tau_1) & C(\tau_0) & C(\tau_1) & \cdots & C(\tau_{n-1}) \\ C(\tau_2) & C(\tau_1) & C(\tau_0) & \cdots & C(\tau_{n-2}) \\ \vdots & \vdots & \vdots & \ddots & \vdots \\ C(\tau_n) & C(\tau_{n-1}) & C(\tau_{n-2}) & \cdots & C(\tau_0) \end{bmatrix} \quad (3.21)$$

where τ_i is the time shift (lag) between i epochs, $C(\tau_0)$ is covariance submatrix of the single epoch observations and $C(\tau_i)$ is the covariance submatrix between the observations of two epochs separated by i . If the empirical autocovariance and crosscovariance functions are available, then for each $C(\tau_i)$, the diagonal elements are obtained from the autocovariance function at the i -th lag while off-diagonal elements are obtained from the crosscovariance function at the i -th lag. To have a closer look at the nature of the covariance matrix (3.20), let us consider, without loss of generality, that \mathbf{c}_{ϕ_i} equals the identity matrix. Also we can consider, $\mathbf{c}_{\phi_i\phi_j} = f_{|j-i|} \mathbf{c}_{\phi_i}$ where $f_{|j-i|}$ is the correlation coefficient between the observations of the two epochs i and j . The covariance matrix of the observations for n epochs is then given by

$$\mathbf{C}_\ell = \begin{bmatrix} \mathbf{a} & \mathbf{0} & \cdots & \mathbf{0} \\ \mathbf{0} & \mathbf{a} & \cdots & \mathbf{0} \\ \vdots & \vdots & \ddots & \vdots \\ \mathbf{0} & \mathbf{0} & \cdots & \mathbf{a} \end{bmatrix} \begin{bmatrix} \mathbf{I} & f_1 \mathbf{I} & \cdots & f_{n-1} \mathbf{I} \\ f_1 \mathbf{I} & \mathbf{I} & \cdots & f_{n-2} \mathbf{I} \\ \vdots & \vdots & \ddots & \vdots \\ f_{n-1} \mathbf{I} & f_{n-2} \mathbf{I} & \cdots & \mathbf{I} \end{bmatrix} \begin{bmatrix} \mathbf{a} & \mathbf{0} & \cdots & \mathbf{0} \\ \mathbf{0} & \mathbf{a} & \cdots & \mathbf{0} \\ \vdots & \vdots & \ddots & \vdots \\ \mathbf{0} & \mathbf{0} & \cdots & \mathbf{a} \end{bmatrix}^T \quad (3.22)$$

or

$$\mathbf{C}_\ell = \begin{bmatrix} \mathbf{a} \mathbf{a}^T & f_1 \mathbf{a} \mathbf{a}^T & \cdots & f_{n-1} \mathbf{a} \mathbf{a}^T \\ f_1 \mathbf{a} \mathbf{a}^T & \mathbf{a} \mathbf{a}^T & \cdots & f_{n-2} \mathbf{a} \mathbf{a}^T \\ \vdots & \vdots & \ddots & \vdots \\ f_{n-1} \mathbf{a} \mathbf{a}^T & f_{n-2} \mathbf{a} \mathbf{a}^T & \cdots & \mathbf{a} \mathbf{a}^T \end{bmatrix}. \quad (3.23)$$

The matrix (3.23) shows that the crosscovariance submatrix $f_i \mathbf{a} \mathbf{a}^T$ is equal to the covariance submatrix $\mathbf{a} \mathbf{a}^T$ scaled by the correlation coefficient f_i , which is obtained from the empirical autocovariance function. This means that the fully populated covariance matrix can be obtained without having the empirical crosscovariance function. If different satellites are tracked over time, then (3.22) and (3.23) take the form

$$\mathbf{C}_\ell = \begin{bmatrix} \mathbf{a}_1 & \mathbf{0} & \cdots & \mathbf{0} \\ \mathbf{0} & \mathbf{a}_2 & \cdots & \mathbf{0} \\ \vdots & \vdots & \ddots & \vdots \\ \mathbf{0} & \mathbf{0} & \cdots & \mathbf{a}_n \end{bmatrix} \begin{bmatrix} \mathbf{I}_{11} & f_1 \mathbf{I}_{12} & \cdots & f_{n-1} \mathbf{I}_{1n} \\ f_1 \mathbf{I}_{21} & \mathbf{I}_{22} & \cdots & f_{n-2} \mathbf{I}_{2n} \\ \vdots & \vdots & \ddots & \vdots \\ f_{n-1} \mathbf{I}_{n1} & f_{n-2} \mathbf{I}_{n2} & \cdots & \mathbf{I}_{nn} \end{bmatrix} \times \\ \times \begin{bmatrix} \mathbf{a}_1 & \mathbf{0} & \cdots & \mathbf{0} \\ \mathbf{0} & \mathbf{a}_2 & \cdots & \mathbf{0} \\ \vdots & \vdots & \ddots & \vdots \\ \mathbf{0} & \mathbf{0} & \cdots & \mathbf{a}_n \end{bmatrix}^T \quad (3.24)$$

or

$$\mathbf{C}_\ell = \begin{bmatrix} \mathbf{a}_1 \mathbf{a}_1^T & f_1 \mathbf{a}_1 \mathbf{I}_{12} \mathbf{a}_2^T & \cdots & f_{n-1} \mathbf{a}_1 \mathbf{I}_{1n} \mathbf{a}_n^T \\ f_1 \mathbf{a}_2 \mathbf{I}_{21} \mathbf{a}_1^T & \mathbf{a}_2 \mathbf{a}_2^T & \cdots & f_{n-2} \mathbf{a}_2 \mathbf{I}_{2n} \mathbf{a}_n^T \\ \vdots & \vdots & \ddots & \vdots \\ f_{n-1} \mathbf{a}_n \mathbf{I}_{n1} \mathbf{a}_1^T & f_{n-2} \mathbf{a}_n \mathbf{I}_{n2} \mathbf{a}_2^T & \cdots & \mathbf{a}_n \mathbf{a}_n^T \end{bmatrix} \quad (3.25)$$

where the matrix \mathbf{I}_{jj} is the identity matrix with dimension equal to the number of double differences at epoch j and the matrix \mathbf{I}_{jk} , $j \neq k$, consists of an identity submatrix with a dimension equal to the number of common double differences at epochs j and k and zero elements elsewhere.

Chapter 4

ALGORITHM FOR THE INVERSE OF THE FULLY POPULATED COVARIANCE MATRIX

Stochastic modelling of the GPS residual errors yields a fully populated covariance matrix for the GPS carrier phase double difference observations. Implementing this fully populated covariance matrix into a software package usually slows down the numerical computations. However, this is not the case if an exponential function can be used to approximate the actual covariance function of the GPS residual errors. Using the exponential function results in a block diagonal weight matrix for the double difference observations. In this chapter, the algorithm for efficient computation of the inverse of this fully populated covariance matrix is developed. Also the storage requirements for the adjustment process are discussed.

4.1 The Covariance Matrix of Carrier Phase Double Differences

The carrier phase double difference for a particular epoch i may be written as

$$\Delta\nabla\Phi_i = \mathbf{a}_i \Phi_i \quad (4.1)$$

where $\Delta\nabla\Phi_i$ is the vector of carrier phase double differences at epoch i , \mathbf{a}_i is a differencing operator matrix and Φ_i is the vector of the observed phase values at epoch i . If different satellites are tracked over time, the operator matrix \mathbf{a}_i is different as well. In this case, the covariance matrix is given as (see section 3.3)

$$\mathbf{C}_\ell = \begin{bmatrix} \mathbf{a}_1 \mathbf{a}_1^T & f_1 \mathbf{a}_1 \mathbf{I}_{12} \mathbf{a}_2^T & \cdots & f_{n-1} \mathbf{a}_1 \mathbf{I}_{1n} \mathbf{a}_n^T \\ f_1 \mathbf{a}_2 \mathbf{I}_{21} \mathbf{a}_1^T & \mathbf{a}_2 \mathbf{a}_2^T & \cdots & f_{n-2} \mathbf{a}_2 \mathbf{I}_{2n} \mathbf{a}_n^T \\ \vdots & \vdots & \vdots & \vdots \\ f_{n-1} \mathbf{a}_n \mathbf{I}_{n1} \mathbf{a}_1^T & f_{n-2} \mathbf{a}_n \mathbf{I}_{n2} \mathbf{a}_2^T & \cdots & \mathbf{a}_n \mathbf{a}_n^T \end{bmatrix} \quad (4.2)$$

assuming that the original phase measurements are uncorrelated. The measurement variance is assumed to be constant and is omitted in equation (4.2) and in its sequel. The matrix \mathbf{I}_{jk} consists of an identity submatrix and zero elements as shown in chapter 3. The factor f_i is the correlation coefficient for a time lag of i epochs. In chapter 3, it was shown that the exponential covariance function

$$f_i = \exp(-i \tau_i / T) \quad (4.3)$$

is a good approximation of the actual covariance function of GPS carrier phase measurements. τ_i is the time lag of i epochs and T is the correlation time in seconds. Assuming a constant data rate, the correlation coefficient between any two epochs can be written as

$$f_i = f_1 f_{i-1} = f_1^2 f_{i-2} = \cdots = f_1^i . \quad (4.4)$$

With equation (4.4), the covariance matrix (4.2) can be written as

$$\mathbf{C}_\ell = \begin{bmatrix} \mathbf{a}_1 \mathbf{a}_1^T & f_1 \mathbf{a}_1 \mathbf{I}_{12} \mathbf{a}_2^T & \cdots & f_1^{n-1} \mathbf{a}_1 \mathbf{I}_{1n} \mathbf{a}_n^T \\ f_1 \mathbf{a}_2 \mathbf{I}_{21} \mathbf{a}_1^T & \mathbf{a}_2 \mathbf{a}_2^T & \cdots & f_1^{n-2} \mathbf{a}_2 \mathbf{I}_{2n} \mathbf{a}_n^T \\ \vdots & \vdots & \vdots & \vdots \\ f_1^{n-1} \mathbf{a}_n \mathbf{I}_{n1} \mathbf{a}_1^T & f_1^{n-2} \mathbf{a}_n \mathbf{I}_{n2} \mathbf{a}_2^T & \cdots & \mathbf{a}_n \mathbf{a}_n^T \end{bmatrix} \quad (4.5)$$

which may be written in a further simplified form as

$$\mathbf{C}_\ell = \begin{bmatrix} \mathbf{M}_{11} & f_1 \mathbf{M}_{12} & \cdots & f_1^{n-1} \mathbf{M}_{1n} \\ f_1 \mathbf{M}_{21} & \mathbf{M}_{22} & \cdots & f_1^{n-2} \mathbf{M}_{2n} \\ \vdots & \vdots & \vdots & \vdots \\ f_1^{n-1} \mathbf{M}_{n1} & f_1^{n-2} \mathbf{M}_{n2} & \cdots & \mathbf{M}_{nn} \end{bmatrix} \quad (4.6)$$

where $\mathbf{M}_{ij} = \mathbf{a}_i \mathbf{a}_j^T$ and $\mathbf{M}_{ij} = \mathbf{a}_i \mathbf{I}_{ij} \mathbf{a}_j^T$.

4.2 Inverting the Covariance Matrix

In this section, two different cases are treated. The first one is the ideal case where the same satellites are observed over the whole observation time span. The second case is a more realistic case which allows different satellites to be observed over the observation time span.

4.2.1 Ideal Case: The Same Satellites are Tracked Over Time

To find the inverse of the covariance matrix when tracking the same satellites during the observation time span, let us first introduce some matrix operations. If we have a regular and symmetric matrix \mathbf{C} given by

$$\mathbf{C} = \begin{bmatrix} C_{11} & C_{12} \\ C_{21} & C_{22} \end{bmatrix}, \quad (4.7)$$

and C_{11}^{-1} exists, then through partitioning, the inverse of \mathbf{C} can be written as (Mikhail, 1976)

$$\mathbf{C}^{-1} = \begin{bmatrix} P_{11} & P_{12} \\ P_{21} & P_{22} \end{bmatrix} \quad (4.8)$$

where

$$P_{22} = (C_{22} - C_{21} C_{11}^{-1} C_{12})^{-1}, \quad (4.9)$$

$$P_{12} = -C_{11}^{-1} C_{12} P_{22}, \quad (4.10)$$

$$P_{21} = -P_{22} C_{21} C_{11}^{-1} = P_{12}^T, \quad (4.11)$$

$$P_{11} = C_{11}^{-1} + C_{11}^{-1} C_{12} P_{22} C_{21} C_{11}^{-1}. \quad (4.12)$$

Using (4.9) through (4.12), the inverse of the observations' covariance matrix can be obtained epoch by epoch. In the first epoch, we have only one submatrix. Thus, its inverse can be easily obtained (see e.g. Hofmann-Wellenhof et al., 1992). In the second epoch, the covariance matrix takes the form

$$C_{\ell} = \begin{bmatrix} \mathbf{M} & f_1 \mathbf{M} \\ f_1 \mathbf{M} & \mathbf{M} \end{bmatrix}, \quad (4.13)$$

where the symmetric submatrix \mathbf{M} represents the mathematical correlation for one epoch.

The inverse of the matrix (4.13) can be computed using (4.6) through (4.9) as

$$C_{\ell}^{-1} = \begin{bmatrix} P & -f_1 P \\ -f_1 P & P \end{bmatrix}, \quad (4.14)$$

$$\text{where } P = \frac{1}{1 - f_1^2} \mathbf{M}^{-1}. \quad (4.15)$$

This means that only the submatrix P is stored. If the observations' covariance matrix is extended to include the n -th epoch, it takes the form

$$\mathbf{C}_\ell = \begin{bmatrix} \mathbf{M} & f_1 \mathbf{M} & \cdots & f_1^{n-1} \mathbf{M} \\ f_1 \mathbf{M} & \mathbf{M} & \cdots & f_1^{n-2} \mathbf{M} \\ \vdots & \vdots & \vdots & \vdots \\ f_1^{n-1} \mathbf{M} & f_1^{n-2} \mathbf{M} & \cdots & \mathbf{M} \end{bmatrix}. \quad (4.16)$$

Again using (4.9) through (4.12), we end up with

$$\mathbf{C}_\ell^{-1} = \begin{bmatrix} \mathbf{P} & -f_1 \mathbf{P} & \mathbf{0} & \cdots & \mathbf{0} & \mathbf{0} \\ -f_1 \mathbf{P} & (1+f_1^2) \mathbf{P} & -f_1 \mathbf{P} & \cdots & \mathbf{0} & \mathbf{0} \\ \mathbf{0} & -f_1 \mathbf{P} & (1+f_1^2) \mathbf{P} & \cdots & \mathbf{0} & \mathbf{0} \\ \cdots & \cdots & \cdots & \cdots & \cdots & \cdots \\ \mathbf{0} & \mathbf{0} & \mathbf{0} & \cdots & (1+f_1^2) \mathbf{P} & -f_1 \mathbf{P} \\ \mathbf{0} & \mathbf{0} & \mathbf{0} & \cdots & -f_1 \mathbf{P} & \mathbf{P} \end{bmatrix}, \quad (4.17)$$

which reveals that the weight matrix is in fact a band structure matrix with only one off-diagonal submatrix. This simplification saves a lot of computational time and reduces memory requirements.

4.2.2 Real Case: Different Satellites are Tracked Over Time

Let us now consider the more general case where the same satellites have been observed over the first n epochs and different satellites have been observed at epoch $n+1$. Up to the n -th epoch, the inverse of the covariance matrix will be as described by (4.17). At epoch $n+1$, the covariance matrix will take the form

$$\mathbf{C}_\ell = \begin{bmatrix} \mathbf{M} & f_1 \mathbf{M} & \cdots & f_1^{n-1} \mathbf{M} & f_1^n \mathbf{M}_{n+1,1}^T \\ f_1 \mathbf{M} & \mathbf{M} & \cdots & f_1^{n-2} \mathbf{M} & f_1^{n-1} \mathbf{M}_{n+1,2}^T \\ \vdots & \vdots & \vdots & \vdots & \vdots \\ f_1^{n-1} \mathbf{M} & f_1^{n-2} \mathbf{M} & \cdots & \mathbf{M} & f_1 \mathbf{M}_{n+1,n}^T \\ f_1^n \mathbf{M}_{n+1,1} & f_1^{n-1} \mathbf{M}_{n+1,2} & \cdots & f_1 \mathbf{M}_{n+1,n} & \mathbf{M}_{n+1,n+1} \end{bmatrix}. \quad (4.19)$$

It should be noted that

$$\mathbf{M}_{n+1, i} = \mathbf{M}_{n+1, j}, \quad i, j = 1, \dots, n. \quad (4.20)$$

Using (4.9) through (4.12), the inverse of the covariance matrix (4.19) can be obtained as

$$\mathbf{C}_\ell^{-1} = \begin{bmatrix} \mathbf{P} & -f_1 \mathbf{P} & \dots & \mathbf{0} & \mathbf{0} & \mathbf{0} \\ -f_1 \mathbf{P} & (1 + f_1^2) \mathbf{P} & \dots & \mathbf{0} & \mathbf{0} & \mathbf{0} \\ \vdots & \vdots & \vdots & \vdots & \vdots & \vdots \\ \mathbf{0} & \mathbf{0} & \dots & (1 + f_1^2) \mathbf{P} & -f_1 \mathbf{P} & \mathbf{0} \\ \mathbf{0} & \mathbf{0} & \dots & -f_1 \mathbf{P} & \mathbf{Q}_{11} & \mathbf{Q}_{21}^T \\ \mathbf{0} & \mathbf{0} & \dots & \mathbf{0} & \mathbf{Q}_{21} & \mathbf{Q}_{22} \end{bmatrix}, \quad (4.21)$$

where

$$\mathbf{Q}_{11} = \mathbf{P} - f_1 \mathbf{M}^{-1} \mathbf{M}_{n+1, n}^T \mathbf{Q}_{21} \quad (4.22)$$

$$\mathbf{Q}_{21} = f_1 \mathbf{Q}_{22} \mathbf{M}_{n+1, n} \mathbf{M}^{-1} \quad (4.23)$$

$$\mathbf{Q}_{22} = \{\mathbf{M}_{n+1, n+1} - f_1^2 \mathbf{M}_{n+1, n} \mathbf{M}^{-1} \mathbf{M}_{n+1, n}^T\}^{-1}. \quad (4.24)$$

Even though different satellites were tracked at epoch $n+1$, the simple band structure with only one off-diagonal submatrix remains unchanged. However, as shown below, this is not true if tracked satellites were different for more than two consecutive epochs.

If the first group of satellites was re-tracked again at epochs $n+2$ and $n+3$, then the covariance matrix at epoch $n+2$ will take the form

$$\mathbf{C}_\ell = \begin{bmatrix} \mathbf{M} & f_1 \mathbf{M} & \cdots & f_1^{n-1} \mathbf{M} & f_1^n \mathbf{M}_{n+1,1}^T & f_1^{n+1} \mathbf{M} \\ f_1 \mathbf{M} & \mathbf{M} & \cdots & f_1^{n-2} \mathbf{M} & f_1^{n-1} \mathbf{M}_{n+1,2}^T & f_1^n \mathbf{M} \\ \vdots & \vdots & \vdots & \vdots & \vdots & \vdots \\ f_1^{n-1} \mathbf{M} & f_1^{n-2} \mathbf{M} & \cdots & \mathbf{M} & f_1 \mathbf{M}_{n+1,n}^T & f_1^2 \mathbf{M} \\ f_1^n \mathbf{M}_{n+1,1} & f_1^{n-1} \mathbf{M}_{n+1,2} & \cdots & f_1 \mathbf{M}_{n+1,n} & \mathbf{M}_{n+1,n+1} & f_1 \mathbf{M}_{n+1,n} \\ f_1^{n+1} \mathbf{M} & f_1^n \mathbf{M} & \cdots & f_1^2 \mathbf{M} & f_1 \mathbf{M}_{n+1,n}^T & \mathbf{M} \end{bmatrix} \quad (4.25)$$

Again using (4.9) through (4.12), the new weight matrix can be written as

$$\mathbf{C}_\ell^{-1} = \begin{bmatrix} \mathbf{P} & -f_1 \mathbf{P} & \cdots & \mathbf{0} & \mathbf{0} & \mathbf{0} & \mathbf{0} \\ -f_1 \mathbf{P} & (1 + f_1^2) \mathbf{P} & \cdots & \mathbf{0} & \mathbf{0} & \mathbf{0} & \mathbf{0} \\ \vdots & \vdots & \vdots & \vdots & \vdots & \vdots & \vdots \\ \mathbf{0} & \mathbf{0} & \cdots & (1 + f_1^2) \mathbf{P} & -f_1 \mathbf{P} & \mathbf{0} & \mathbf{0} \\ \mathbf{0} & \mathbf{0} & \cdots & -f_1 \mathbf{P} & \mathbf{R}_{11} & \mathbf{R}_{21}^T & \mathbf{R}_{31}^T \\ \mathbf{0} & \mathbf{0} & \cdots & \mathbf{0} & \mathbf{R}_{21} & \mathbf{R}_{22} & \mathbf{R}_{32}^T \\ \mathbf{0} & \mathbf{0} & \cdots & \mathbf{0} & \mathbf{R}_{31} & \mathbf{R}_{32} & \mathbf{R}_{33} \end{bmatrix}, \quad (4.26)$$

where

$$\mathbf{R}_{11} = \mathbf{Q}_{11} + \mathbf{E}_1^T \mathbf{R}_{33} \mathbf{E}_1 \quad (4.27)$$

$$\mathbf{R}_{21} = \mathbf{Q}_{21} + \mathbf{E}_2^T \mathbf{R}_{33} \mathbf{E}_1 \quad (4.28)$$

$$\mathbf{R}_{22} = \mathbf{Q}_{22} + \mathbf{E}_2^T \mathbf{R}_{33} \mathbf{E}_2 \quad (4.29)$$

$$\mathbf{R}_{31} = -\mathbf{R}_{33} \mathbf{E}_1 \quad (4.30)$$

$$\mathbf{R}_{32} = -\mathbf{R}_{33} \mathbf{E}_2 \quad (4.31)$$

$$\mathbf{R}_{33} = \{\mathbf{M} - f_1^2 \mathbf{E}_1 \mathbf{M} - f_1 \mathbf{E}_2 \mathbf{M}_{n+1,n}\}^{-1} \quad (4.32)$$

$$\mathbf{E}_1 = f_1^2 (1 - f_1^2) (\mathbf{M} \mathbf{P} - \mathbf{M}_{n+1,n}^T \mathbf{Q}_2 \mathbf{M}_{n+1,n} \mathbf{M}^{-1}) \quad (4.33)$$

$$E_2 = f_1 (1 - f_1^2) \mathbf{M}_{n+1,n}^T \mathbf{Q}_2. \quad (4.34)$$

Equation (4.26) shows that a second off-diagonal line with non zero submatrices appears in this case. This is caused by having different groups of satellites tracked during three subsequent measurements epochs. However, except for the lower 3 by 3 submatrices which correspond to the three different groups of satellites, the inverse of the covariance matrix remains unchanged and is in fact identical with the ideal case (4.17). At epoch $n+3$, the covariance matrix will take the form

$$\mathbf{C}_\ell = \begin{bmatrix} \mathbf{M} & f_1 \mathbf{M} & \cdots & f_1^{n-1} \mathbf{M} & f_1^n \mathbf{M}_{n+1,1}^T & f_1^{n+1} \mathbf{M} & f_1^{n+2} \mathbf{M} \\ f_1 \mathbf{M} & \mathbf{M} & \cdots & f_1^{n-2} \mathbf{M} & f_1^{n-1} \mathbf{M}_{n+1,2}^T & f_1^n \mathbf{M} & f_1^{n+1} \mathbf{M} \\ \vdots & \vdots & \vdots & \vdots & \vdots & \vdots & \vdots \\ f_1^{n-1} \mathbf{M} & f_1^{n-2} \mathbf{M} & \cdots & \mathbf{M} & f_1 \mathbf{M}_{n+1,n}^T & f_1^2 \mathbf{M} & f_1^3 \mathbf{M} \\ f_1^n \mathbf{M}_{n+1,1} & f_1^{n-1} \mathbf{M}_{n+1,2} & \cdots & f_1 \mathbf{M}_{n+1,n} & \mathbf{M}_{n+1,n+1} & f_1 \mathbf{M}_{n+1,n} & f_1^2 \mathbf{M}_{n+1,n} \\ f_1^{n+1} \mathbf{M} & f_1^n \mathbf{M} & \cdots & f_1^2 \mathbf{M} & f_1 \mathbf{M}_{n+1,n}^T & \mathbf{M} & f_1 \mathbf{M} \\ f_1^{n+2} \mathbf{M} & f_1^{n+1} \mathbf{M} & \cdots & f_1^3 \mathbf{M} & f_1^2 \mathbf{M}_{n+1,n}^T & f_1 \mathbf{M} & \mathbf{M} \end{bmatrix}. \quad (4.35)$$

The new weight matrix will be given by (see Appendix IV for detailed derivation)

$$\mathbf{C}_\ell^{-1} = \begin{bmatrix} P & -f_1 P & \cdots & \mathbf{0} & \mathbf{0} & \mathbf{0} & \mathbf{0} & \mathbf{0} \\ -f_1 P & (1 + f_1^2) P & \cdots & \mathbf{0} & \mathbf{0} & \mathbf{0} & \mathbf{0} & \mathbf{0} \\ \vdots & \vdots \\ \mathbf{0} & \mathbf{0} & \cdots & (1 + f_1^2) P & -f_1 P & \mathbf{0} & \mathbf{0} & \mathbf{0} \\ \mathbf{0} & \mathbf{0} & \cdots & -f_1 P & R_{11} & R_{21}^T & R_{31}^T & \mathbf{0} \\ \mathbf{0} & \mathbf{0} & \cdots & \mathbf{0} & R_{21} & R_{22} & R_{32}^T & \mathbf{0} \\ \mathbf{0} & \mathbf{0} & \cdots & \mathbf{0} & R_{31} & R_{32} & RR_{33} & -f_1 P \\ \mathbf{0} & \mathbf{0} & \cdots & \mathbf{0} & \mathbf{0} & \mathbf{0} & -f_1 P & P \end{bmatrix}, \quad (4.36)$$

where

$$\mathbf{RR}_{33} = \mathbf{R}_{33} + f_1 \mathbf{P}. \quad (4.37)$$

It is interesting to note that the last row and column in (4.36) are identical to the corresponding ones in the ideal case because the satellites at the last two epochs were identical. It is also important to know that, as a general rule, if the same satellites are tracked at two consecutive epochs, then the last row and column in the weight matrix are identical to the corresponding ones in the ideal case with the same number of satellites regardless of whether the previously observed satellites were the same. Whatever groups of satellites are to be tracked in the following epochs, the first $n+3$ by $n+3$ submatrices will always be identical to (4.36) except for the lower right corner submatrix. Another important feature is that if in the following epochs the tracked satellites are identical to the ones at epoch $n+3$, the inverse of the covariance matrix will be identical to the ideal case (4.17) except for the part(s) where the tracked satellites in consecutive epochs were different. It is concluded that if different satellites are observed every other epoch, the inverse of the covariance matrix will take the band structure with only one off-diagonal submatrix but it will not be identical to the ideal case.

4.3 Storage Requirements

The analysis shown above reveals some important facts in terms of the required storage space. When multiplying the matrix \mathbf{C}_{21} and the inverse of the matrix \mathbf{C}_{11} (section 4.2.1), the result contains some zero submatrices even if different groups of satellites were observed. These zero submatrices will yield zero submatrices in the weight matrix as well (see e.g. (IV.12)). Also, since we know that some zero submatrices will be produced, certain matrix multiplications can be avoided. As shown in (IV.2) multiplying the last row submatrix in the covariance matrix with the first $n-1$ columns of the previous epoch weight matrix can be avoided. This is because, as shown in (IV.3), the results will

be $n-1$ zero submatrices. These zero submatrices in the weight matrix allow a reduction in the required storage space for the covariance matrix. Since the weight matrix is updated every epoch, only the last row of the covariance matrix at every epoch is required. Because of the zero submatrices in the weight matrix, only a few submatrices in the last row of the covariance matrix are actually required. If, for example, the current epoch is the n -th epoch and the tracked satellites at epochs $m-1$ and m ($m < n$) were identical but they were different after that, then only the last $n-m+1$ submatrices in the last row of the covariance matrix are required. The first $m-2$ submatrices are not required because they are to be multiplied by zero submatrices. In reality, $m-n$ is a small number. Usually, it is less than three.

If in the current epoch and the previous one the same satellites are tracked, the lengthy computations for the inverse of the covariance matrix are not necessary. In this case, not a single submatrix in the covariance matrix is required. The changes in the updated weight matrix will be similar to the results obtained in (4.36) which can be done automatically.

Chapter 5

MODIFIED LEAST SQUARES ADJUSTMENT FOR THE DETERMINATION OF POSITIONS AND AMBIGUITIES

In this chapter, a modified least squares adjustment algorithm incorporating the new developed fully populated covariance matrix for the determination of the position parameters and the ambiguities is developed. However, the estimated ambiguities are generally not integers. To obtain the most likely integer ambiguity parameters, the resulting covariance matrix of the ambiguity parameters is used to form a confidence region of a hyperellipsoid centered at the estimated real ambiguity parameters. The hyperellipsoid is used for searching the most likely integer ambiguity parameters. The searching time is optimized by using Cholesky roots of the covariance matrix of the ambiguity parameters. Once the integer ambiguity parameters are determined, they are used as functional constraints in another least squares adjustment to obtain the final station coordinates and their covariance matrix. Finally, the storage requirements for the different parameters are discussed at the end of this chapter.

5.1 Modified Sequential Least Squares Adjustment

In this section a modified least squares parametric adjustment for positions and ambiguities, including stochastic modelling of the remaining unmodelled errors, is developed. The linearized mathematical model describing the observations is given by Wells (1990) and Vanicek and Krakiwsky (1986) as

$$\mathbf{A} \hat{\mathbf{d}} = \hat{\mathbf{r}} + \mathbf{W}, \quad \mathbf{C}_\ell \quad (5.1)$$

where \mathbf{A} is the design matrix which depends on the satellite geometry, $\hat{\mathbf{d}}$ is the vector of corrections to the approximate values of the unknown parameters, $\hat{\mathbf{r}}$ is the vector of residuals and \mathbf{W} is the misclosure vector. To obtain a sequential solution, the linearized mathematical model (5.1) has to be partitioned into two sets as

$$\mathbf{A}_{i-1} \hat{\mathbf{d}} = \hat{\mathbf{r}}_{i-1} + \mathbf{W}_{i-1}, \quad (5.2)$$

$$\mathbf{A}_i \hat{\mathbf{d}} = \hat{\mathbf{r}}_i + \mathbf{W}_i \quad (5.3)$$

where the first set represents all previous observations (i.e. up to and including the previous epoch) while the second set represents a new set of observations (i.e. for the current epoch only). The observation covariance matrix and its inverse can be partitioned in a similar manner as

$$\mathbf{C}_\ell = \begin{bmatrix} \mathbf{C}_{i-1, i-1} & \mathbf{C}_{i-1, i} \\ \mathbf{C}_{i, i-1} & \mathbf{C}_{i, i} \end{bmatrix}, \quad (5.4)$$

$$\mathbf{C}_\ell^{-1} = \begin{bmatrix} \mathbf{P}_{i-1, i-1} & \mathbf{P}_{i-1, i} \\ \mathbf{P}_{i, i-1} & \mathbf{P}_{i, i} \end{bmatrix}. \quad (5.5)$$

The least squares adjustment can be based on minimizing the so-called variation function Φ (Wells and Krakiwsky, 1971; Vanicek and Krakiwsky, 1986) which is given by

$$\Phi = \hat{\mathbf{r}}^T \mathbf{C}_\ell^{-1} \hat{\mathbf{r}} + \hat{\mathbf{d}}^T \mathbf{P}_{x^0} \hat{\mathbf{d}} + 2 \hat{\mathbf{K}}_1^T (\mathbf{A}_{i-1} \hat{\mathbf{d}} - \hat{\mathbf{r}}_{i-1} - \mathbf{W}_{i-1}) + 2 \hat{\mathbf{K}}_2^T (\mathbf{A}_i \hat{\mathbf{d}} - \hat{\mathbf{r}}_i - \mathbf{W}_i) \quad (5.6)$$

where $\hat{\mathbf{r}} = [\hat{\mathbf{r}}_{i-1}^T, \hat{\mathbf{r}}_i^T]^T$, $\hat{\mathbf{K}}_1$ and $\hat{\mathbf{K}}_2$ are Lagrange correlates, \mathbf{x}^0 is the vector of the approximate values of the unknown parameters and \mathbf{P}_{x^0} is the a priori weight matrix for the approximate values of the unknown parameters. Minimizing the function Φ means that its partial derivatives with respect to $\hat{\mathbf{r}}$, $\hat{\mathbf{d}}$, $\hat{\mathbf{K}}_1$, and $\hat{\mathbf{K}}_2$ are set to zero. Combining the results of these partial derivatives with equation (5.1) leads to the normal equations

$$\begin{bmatrix} \mathbf{P}_{i-1, i-1} & \mathbf{P}_{i-1, i} & \mathbf{I} & \mathbf{0} & \mathbf{0} \\ \mathbf{P}_{i, i-1} & \mathbf{P}_{i, i} & \mathbf{0} & \mathbf{I} & \mathbf{0} \\ \mathbf{I} & \mathbf{0} & \mathbf{0} & \mathbf{0} & \mathbf{A}_{i-1} \\ \mathbf{0} & \mathbf{I} & \mathbf{0} & \mathbf{0} & \mathbf{A}_i \\ \mathbf{0} & \mathbf{0} & \mathbf{A}_{i-1}^T & \mathbf{A}_i^T & \mathbf{P}_{x^0} \end{bmatrix} \begin{bmatrix} \widehat{\mathbf{r}}_{i-1} \\ \widehat{\mathbf{r}}_i \\ \widehat{\mathbf{K}}_1 \\ \widehat{\mathbf{K}}_2 \\ \widehat{\mathbf{d}} \end{bmatrix} - \begin{bmatrix} \mathbf{0} \\ \mathbf{0} \\ \mathbf{W}_{i-1} \\ \mathbf{W}_i \\ \mathbf{0} \end{bmatrix} = \mathbf{0}. \quad (5.7)$$

Eliminating \mathbf{r}_{i-1} and \mathbf{r}_i from (5.7) through matrix partitioning, we obtain

$$\begin{bmatrix} -\mathbf{C}_{i-1, i-1} & -\mathbf{C}_{i-1, i} & \mathbf{A}_{i-1} \\ -\mathbf{C}_{i, i-1} & -\mathbf{C}_{i, i} & \mathbf{A}_i \\ \mathbf{A}_{i-1}^T & \mathbf{A}_i^T & \mathbf{P}_{x^0} \end{bmatrix} \begin{bmatrix} \widehat{\mathbf{K}}_1 \\ \widehat{\mathbf{K}}_2 \\ \widehat{\mathbf{d}} \end{bmatrix} - \begin{bmatrix} \mathbf{W}_{i-1} \\ \mathbf{W}_i \\ \mathbf{0} \end{bmatrix} = \mathbf{0}. \quad (5.8)$$

Eliminating \mathbf{K}_1 from (5.8) through matrix partitioning, we obtain

$$\begin{bmatrix} (-\mathbf{C}_{i, i} + \mathbf{C}_{i, i-1} \mathbf{C}_{i-1, i-1}^{-1} \mathbf{C}_{i-1, i}) & (\mathbf{A}_i - \mathbf{C}_{i, i-1} \mathbf{C}_{i-1, i-1}^{-1} \mathbf{A}_{i-1}) \\ (\mathbf{A}_i^T - \mathbf{A}_{i-1}^T \mathbf{C}_{i-1, i-1}^{-1} \mathbf{C}_{i-1, i}) & (\mathbf{P}_{x^0} + \mathbf{A}_{i-1}^T \mathbf{C}_{i-1, i-1}^{-1} \mathbf{A}_{i-1}) \end{bmatrix} \begin{bmatrix} \widehat{\mathbf{K}}_2 \\ \widehat{\mathbf{d}} \end{bmatrix} - \begin{bmatrix} (\mathbf{W}_i - \mathbf{C}_{i, i-1} \mathbf{C}_{i-1, i-1}^{-1} \mathbf{W}_{i-1}) \\ \mathbf{A}_{i-1}^T \mathbf{C}_{i-1, i-1}^{-1} \mathbf{W}_{i-1} \end{bmatrix} = \mathbf{0}. \quad (5.9)$$

Rewriting (5.9) in an equivalent compacted form we obtain

$$\begin{bmatrix} -\mathbf{P}_{i, i}^{-1} & \mathbf{A}_i^* \\ \mathbf{A}_i^{*T} & \mathbf{N}_{i-1} \end{bmatrix} \begin{bmatrix} \widehat{\mathbf{K}}_2 \\ \widehat{\mathbf{d}} \end{bmatrix} - \begin{bmatrix} \mathbf{W}_i^* \\ \mathbf{A}_{i-1}^T \mathbf{C}_{i-1, i-1}^{-1} \mathbf{W}_{i-1} \end{bmatrix} = \mathbf{0} \quad (5.10)$$

where

$$\mathbf{A}_i^* = \mathbf{A}_i - \mathbf{C}_{i, i-1} \mathbf{C}_{i-1, i-1}^{-1} \mathbf{A}_{i-1} \quad (5.11)$$

$$\mathbf{W}_i^* = \mathbf{W}_i - \mathbf{C}_{i, i-1} \mathbf{C}_{i-1, i-1}^{-1} \mathbf{W}_{i-1} \quad (5.12)$$

$$\mathbf{N}_{i-1} = \mathbf{P}_{x_0} + \mathbf{A}_{i-1}^T \mathbf{C}_{i-1,i-1}^{-1} \mathbf{A}_{i-1}. \quad (5.13)$$

To obtain a sequential solution for $\hat{\mathbf{d}}$, $\hat{\mathbf{K}}_2$ has to be obtained first by eliminating $\hat{\mathbf{d}}$ from (5.10). That is,

$$\hat{\mathbf{K}}_2 = - [\mathbf{P}_{i,i}^{-1} + \mathbf{A}_i^* \mathbf{N}_{i-1}^{-1} \mathbf{A}_i^{*T}]^{-1} [\mathbf{W}_i^* - \mathbf{A}_i^* \mathbf{N}_{i-1}^{-1} \mathbf{A}_{i-1}^T \mathbf{C}_{i-1,i-1}^{-1} \mathbf{W}_{i-1}]. \quad (5.14)$$

Back-substituting (5.14) in (5.10) to obtain a sequential solution for $\hat{\mathbf{d}}$ results in

$$\hat{\mathbf{d}} = \mathbf{N}_{i-1}^{-1} (\mathbf{A}_{i-1}^T \mathbf{C}_{i-1,i-1}^{-1} \mathbf{W}_{i-1} - \mathbf{A}_i^{*T} \hat{\mathbf{K}}_2). \quad (5.15)$$

Using (5.14) and (5.15), the sequential solution for $\hat{\mathbf{d}}$, in its general form, can be written as

$$\hat{\mathbf{d}}_i = \hat{\mathbf{d}}_{i-1} + \mathbf{N}_{i-1}^{-1} \mathbf{A}_i^{*T} [\mathbf{P}_{i,i}^{-1} + \mathbf{A}_i^* \mathbf{N}_{i-1}^{-1} \mathbf{A}_i^{*T}]^{-1} [\mathbf{W}_i^* - \mathbf{A}_i^* \hat{\mathbf{d}}_{i-1}] \quad (5.16)$$

where $\hat{\mathbf{d}}_{i-1}$ is the previous solution for the adjusted parameters and \mathbf{N}_{i-1}^{-1} is the inverse of the previous normal equation matrix which is developed in a sequential form in the following section. It should be noted that the usual batch least squares adjustment should be used before the first use of (5.16). The batch solution for the adjusted parameters and the inverse of the normal equation matrix are given by

$$\hat{\mathbf{d}} = (\mathbf{P}_{x_0} + \mathbf{A}^T \mathbf{C}_{\ell}^{-1} \mathbf{A})^{-1} \mathbf{A}^T \mathbf{C}_{\ell}^{-1} \mathbf{W}, \quad (5.17)$$

$$\mathbf{N}^{-1} = (\mathbf{P}_{x_0} + \mathbf{A}^T \mathbf{C}_{\ell}^{-1} \mathbf{A})^{-1}. \quad (5.18)$$

5.2 Updating the Inverse of the Normal Equation Matrix

As shown in (5.16), it is necessary to update the inverse of the normal equation matrix with every update for $\hat{\mathbf{d}}$. For the two sets of observations (5.2) and (5.3), the normal equation matrix \mathbf{N}_i can be written as

$$\mathbf{N}_i = \mathbf{P}_{x^0} + \begin{bmatrix} \mathbf{A}_{i-1}^T & \mathbf{A}_i^T \end{bmatrix} \begin{bmatrix} \mathbf{P}_{i-1, i-1} & \mathbf{P}_{i-1, i} \\ \mathbf{P}_{i, i-1} & \mathbf{P}_{i, i} \end{bmatrix} \begin{bmatrix} \mathbf{A}_{i-1} \\ \mathbf{A}_i \end{bmatrix} \quad (5.19)$$

or after multiplication

$$\mathbf{N}_i = \mathbf{P}_{x^0} + \mathbf{A}_{i-1}^T \mathbf{P}_{i-1, i-1} \mathbf{A}_{i-1} + \mathbf{A}_i^T \mathbf{P}_{i, i-1} \mathbf{A}_{i-1} + \mathbf{A}_{i-1}^T \mathbf{P}_{i-1, i} \mathbf{A}_i + \mathbf{A}_i^T \mathbf{P}_{i, i} \mathbf{A}_i. \quad (5.20)$$

Substituting the values of \mathbf{P}_{11} , \mathbf{P}_{21} and \mathbf{P}_{12} (see section 4.2.1), we obtain

$$\begin{aligned} \mathbf{N}_i = \mathbf{P}_{x^0} + \mathbf{A}_{i-1}^T (\mathbf{C}_{i-1, i-1}^{-1} + \mathbf{C}_{i-1, i-1}^{-1} \mathbf{C}_{i-1, i} \mathbf{P}_{i, i} \mathbf{C}_{i, i-1} \mathbf{C}_{i-1, i-1}^{-1}) \mathbf{A}_{i-1} \\ - \mathbf{A}_i^T \mathbf{P}_{i, i} \mathbf{C}_{i, i-1} \mathbf{C}_{i-1, i-1}^{-1} \mathbf{A}_{i-1} - \mathbf{A}_{i-1}^T \mathbf{C}_{i-1, i-1}^{-1} \mathbf{C}_{i-1, i} \mathbf{P}_{i, i} \mathbf{A}_i + \mathbf{A}_i^T \mathbf{P}_{i, i} \mathbf{A}_i. \end{aligned} \quad (5.21)$$

Rearranging (5.21) and using (5.11) and (5.13) we end up with

$$\mathbf{N}_i = \mathbf{N}_{i-1} + \mathbf{A}_i^{*T} \mathbf{P}_{i, i} \mathbf{A}_i^* \quad (5.22)$$

or

$$\mathbf{N}_i^{-1} = (\mathbf{N}_{i-1} + \mathbf{A}_i^{*T} \mathbf{P}_{i, i} \mathbf{A}_i^*)^{-1}. \quad (5.23)$$

Using the matrix identity (Mikhail, 1976)

$$(\mathbf{Y} \pm \mathbf{U} \mathbf{Z} \mathbf{V})^{-1} = \mathbf{Y}^{-1} \mp \mathbf{Y}^{-1} \mathbf{U} (\mathbf{Z}^{-1} \pm \mathbf{V} \mathbf{Y}^{-1} \mathbf{U})^{-1} \mathbf{V} \mathbf{Y}^{-1}, \quad (5.24)$$

provided that \mathbf{Y} and \mathbf{Z} are regular matrices, equation (5.23) may be written as

$$\mathbf{N}_i^{-1} = \mathbf{N}_{i-1}^{-1} - \mathbf{N}_{i-1}^{-1} \mathbf{A}_i^{*T} (\mathbf{P}_{i, i}^{-1} + \mathbf{A}_i^{*T} \mathbf{N}_{i-1}^{-1} \mathbf{A}_i^*)^{-1} \mathbf{A}_i^* \mathbf{N}_{i-1}^{-1}. \quad (5.25)$$

This representation of \mathbf{N}_i^{-1} is used in (5.16) to obtain an updated solution for the unknown parameters. It should be noted that the size of the matrix to be inverted in (5.25) is equal to the number of the double difference observations at the current epoch, while the size of the matrix to be inverted in (5.23) is equal to the number of the unknown parameters.

Therefore, using either of (5.23) or (5.25) depends on the size of the matrix to be inverted.

5.3 Ambiguity Resolution Technique

Equation (5.16) is used to obtain the sequential least squares solution for the parameters \mathbf{d} . The estimated ambiguities are generally not integers. Therefore, this solution does not exploit the integer nature of the ambiguities (see section 2.2.2). To obtain the integer set of the ambiguity parameters at a certain probability level, the covariance matrix of the ambiguities is used to form a confidence hyperellipsoid around the estimated real ambiguity values. It should be noted that the covariance matrix has to be scaled by the a posteriori variance factor given by Vanicek and Krakiwsky (1986) as

$$\hat{\sigma}_0^2 = \hat{\mathbf{r}}^T \mathbf{C}_\ell^{-1} \hat{\mathbf{r}} / v \quad (5.26)$$

where v is the number of degrees of freedom (i.e. the total number of the observations, n , minus the total number of the unknown parameters, u). The scaled covariance matrix of the estimated parameters is given by

$$\hat{\mathbf{C}}_{\mathbf{d}_i} = \hat{\sigma}_0^2 \mathbf{N}_i^{-1} = \hat{\sigma}_0^2 \{ \mathbf{N}_{i-1}^{-1} - \mathbf{N}_{i-1}^{-1} \mathbf{A}_i^{*T} (\mathbf{P}_{i,i}^{-1} + \mathbf{A}_i^{*T} \mathbf{N}_{i-1}^{-1} \mathbf{A}_i^*)^{-1} \mathbf{A}_i^* \mathbf{N}_{i-1}^{-1} \} \quad (5.27)$$

and may be partitioned as

$$\hat{\mathbf{C}}_{\mathbf{d}} = \hat{\sigma}_0^2 \begin{bmatrix} \mathbf{N}_{XX} & \mathbf{N}_{XN} \\ \mathbf{N}_{NX} & \mathbf{N}_{NN} \end{bmatrix}^{-1} \quad (5.28)$$

where \mathbf{N}_{XX} and \mathbf{N}_{NN} are the normal equation submatrices corresponding to the estimated coordinate increments and the ambiguity parameters respectively. The index i has been omitted in (5.28) and unless it is necessary will be omitted in the remaining part of this section.

The hyperellipsoid is centered on the estimated values of the ambiguity parameters with semi-axes equal to the square root of the eigenvalues of the scaled covariance matrix of the ambiguity parameters. As the dimension of the ambiguity parameters increases, the probability associated with the hyperellipsoid decreases. Therefore, the hyperellipsoid has to be scaled with an expansion factor \mathbf{k} to make the hyperellipsoid volume correspond to a certain desired probability level such as 99%. Since the a priori variance factor is not known, the Fisher distribution is used to determine the value of \mathbf{k} (Mikhail, 1976). In this case, the expansion factor \mathbf{k} is given by

$$\mathbf{k} = \sqrt{u \xi_{F_{u, n-u, 1-\alpha}}} \quad (5.29)$$

where u is the total number of the unknown parameters, n is the total number of the observations, α is the significance level and $\xi_{F_{u, n-u, 1-\alpha}}$ is the value of the F-distribution with u and $n-u$ degrees of freedom and $1-\alpha$ probability level (Vanicek and Krakiwsky, 1986). The confidence region is searched for the integer values of the ambiguity parameters to find the most likely integer ambiguities. In general, there are many different sets of solutions inside the hyperellipsoid. The best solution, in the least squares sense, is selected to be the one which gives the minimal a posteriori variance factor, based on integer ambiguities, and does not have any other compatible solution. To do this, the rounded values of the estimated real ambiguities are first selected to be the initial solution. All other points inside the hyperellipsoid are then tested for compatibility with the initial solution (i.e. the rounded values of the estimated real ambiguities). The following inequality is used to check whether a point (i.e. a set of integers) is located inside the hyperellipsoid

$$(\mathbf{N}_{re} - \mathbf{Z})^T \hat{\mathbf{C}}_N^{-1} (\mathbf{N}_{re} - \mathbf{Z}) \leq \mathbf{k}^2 \quad (5.30)$$

where \mathbf{N}_{re} are the real values estimated ambiguities, \mathbf{Z} is a possible set of integers for the ambiguities to be initially selected based on the estimated ambiguities and their standard

deviations and $\widehat{\mathbf{C}}_N^{-1}$ is defined in terms of the normal equation submatrices corresponding to the estimated coordinate increments and the ambiguity parameters as

$$\widehat{\mathbf{C}}_N^{-1} = \widehat{\sigma}_0^{-2} \{ \mathbf{N}_{NN} - \mathbf{N}_{NX} \mathbf{N}_{XX}^{-1} \mathbf{N}_{XN} \}. \quad (5.31)$$

It is, however, much faster to decompose the symmetric matrix $\widehat{\mathbf{C}}_N^{-1}$ using Cholesky decomposition (Euler and Landau, 1992). The hyperellipsoid inequality is then given by

$$[(\mathbf{N}_{re} - \mathbf{Z})^T \mathbf{L}] [(\mathbf{N}_{re} - \mathbf{Z})^T \mathbf{L}]^T \leq \mathbf{k}^2 \quad (5.32)$$

where \mathbf{L} is the Cholesky root of $\widehat{\mathbf{C}}_N^{-1}$. If (5.32) is satisfied, \mathbf{Z} is located inside the hyperellipsoid. The purpose of decomposing the matrix $\widehat{\mathbf{C}}_N^{-1}$ is that if the quadratic form on the left hand side of (5.32) for any tested point exceeds \mathbf{k}^2 during the computations, the point is rejected without completing the multiplications. Once a point is found inside the hyperellipsoid, a statistical test using the Fisher distribution is to be performed to check if the a posteriori variance factor for that point is compatible with that of the selected initial solution. For any tested solution, the corresponding set of integer ambiguities is considered as a functional constraint. Equation (5.26) can be used to compute the a posteriori variance factor with degrees of freedom given by

$$v = n + nc - u \quad (5.33)$$

where nc is the number of constraints (i.e. the number of ambiguity parameters). The quadratic form $\widehat{\mathbf{r}}^T \mathbf{C}_\ell^{-1} \widehat{\mathbf{r}}$ is given by Euler and Landau (1992) as

$$\widehat{\mathbf{r}}^T \mathbf{C}_\ell^{-1} \widehat{\mathbf{r}} = \mathbf{W}^T \mathbf{C}_\ell^{-1} \mathbf{W} - \mathbf{U}^T \widehat{\mathbf{d}} + (\mathbf{N}_{re} - \mathbf{Z})^T \widehat{\mathbf{C}}_N^{-1} (\mathbf{N}_{re} - \mathbf{Z}) \quad (5.34)$$

where the vector \mathbf{U} can be obtained in a similar way to the matrix of the normal equation discussed above as

$$\mathbf{U}_i = \mathbf{A}^T \mathbf{C}_\ell^{-1} \mathbf{W} = \mathbf{U}_{i-1} + \mathbf{A}_i^{*T} \mathbf{P}_{i,i} \mathbf{W}_i^* \quad (5.35)$$

Using (5.26) and (5.33) through (5.35), the a posteriori variance factor for any least squares solution based on integer ambiguities can be obtained. These solutions can be subjected to the F-test. The null hypothesis $\hat{\sigma}_{o_s}^2 = \hat{\sigma}_{o_a}^2$ is to be tested against the alternative $\hat{\sigma}_{o_s}^2 \neq \hat{\sigma}_{o_a}^2$, where $\hat{\sigma}_{o_s}^2$ is the a posteriori variance factor for the selected solution and $\hat{\sigma}_{o_a}^2$ is the a posteriori variance factor for an alternative solution. The statistical test may be written using (5.26) and (5.33) through (5.35) as

$$(\mathbf{LHS})_a > \xi_{F_{v, v, \alpha/2}} (\mathbf{LHS})_s + (\xi_{F_{v, v, \alpha/2}} - 1) (\mathbf{W}^T \mathbf{C} \ell^{-1} \mathbf{W} - \mathbf{U}^T \hat{\mathbf{d}}) \quad (5.36)$$

where $(\mathbf{LHS})_a$ is the quadratic form on the left hand side of (5.32) for the alternative point, $(\mathbf{LHS})_s$ is the quadratic form on the left hand side of (5.32) for the selected point and $\xi_{F_{v, v, \alpha/2}}$ is the value of the F-distribution corresponding to v degrees of freedom for both solutions and α significance level. If the statement (5.36) is true for all the tested points, then a unique solution is obtained. In other words, the selected solution is the best solution. If during the test a point was found to give a smaller a posteriori variance factor than the selected solution, then this point is selected to be the best solution and the test is to be completed with reference to this point. If the statement (5.36) is not true for all the points inside the confidence area, then a unique solution cannot be obtained at the specified probability level and additional observations are needed.

5.4 Solution with Ambiguities as Functional Constraints

Once the most likely integer values of the ambiguities, \mathbf{N}_{int} , are obtained, they are considered as constraint parameters and another least squares adjustment with functional constraints is to be performed to obtain the final estimated parameters. The mathematical model for functional constraints can be written as (Mikhail, 1976)

$$\mathbf{A}_f \mathbf{d} = \mathbf{N}_{\text{int}} \quad (5.37)$$

where, in our case, \mathbf{A}_f is an nc by u matrix consisting of a zero submatrix with dimension nc by $u-nc$ and an identity submatrix with dimension nc , nc is the number of the ambiguity parameters and u is the total number of the estimated parameters. The final modified solution for the parameters, $\hat{\mathbf{d}}_m$, is given by Wells (1990) as

$$\hat{\mathbf{d}}_m = \hat{\mathbf{d}} + \mathbf{N}^{-1} \mathbf{A}_f^T (\mathbf{A}_f \mathbf{N}^{-1} \mathbf{A}_f^T)^{-1} (\mathbf{N}_{int} - \mathbf{A}_f \hat{\mathbf{d}}) \quad (5.38)$$

and the modified covariance matrix for the unknown parameters, \mathbf{C}_{d_m} , is given by

$$\mathbf{C}_{d_m} = \mathbf{N}^{-1} - \mathbf{N}^{-1} \mathbf{A}_f^T (\mathbf{A}_f \mathbf{N}^{-1} \mathbf{A}_f^T)^{-1} \mathbf{A}_f \mathbf{N}^{-1}. \quad (5.39)$$

5.5 Storage Requirements

The main obstacle in implementing a fully populated observations' covariance matrix in a least squares adjustment is the required huge numerical mathematical operations. The design matrix, the weight matrix and the misclosure vector have to be stored from the beginning until the end of the observation time span. However, with the exponential function, the situation is different. As shown in chapter 4, when tracking the same satellites during the observation time span, the weight matrix will be a band structure matrix with only one off-diagonal submatrix. In this case, only the lower diagonal elements of one submatrix is to be stored in the weight matrix. The design matrix (5.11) and the misclosure vector (5.12) will be given as

$$\mathbf{A}_i^* = \mathbf{A}_i - f_1 \mathbf{A}_{i-1}, \quad (5.40)$$

$$\mathbf{W}_i^* = \mathbf{W}_i - f_1 \mathbf{W}_{i-1} \quad (5.41)$$

where f_1 is the correlation coefficient (see chapter 4). This means, only the design matrix and the misclosure vector for the current and the previous epochs are required.

In reality, different groups of satellites may be observed for sometime during the observation time span. In this case, the weight matrix will be a block diagonal matrix. If different groups of satellites were observed during the epochs from j through k , then the required storage for the weight matrix is given by the shaded area in Figure 5.1.

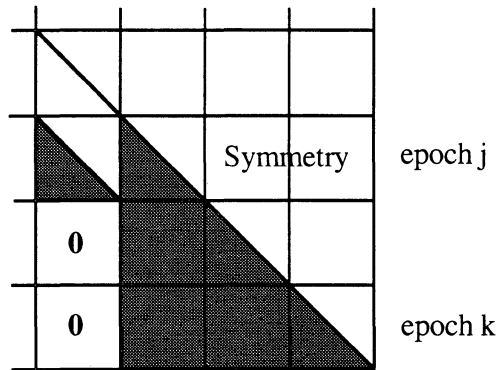


Figure 5.1. Required Storage for the Weight Matrix When Tracking Different Groups of Satellites Between Epochs j and k .

The required storage for the design matrix and the misclosure vector would be the part from epoch $j-1$ up to the current epoch k only. It should be noted that if the observed satellites in the current epoch and the previous one were identical, the required storage and computations will be identical to the ideal case of tracking the same groups of satellites all the time. In reality, the same satellites are tracked most of the observation time. Resulting in, great savings in the required storage and the computation time. It should be noted that the term $\mathbf{W}^T \mathbf{C}_\ell^{-1} \mathbf{W}$ in (5.34) will be needed in computing the quadratic form $\hat{\mathbf{r}}^T \mathbf{C}_\ell^{-1} \hat{\mathbf{r}}$. It may appear that the whole vector \mathbf{W} has to be stored to perform the above computation. However, if the quadratic form $\mathbf{W}^T \mathbf{C}_\ell^{-1} \mathbf{W}$ is updated each epoch, the required storage for \mathbf{W} will be the same as mentioned above.

Chapter 6

SOFTWARE DEVELOPMENT AND DISCUSSION OF THE RESULTS

This chapter discusses the effect of the physical correlations on the ambiguity resolution and the accuracy estimation. The measurements of several baselines of different lengths were analyzed to show this effect. The baselines were observed under different ionospheric activities and were located in various areas in North America. These data sets were first preprocessed using PREDD, the UNB preprocessor program (Kleusberg et al., 1989). This program detects and corrects the cycle slips in the measurements, forms the double differences of the carrier phases and pseudoranges and computes the satellite coordinates at the same epochs as the carrier phase double differences.

After preprocessing the data sets, DIFGPS, the newly developed software was used for the postprocessing. For comparison, the Ashtech software, GPPS 5.0 (Ashtech, 1993), was used in the analyses of the measurements of two baselines. Only L1 carrier phase data was used for these analyses.

6.1 Description of the Software

DIFGPS software is based on the least squares adjustment algorithm described in the previous chapter. The physical correlation is modelled using the developed exponential covariance function. The correlation times shown in Table 3.4 are used by the program

as default values. However, the user can introduce any other desired values for the correlation times. The program also allows the user to specify a particular part of the data set to be analyzed.

DIFGPS first determines the float solution for the ambiguity parameters as well as their covariance matrix from the least squares adjustment described in the previous chapter. The covariance matrix is then used to form a confidence region of a hyperellipsoid around the estimated real values of the ambiguity parameters. The hyperellipsoid is scaled with an expansion factor given by Equation 5.29 to make its volume correspond to a certain desired probability level of $1-\alpha$ introduced by the user. The confidence region is then used for searching the likely integer values of the ambiguity parameters. It should be pointed out that as the size of the hyperellipsoid increases, the number of ambiguities to be tested increases. However, with the help of the powerful rejection criteria of the Cholesky decomposition described in Chapter 5, searching the ambiguities usually does not take more than two seconds on the Macintosh SE/30. To reach this speed, the first Cholesky root should be an upper triangle. The statistical test given by Equation 5.36 is used to determine the most likely integer ambiguity parameters at a certain desired probability level of $1-\alpha$ introduced by the user. Once the integer ambiguities are determined they are used as constraint parameters to obtain the final constraint solution for the unknown coordinates. If a non unique solution for the integer ambiguity parameters is obtained, a warning message appears to the user. In this case, the user can either lower the probability level of $1-\alpha$ or select the solution with the minimum a posteriori variance factor. If the first option is selected, the searching operation is repeated. However, if the second option is selected, the solution with the minimum a posteriori variance factor is used to determine the final constraint solution for the unknown coordinates. In this case, to avoid confusion, a warning message appears in the output file indicating that the solution for the ambiguity parameters is not unique. It

should be noted that a third option may be added to allow processing some more observations without terminating the program.

The input files to this software are the meteorological data and the double difference data file obtained from the UNB GPS preprocessing software. The output files include the preliminary solution before fixing the ambiguities, the dimension and size of the hyperellipsoid used for searching the ambiguities, the determined integer ambiguities, the time of searching the ambiguities and the final constraint solution for the unknown coordinates and their covariance matrix.

6.2 Discussion of the Results

As mentioned before, several baselines were analyzed to test the effect of including or neglecting the physical correlations on the ambiguity resolution and the accuracy estimation. The lengths of these baselines were selected to represent a range of up to 100 km. The baselines were separated into two groups. The first group consisted of three baselines of lengths 20, 60 and 81 km which were observed with TI 4100 receivers in 1986. The measurements of this set of baselines had a 60 second sampling interval. The second group consisted of three baselines of lengths 13, 55 and 90 km which were observed with Ashtech, Rogue, and Trimble receivers in 1992 and 1993. The measurements of this set of baselines had a 20 second sampling interval for the 13 km baseline and 120 second interval for the other two baselines. It should be pointed out that only the first group of baselines were among the baselines used for developing the empirical covariance function discussed in Chapter 3.

After preprocessing these data sets, the program DIFGPS was used for postprocessing. To compare the results, a reference truth had to be determined. The observation time span was long enough to ensure that the errors were averaged out when processing the

entire data set of each baseline. The reference truth selected resulted from processing the entire data set with physical correlations included. In all cases, unique solutions were obtained at the 99.9% probability level, except with the 81 km baseline where a unique solution was obtained at the 96% probability level. This decrease in probability is due to the relatively short observation time span for that baseline (2.6 hours). In all cases, the probability level used to scale the hyperellipsoid was 99.999%.

6.2.1 Results for TI 4100 Data

Three baselines of lengths 20, 60 and 81 km were processed. The observation time spans for these baselines were 4.7, 3.2 and 2.6 hours, respectively. These three baselines are part of the Juan de Fuca network observed in 1986 (Kleusberg and Wanninger, 1987). The surface meteorological data were available and used in modelling the tropospheric delay. With the TI 4100 receivers, the maximum number of the satellites at any epoch is four. Although this may require more epochs to obtain a unique solution, the processed data was observed under low ionospheric activities which means less epochs are required to find the unique solution. The results for the three baselines are summarized below.

For each baseline, the whole data set was first processed to obtain reference values as described above. Unique solutions were obtained for the 20 and 60 km baselines at the significance level of 0.001. However, for the 81 km baseline, a unique solution was obtained at the 0.04 significance level. This increased significance level is mainly due to its relatively short observation time span (2.6 hours). Subsets of each of these data sets were also processed to obtain solutions at the 5%, 1% and 0.1% significance levels. Tables 6.1 through 6.3 show the resulting estimated real ambiguity parameters in cycles (Columns 2 and 3) obtained from DIFGPS with and without physical correlations included. It should be noted that the values shown in Columns 2 and 3 represent the estimated real ambiguity parameters minus the most likely integer ambiguity parameters.

In other words, if the estimated ambiguity parameters are close to the most likely ones, they appear in the tables as close to zero values. It can be seen from the tables that the set of integers obtained from direct rounding of the estimated real ambiguities does not necessarily agree with the most likely set of integers. It can also be seen that neglecting the physical correlations does not significantly affect the estimated real ambiguities. The reason could be that the errors are averaged out. Also shown in these tables are the corresponding integer search ranges (Columns 4 through 7). The integer search ranges represent possible candidates for each of the ambiguity parameters. In other words, they represent all integer sets inside the hyperbox which encloses the hyperellipsoid. The search ranges are generally larger when the physical correlations are included. This is due to the larger standard deviations obtained when the physical correlations are included as discussed below. As mentioned before, the length of data (LD) shown in these tables represents the required data length in minutes to obtain a unique integer set of ambiguities at the 5% significance level.

Table 6.1 Estimated Real Ambiguities and the Search Ranges for a 20 km Baseline

	Real Ambiguities (cyc)		Search Range			
	math. corr.	math & ph	math. corr. ($\alpha = 1.E-5$)		math & ph ($\alpha = 1.E-5$)	
	LD*=42	LD*=52	min.	max.	min.	max.
#1	0.33	0.43	-5	6	-5	6
#2	0.32	0.54	-7	8	-8	9
#3	-0.10	-0.05	-3	2	-3	3

* LD is the length of data in minutes.

Table 6.2 Estimated Real Ambiguities and the Search Ranges for a 60 km Baseline

	Real Ambiguities (cyc)		Search Range			
	math. corr.	math & ph	math. corr. ($\alpha = 1.E-5$)		math & ph ($\alpha = 1.E-5$)	
	LD*=52	LD*=90	min.	max.	min.	max.
#1	0.16	-0.04	-2	3	-4	3
#2	-0.47	-0.17	-4	3	-4	3
#3	-0.70	-0.09	-4	3	-3	3

* LD is the length of data in minutes.

Table 6.3 Estimated Real Ambiguities and the Search Ranges for an 81 km Baseline

	Real Ambiguities (cyc)		Search Range			
	math. corr.	math & ph	math. corr. ($\alpha = 1.E-5$)		math & ph ($\alpha = 1.E-5$)	
	LD*=80	LD*=158	min.	max.	min.	max.
#1	0.11	-0.10	-2	2	-5	5
#2	-0.14	-0.24	-2	1	-3	2
#3	-0.25	-0.21	-7	7	-14	13
#4	-0.09	-0.21	-4	4	-9	9
#5	NA **	-0.31	NA **	NA **	-8	8
#6	NA **	0.16	NA **	NA **	-3	3

* LD is the length of data in minutes.

** Not available at this time.

Tables 6.4 through 6.6 show the final constraint solution after fixing the ambiguities for the three baselines. In these tables, the first column indicates whether the physical correlation is included or not. The second column shows the required data length to obtain a unique solution at a certain probability level. The third column shows the significance level used for each processing. The fourth column represents the final constraint solution, based on the fixed ambiguities, less the reference truth for the coordinates of the remote station. The fifth column represents the resulting standard

deviations scaled by the square root of the a posteriori variance factor for the remote station coordinates.

Table 6.4 Effect of Physical correlations on a 20 km Baseline

Software Used	Length of Data	Signif. Level	Coordinate Differences (cm)			Standard Devs. (mm)		
			ΔX	ΔY	ΔZ	σX	σY	σZ
	minutes	α						
DIFGPS math. corr.	42	0.05	-0.8	-0.3	-0.6	6	4	3
DIFGPS math. corr.	48	0.01	-0.7	-0.4	-0.6	5	3	3
DIFGPS math. corr.	50	0.001	-0.8	-0.4	-0.6	5	3	3
DIFGPS math. corr.	280	0.001	-0.1	-0.2	0.3	2	2	2
DIFGPS math & ph	52	0.05	-0.9	-0.5	-0.6	9	5	5
DIFGPS math & ph	56	0.01	-1.1	-0.5	-0.6	9	6	6
DIFGPS math & ph	60	0.001	-1.2	-0.5	-0.6	9	6	6
DIFGPS math & ph	280	0.001	0.0	0.0	0.0	2	2	3

For the 20 km baseline, the ambiguity parameters were identified correctly rather than as most likely after only 11 epochs (11 minutes), if the physical correlations were included. However, without physical correlations, the ambiguity parameters were identified correctly after 12 epochs. In both cases, the ratio between the smallest a posteriori variance factor and the second smallest a posteriori variance factor was just above one. Without physical correlations included, the ambiguity parameters were uniquely obtained after 42, 48 and 50 minutes at 0.05, 0.01 and 0.001 significance levels, respectively. However, with physical correlations included, they were obtained after 52, 56 and 60 minutes at 0.05, 0.01 and 0.001 significance levels. For the 60 km baseline, without physical correlations, data lengths of 52, 55 and 77 minutes were needed to obtain a

unique solution at the same significance levels mentioned above. However, with physical correlations included, they were 90, 96 and 104 minutes. For the 81 km baseline, with physical correlations neglected, the lengths of data required to obtain a unique solution at the above mentioned significance levels were 80, 83 and 88 minutes. If physical correlations were included, the only unique solution obtained was at 0.04 significance level. To obtain this solution, it was necessary to process the whole data set. It is obvious that, for all of the three baselines, including the physical correlations requires more data to obtain a unique solution.

Table 6.5 Effect of Physical correlations on a 60 km Baseline

Software Used	Length of Data	Signif. Level	Coordinate Differences (cm)			Standard Devs. (mm)		
			ΔX	ΔY	ΔZ	σX	σY	σZ
	minutes	α						
DIFGPS math. corr.	52	0.05	-3.7	-1.4	3.3	6	4	5
DIFGPS math. corr.	55	0.01	-3.6	-1.3	3.1	6	4	5
DIFGPS math. corr.	77	0.001	-3.7	-1.0	2.9	6	4	5
DIFGPS math. corr.	193	0.001	-0.4	-0.1	0.3	3	2	3
DIFGPS math & ph	90	0.05	-4.6	-1.7	4.2	12	8	10
DIFGPS math & ph	96	0.01	-4.3	-1.6	4.2	11	8	9
DIFGPS math & ph	104	0.001	-4.8	-1.6	4.0	9	6	7
DIFGPS math & ph	193	0.001	0.0	0.0	0.0	5	4	4

As shown in Tables 6.4 through 6.6, including the physical correlations has no significance influence on the resulting coordinates. Again, the reason could be that the errors are averaged out. However, neglecting the physical correlations can significantly affect the resulting covariance matrix of the estimated parameters.

Table 6.6 Effect of Physical correlations on an 81 km Baseline

Software Used	Length of Data	Signif. Level	Coordinate Differences (cm)			Standard Devs. (mm)		
			ΔX	ΔY	ΔZ	σX	σY	σZ
	minutes	α						
DIFGPS math. corr.	80	0.05	-0.2	1.3	0.8	4	4	5
DIFGPS math. corr.	83	0.01	-0.1	1.3	0.8	3	4	5
DIFGPS math. corr.	88	0.001	0.0	1.3	0.7	3	3	5
DIFGPS math. corr.	158	0.001	-0.5	-0.6	-0.8	3	3	4
DIFGPS math & ph	158	0.04	0.0	0.0	0.0	5	6	8

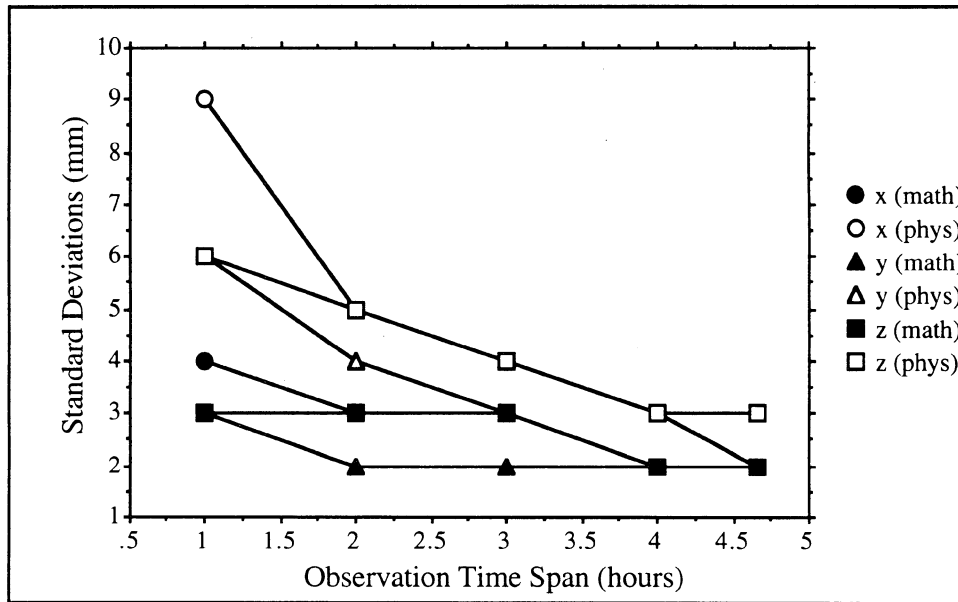


Figure 6.1. Effect of Physical Correlations on the Accuracy Estimation for a 20 km Baseline

Examining the resulting standard deviations of the coordinates of the remote station, Tables 6.4 through 6.6 show that in all cases neglecting the physical correlations leads to smaller standard deviations compared to the ones obtained with physical correlations

included. In other words, neglecting the physical correlations leads to an overly optimistic covariance matrix. Figures 6.1 and 6.2 show the resulting standard deviations, obtained with and without physical correlations included as a function of the observation time span for the 20 km and the 60 km baselines.

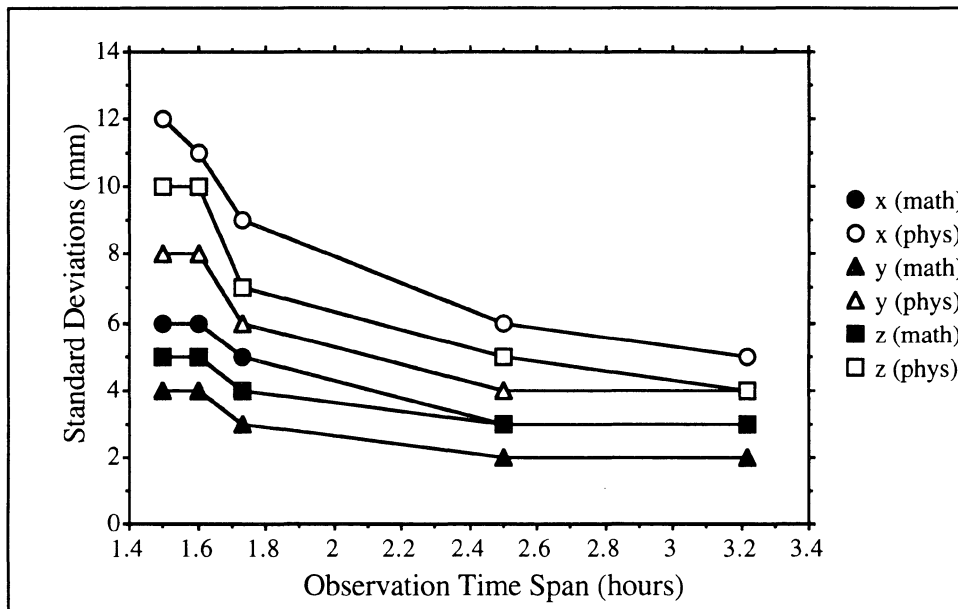


Figure 6.2. Effect of Physical Correlations on the Accuracy Estimation for a 60 km Baseline

6.2.2 Results for Other Data Sets

Three other data sets for baselines of lengths 13, 55 and 90 km were also processed. The 13 km baseline was observed in 1992 with Ashtech receivers. The 55 km baseline was observed in 1993 with a Trimble receiver at one end and a Rogue receiver at the other. The 90 km baseline was observed in 1993 with the Trimble receivers. The observation time spans for these three baselines were approximately 1.1, 2.5 and 3.5 hours. The

surface meteorological data were not available and default values of 1010 MB for pressure, 20° C for temperature, and 50% for relative humidity were used.

The results for these baselines are given in Tables 6.7 through 6.12. The contents of these tables can be described the same way as the case of TI 4100 data. As before, for each of the three baselines, the whole data set was first processed to obtain the reference values. Unique solutions were obtained at the 0.1% significance level. Also subsets of these data sets were processed to determine the required data length to obtain a unique solution at the 5%, 1% and 0.1% significance levels. Tables 6.7 through 6.9 summarize the results for the estimated real ambiguity parameters and the corresponding search ranges. These tables are based on a 5% significance level.

Table 6.7 Estimated Real Ambiguities and the Search Ranges for a 13 km Baseline

	Real Ambiguities (cyc)		Search Range			
	math. corr.	math & ph	math. corr. ($\alpha = 1.E-5$)		math & ph ($\alpha = 1.E-5$)	
$\alpha = 0.05$	LD*=19	LD*=47	min.	max.	min.	max.
#1	-0.52	-0.38	-4	3	-9	8
#2	-1.27	-0.65	-8	5	-15	14
#3	-0.78	-0.48	-5	4	-10	9

* LD is the length of data in minutes.

As with the case of TI 4100 data, no significant influence of neglecting or including the physical correlations on the estimated real ambiguity parameters. Note that the relatively big difference between the estimated real ambiguity parameters obtained with and without physical correlations included in Table 6.7 is due to the relatively short data length when physical correlations were neglected. It is again obvious that the set of integers obtained from rounding the estimated real ambiguity parameters to the nearest integers does not agree with the most likely set of integers.

Table 6.8 Estimated Real Ambiguities and the Search Ranges for a 55 km Baseline

$\alpha = 0.05$	Real Ambiguities (cyc)		Search Range			
	math. corr.	math & ph	math. corr. ($\alpha = 1.E-5$)		math & ph ($\alpha = 1.E-5$)	
	LD*=44	LD*=76	min.	max.	min.	max.
#1	-0.52	-0.70	-25	24	-27	26
#2	-0.02	0.0	-4	4	-4	4
#3	-0.01	-0.15	-5	5	-5	5
#4	-0.22	-0.46	-18	18	-19	18
#5	NA**	-0.72	NA**	NA**	-23	22

* LD is the length of data in minutes.

** Not available at this time.

Table 6.9 Estimated Real Ambiguities and the Search Ranges for a 90 km Baseline

$\alpha = 0.05$	Real Ambiguities (cyc)		Search Range			
	math. corr.	math & ph	math. corr. ($\alpha = 1.E-5$)		math & ph ($\alpha = 1.E-5$)	
	LD*=180	LD*=180	min.	max.	min.	max.
#1	-0.62	-0.67	-3	1	-3	2
#2	-0.64	-0.68	-2	1	-2	1
#3	-0.55	-0.55	-1	0	-1	0
#4	-0.30	-0.25	-2	2	-2	2
#5	-0.30	-0.37	-2	2	-3	2
#6	-0.59	-0.54	-2	1	-2	1

* LD is the length of data in minutes.

The final constraint solutions for this group of baselines are shown in Tables 6.10 through 6.12. For the 13 km baseline, without physical correlations, the data length required to get the unique solution at the 5%, 1% and 0.1% significance levels were 19, 24 and 25 minutes respectively. However, with the physical correlations included, the required data

lengths were 47, 60 and 62 minutes, respectively. For the 55 km baseline, with physical correlations neglected, subsets of data with lengths 44, 50 and 54 minutes were required to obtain the unique solution at the 5%, 1% and 0.1% significance levels, respectively. With physical correlations included, the required data lengths were 76, 82 and 84 minutes, respectively. The analysis of the last baseline in this group, the 90 km baseline, shows that the required length to obtain a unique solution at the 5% significance level was 180 minutes, whether the physical correlations were included or not. This could be due to the large sampling interval for this baseline. Details about the effects of the sampling interval on the ambiguity resolution and the accuracy estimation are given in the next section.

Table 6.10 Effect of Physical correlations on a 13 km Baseline

Software Used	Length of Data	Signif. Level	Coordinate Differences (cm)			Standard Devs. (mm)		
			ΔX	ΔY	ΔZ	σX	σY	σZ
	minutes	α						
DIFGPS math. corr.	19	0.05	-0.8	-1.3	0.8	2	4	3
DIFGPS math. corr.	24	0.01	-0.2	-0.2	0.1	2	4	3
DIFGPS math. corr.	25	0.001	-0.2	-0.2	0.2	1	4	3
DIFGPS math. corr.	66	0.001	-0.2	0.0	0.3	1	2	2
DIFGPS math & ph	47	0.05	-0.3	-0.5	0.5	5	15	12
DIFGPS math & ph	60	0.01	-0.1	0.3	0.2	4	12	10
DIFGPS math & ph	62	0.001	0.0	0.3	0.0	4	12	10
DIFGPS math & ph	66	0.001	0.0	0.0	0.0	4	12	10

As shown in Tables 6.10 through 6.12, the effect of including or neglecting the physical correlations on the resulting coordinates does not seem to be significant. However,

neglecting the physical correlations leads to smaller standard deviations than the ones obtained with physical correlations included.

Table 6.11 Effect of Physical correlations on a 55 km Baseline

Software Used	Length of Data	Signif. Level	Coordinate Differences (cm)			Standard Devs. (mm)		
			ΔX	ΔY	ΔZ	σX	σY	σZ
	minutes	α						
DIFGPS math. corr.	44	0.05	-2.1	-3.3	1.4	4	5	8
DIFGPS math. corr.	50	0.01	-2.2	-3.3	2.0	3	5	7
DIFGPS math. corr.	54	0.001	-2.2	-3.2	2.0	3	5	6
DIFGPS math. corr.	148	0.001	0.1	0.0	0.0	2	4	3
DIFGPS math & ph	76	0.05	-2.0	-2.8	2.5	5	9	7
DIFGPS math & ph	82	0.01	-1.8	-2.7	2.4	5	9	7
DIFGPS math & ph	84	0.001	-1.8	-2.7	2.3	4	8	6
DIFGPS math & ph	148	0.001	0.0	0.0	0.0	4	6	5

As shown in Table 6.10, the ratio between the standard deviations obtained without and with physical correlations included can reach up to 6. With the 55 km and the 90 km baselines (Tables 6.11 and 6.12), the ratio is not as large as the 13 km baseline. This is again due to the relatively large sampling interval of these two baselines. Figures 6.3 and 6.4 show the resulting standard deviations obtained with and without physical correlations included for the 13 and the 55 km baselines.

Table 6.12 Effect of Physical Correlations on a 90 km Baseline

Software Used	Length of Data	Signif. Level	Coordinate Differences (cm)			Standard Devs. (mm)		
			ΔX	ΔY	ΔZ	σX	σY	σZ
	minutes	α						
DIFGPS math. corr.	180	0.05	-1.0	-0.9	0.8	5	7	5
DIFGPS math. corr.	182	0.01	-0.9	-0.9	0.7	5	7	5
DIFGPS math. corr.	188	0.001	-0.8	-0.8	0.7	4	7	5
DIFGPS math. corr.	208	0.001	-0.2	-0.3	0.3	4	6	4
DIFGPS math & ph	180	0.05	-0.8	-0.7	0.5	5	8	5
DIFGPS math & ph	184	0.01	-0.7	-0.6	0.4	5	8	5
DIFGPS math & ph	190	0.001	-0.6	-0.5	0.3	5	7	5
DIFGPS math & ph	208	0.001	0.0	0.0	0.0	4	7	5

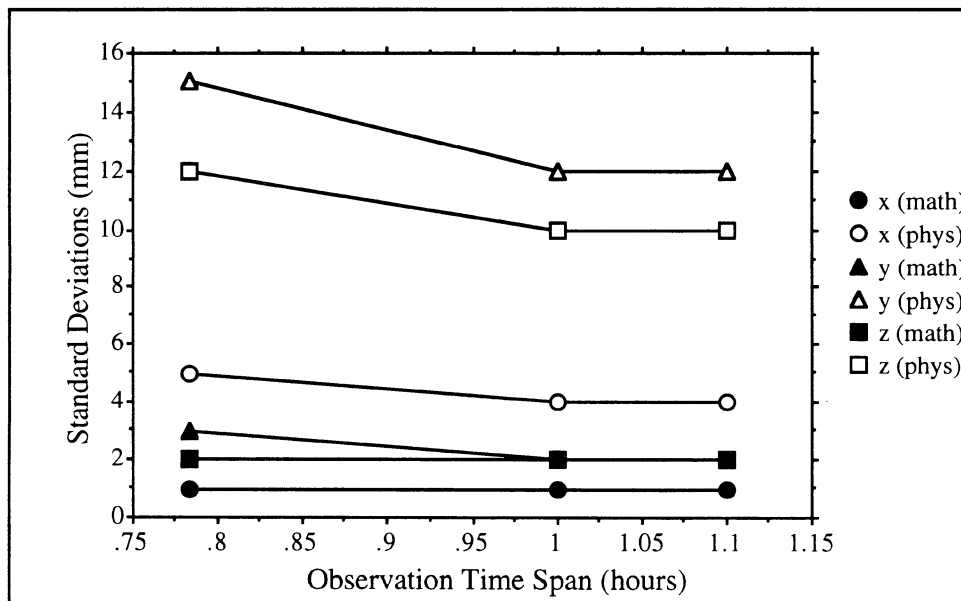


Figure 6.3. Effect of Physical Correlations on the Accuracy Estimation for a 13 km Baseline

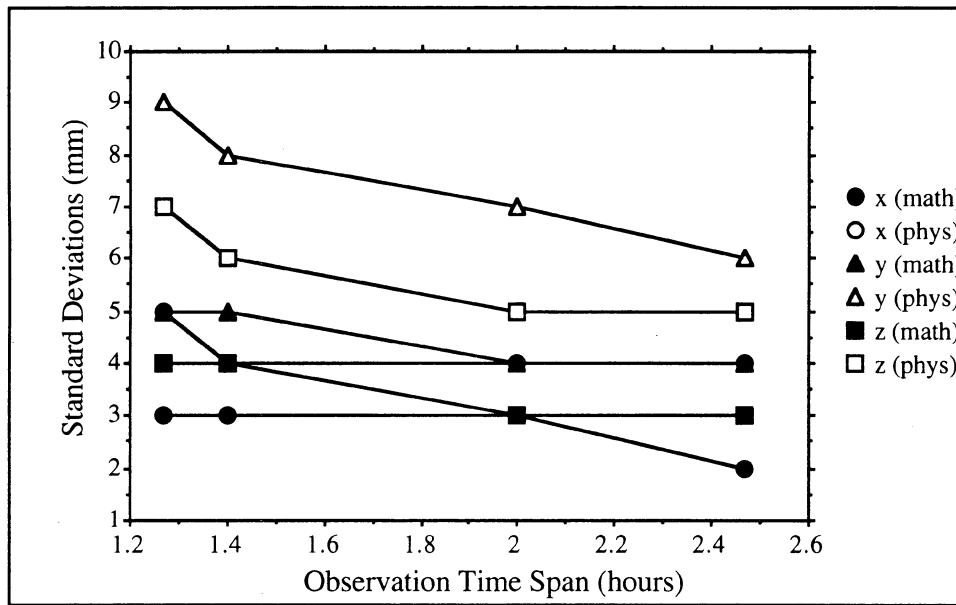


Figure 6.4. Effect of Physical Correlations on the Accuracy Estimation for a 55 km Baseline

6.3 Effect of Sampling Interval

It has been shown in Chapter 3 that the carrier phase double difference observations are positively correlated over a time period of about 20 minutes. However, this correlation decreases exponentially to a high degree of approximation. It is expected that as the sampling interval increases the degree of correlation between the observations of different epochs decreases without physical correlations. In other words, a more realistic covariance matrix for the estimated parameters is expected as the sampling interval increases. To confirm this, the 13 km baseline presented in Section 6.2.2 was processed again using different sampling intervals. The sampling intervals used in the analyses were the original 20 seconds, 1 minute, 2 minutes, 5 minutes and 10 minutes, respectively. The observation time span was one hour for all the cases. To be able to

compare the results, the analyses were performed with and without physical correlations included.

Figure 6.5 shows the resulting standard deviations for the three components of the remote station coordinates as a function of the sampling interval. As expected, as the sampling interval increases, the standard deviations obtained without physical correlation approaches the ones obtained with physical correlations included. However, with physical correlations included, the values of the standard deviations do not change significantly as the sampling interval changes. Furthermore, with 10 minutes sampling interval, the difference between the values of the standard deviations obtained with and without physical correlations included is only 1 mm in each component. If this difference is considered negligible for some applications, the 10 minutes sampling interval is considered optimal. Nevertheless, the optimum sampling interval varies from one baseline to another.

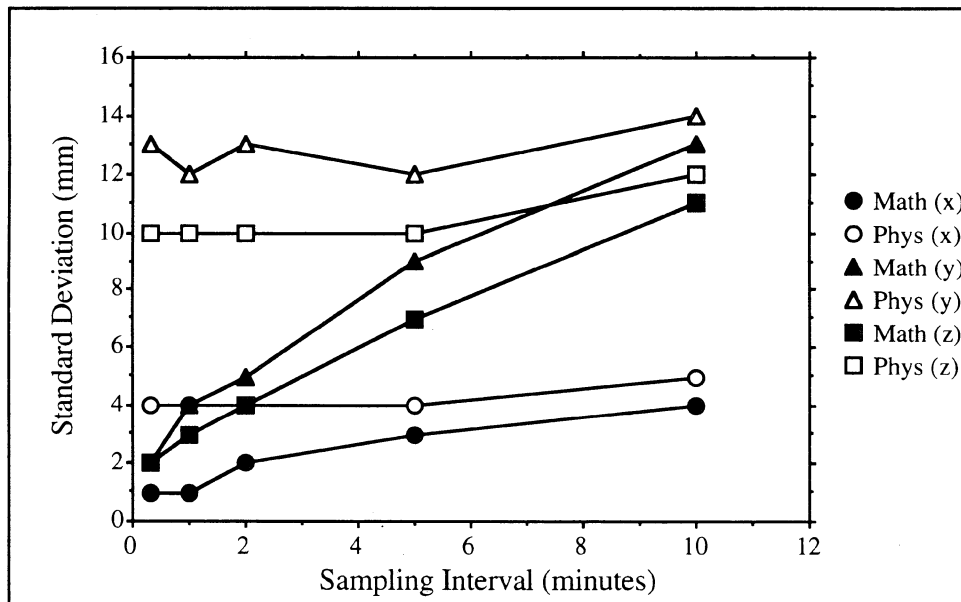


Figure 6.5. Effect of Sampling Interval on the Accuracy Estimation for a 13 km Baseline

The same data sets described above were used to test the effect of sampling interval on the ambiguity resolution. Figure 6.6 shows the ratio between the second smallest a posteriori variance factor and the smallest a posteriori variance factor for the two cases of neglecting or including the physical correlations. Also shown are the values of the F-distribution $\xi_{F_{v, v, \alpha/2}}$ given in the expression (5.36). The significance level used is 0.05.

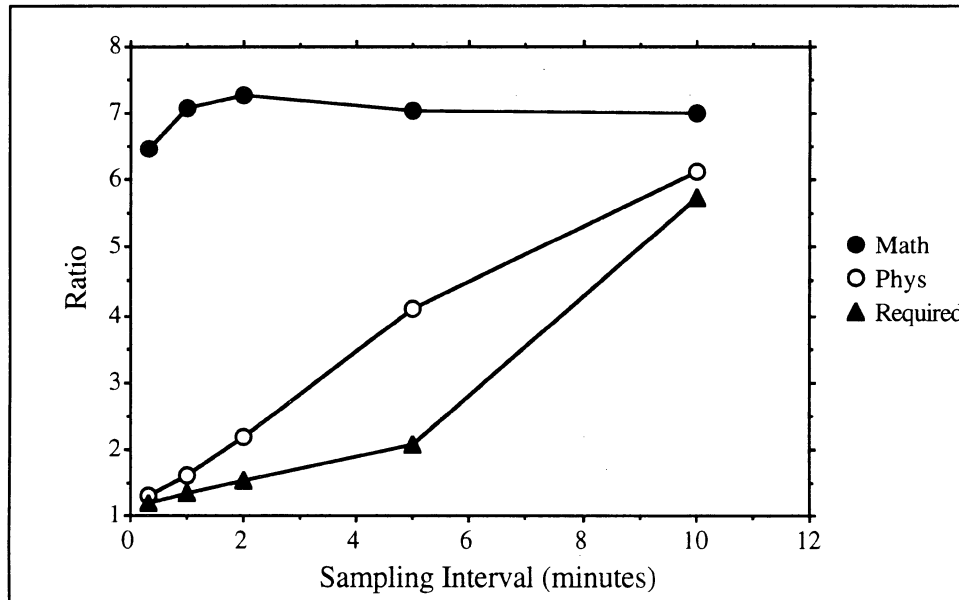


Figure 6.6. Effect of Sampling Interval on the Ratio Between the Second Smallest a posteriori Variance Factor and the Smallest a posteriori Variance Factor for a 13 km Baseline

For small sampling intervals, if the physical correlations are neglected, the ratio between the second smallest a posteriori variance factor and the smallest a posteriori variance factor becomes much larger than the value of $\xi_{F_{v, v, \alpha/2}}$. This means the null hypothesis described in Section 5.3 can pass the test easily. However, as the sampling interval increases the degrees of freedom decrease and the value of $\xi_{F_{v, v, \alpha/2}}$ increases. On the contrary, with physical correlations included, the ratio is just above the value of $\xi_{F_{v, v, \alpha/2}}$ for small sampling intervals. As the sampling interval increases, the ratio between the

second smallest a posteriori variance factor and the smallest a posteriori variance factor changes with a rate higher than that of $\xi_{F_{v, v, \alpha/2}}$. This is true for a sampling interval of up to 5 minutes.

It should be noted that as the significance level decreases the value of $\xi_{F_{v, v, \alpha/2}}$ increases. For a sampling interval of 10 minutes the degrees of freedom for the above data set become 12. Therefore, for a significance level of 0.001, the value of $\xi_{F_{v, v, \alpha/2}}$ becomes 8.09. This means a unique solution cannot be obtained from either cases of neglecting or including the physical correlations. This is, however, not true for smaller sampling intervals. An exception to this is the data set with 20 seconds sampling interval and the physical correlations included.

6.4 Effect of Correlation Time

For all the analyses presented so far in this chapter, the physical correlation was modelled using the general exponential covariance function with correlation time of 263 seconds (Table 3.4). However, as shown in Section 3.2.1, different correlation times are obtained for different baseline lengths. If the actual correlation time is larger than the correlation time of the general covariance function, then using the latter leads to smaller standard deviations than the true ones. On the other hand, if the correlation time of the general covariance function is larger, using it leads to larger smaller standard deviations than the true ones. The same 13 km baseline presented above was reprocessed to test the effect of varying the correlation time on the resulting standard deviations. Based on Table 3.1, the proper correlation time for baselines in the range from 10 to 20 km is 341 seconds. Figure 6.7 shows the standard deviations of the estimated parameters as a function of the sampling interval for the correlation times of 263 seconds and 341 seconds, respectively. It can be seen that if the proper correlation time is used, an increase of about 20% in each component of the resulting standard deviations is obtained. The difference, however,

decreases with a large sampling interval because the observations are less correlated and the effect of including the physical correlations decreases as explained in the previous section.

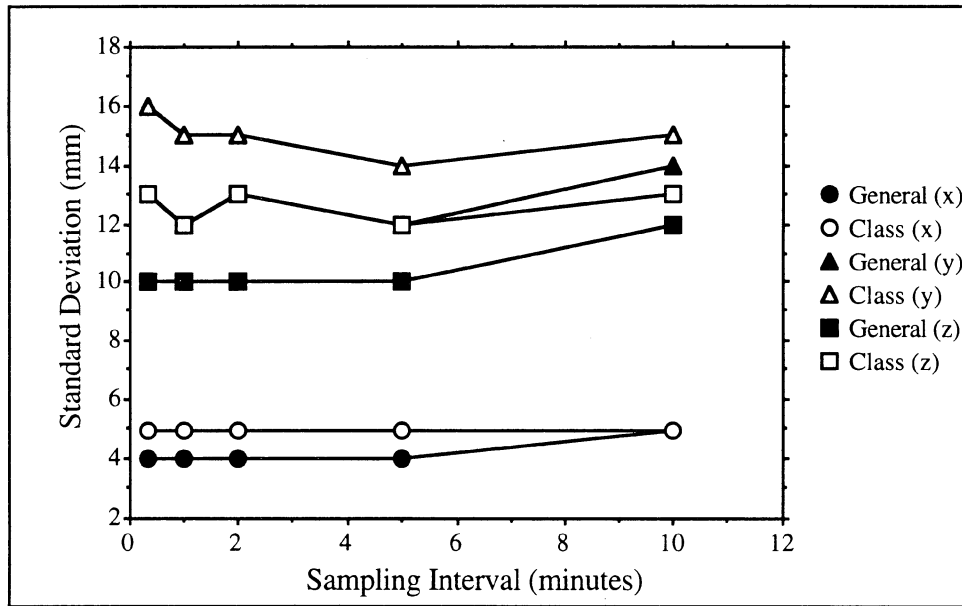


Figure 6.7. Effect of Varying the Correlation Time on the Accuracy Estimation for a 13 km Baseline

As shown in Tables 3.1 through 3.3, there is no particular trend for the correlation times as a function of the baseline length. If the 20% increase discussed above can be considered insignificant, then using the general covariance function is more appropriate.

6.5 Effect of Scaling the Covariance Matrix

As shown in Section 6.2 above, neglecting the physical correlations yields an overly optimistic covariance matrix for the estimated parameters. To account for the neglected physical correlations, some of the available GPS software packages scale the optimistic covariance matrix. However, the scale factor is not guaranteed to work properly

(Craymer et al., 1990). If the scale factor is too small, optimistic results are expected. If it is too large, it leads to pessimistic results.

Two baselines of lengths 13 and 55 km were processed with both DIFGPS with physical correlations included and the Ashtech software GPPS 5.0 (Ashtech, 1993). Figures 6.8 and 6.9 show the standard deviations for the components of the remote station coordinates obtained with both softwares. It can be seen that for all components, the standard deviations obtained with the GPPS software are larger by a factor of two or more than those obtained with DIFGPS. This shows the importance of modelling the physical correlations.

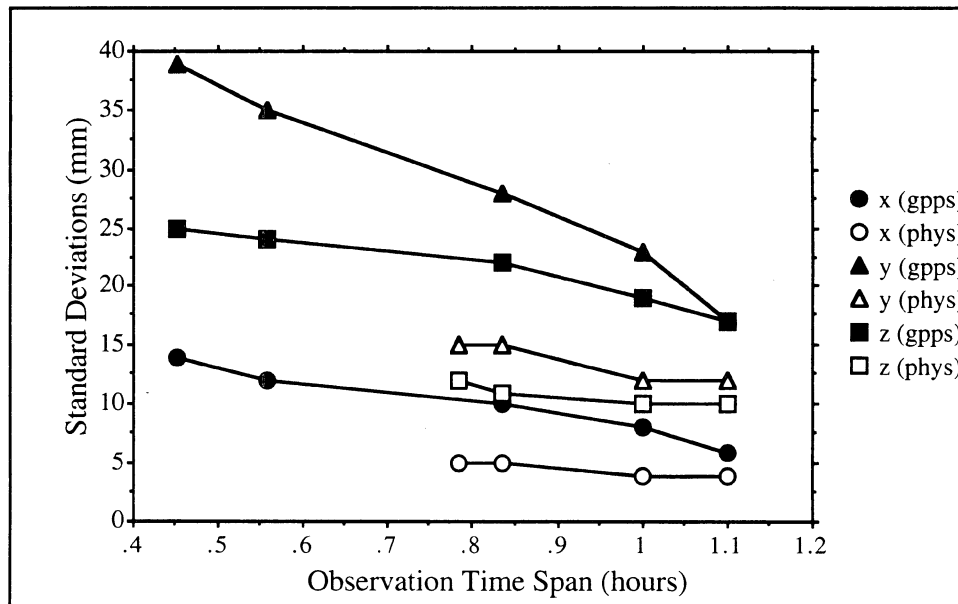


Figure 6.8. The Resulting Standard Deviations from Two Software Packages for a 13 km Baseline

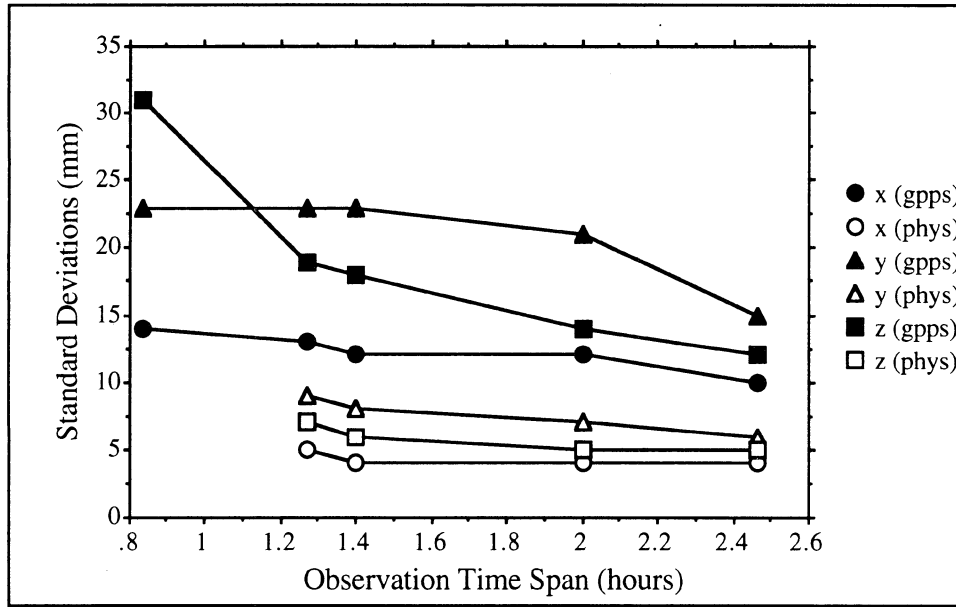


Figure 6.9. The Resulting Standard Deviations from Two Software Packages for a 55 km Baseline

CONCLUSIONS AND RECOMMENDATIONS

7.1 Summary and Conclusions

This research was conducted for two purposes. The first purpose was to model empirically the temporal physical correlations in order to develop a more realistic covariance matrix for the GPS carrier phase double difference observations so that a trustworthy accuracy estimation for the estimated parameters could be obtained. The second objective of this study was to develop an efficient ambiguity resolution technique and to study the effect of the physical correlations on the ambiguity resolution and the accuracy estimation.

7.1.1 Modelling the Physical Correlations

Developing the empirical covariance function which accounts for the temporal physical correlations was based on the analysis of the double difference adjustment residuals obtained without physical correlations included. The adjustment residuals were used to generate a series of autocovariance functions for each double difference series and also crosscovariance functions among the double differences. This was done using a total of 47 baselines of lengths up to 100 km. The least squares technique was then used to develop an empirical covariance function which best fits the estimated covariances. For L1 and L2 data, the exponential function was found to give the best least squares fit (the

least a posteriori variance factor) for the majority of the baselines. However, for L3 (ionosphere free) data, the exponential function gave the best least squares fit for all the baselines.

The analysis indicated that the estimated parameters of the tested empirical functions show small variations. On the other hand, no particular trend was seen for these parameters. For this reason, a general autocovariance function which is valid for the range up to 100 km was developed. It was found that the empirical exponential function always gives the best fit for either L1, L2 or L3. The correlation times (the 1/e point) for the general autocovariance function are 263, 270 and 169 seconds for L1, L2 and L3, respectively. It was also found that the GPS double difference observations are positively correlated over a time period of about 20 minutes. Neglecting this correlation in the least squares adjustment of carrier phase double difference yields an overly optimistic covariance matrix for the estimated parameters.

It was shown that only the autocovariance function needs to be developed. The crosscovariance function can, in fact, be derived from the autocovariance function. This was confirmed mathematically and with simulated GPS data. As a result, the complete covariance matrix can be formed using a simple empirical exponential model.

The empirical exponential covariance function was used to modify the covariance matrix of the carrier phase double difference observations. It was shown that, although the inclusion of physical correlations leads to a fully populated covariance matrix, using the empirical exponential covariance function yields a block diagonal weight matrix. As a result, great savings in both the required computer memory and the computation time can be obtained.

7.1.2 The Effect of the Physical Correlations

A modified sequential least squares adjustment algorithm incorporating the fully populated covariance matrix of the carrier phase double differences was developed. Based on the least squares adjustment, the estimated real ambiguity parameters and their covariance matrix can be obtained. To obtain the most likely integer values for the ambiguities, at a certain probability level, the covariance matrix for the ambiguities was used to form a confidence region of a hyperellipsoid around their estimated values. This confidence region was used to search for the likely integer values of the ambiguity parameters. The use of Cholesky decomposition to break the covariance matrix of the ambiguities was found useful in speeding up the search time. Another least squares adjustment, which introduces the most likely ambiguity parameters as functional constraints, was performed to obtain the final solution.

Data of several baselines of different lengths observed under different ionospheric activities were analyzed to verify the validity of the developed technique. It was found that neglecting the physical correlations does not affect the estimated real ambiguity parameters significantly. However, at the same probability level, the size of the confidence hyperellipsoid is smaller without the physical correlations. If the physical correlations were included, a longer data length is required for the ambiguity parameters to be resolved at a high probability level. As the sampling interval increases, resolving the ambiguity parameters requires more or less the same data length whether the physical correlations were included or not. This situation was faced with the 90 km baseline where the same data length (180 minutes) was required to resolve the ambiguities at the 95% probability level in the cases of neglecting or including the physical correlations.

In all cases, neglecting the physical correlations leads to smaller standard deviations than those obtained with physical correlations included. In other words, neglecting the physical correlations yields an overly optimistic covariance matrix for the estimated

parameters. For this reason, some of the available GPS software packages scale the resulting optimistic covariance matrix to compensate for neglecting the physical correlation. Two baselines of lengths 13 and 55 km were processed using DIFGPS with physical correlations included and the Ashtech software GPPS 5.0. It was shown that the ratio between the resulting standard deviations obtained from GPPS exceeds the corresponding ones obtained from DIFGPS by a factor of two or more. For this reason it is very important to include the physical correlations in any software package and not to rely on using a scale factor.

As the temporal physical correlations may be described by an exponential function, it was expected that, without physical correlations included, using a large sampling interval can lead to a more realistic covariance matrix. A 13 km baseline was processed using sampling intervals varying from 20 seconds up to 10 minutes. It was found that if the physical correlations included, small variations occur. However, without physical correlations, the standard deviations were much smaller than the ones obtained with physical correlations included. As the sampling interval increases the standard deviations obtained without physical correlations tend to be more realistic. For this particular baseline, if a 10 minute sampling interval was used, the difference between each component of the standard deviations obtained with and without physical correlations included is 1 mm.

The effect of varying the correlation time on the obtained covariance matrix was also tested. A 13 km baseline was processed using two different correlation times. The first correlation time was 263 seconds and corresponds to the general covariance function (Table 3.4) while the second one was 341 seconds and corresponds to the covariance function for the class of baselines in the range from 10 to 20 km. An increase of about 20% in the standard deviations was obtained when using a correlation time of 341 seconds. However, as there is no particular trend shown for the correlation times as a

function of the baseline length, it is more appropriate to use a general covariance function which is valid for any baseline length in the range up to 100 km.

7.2 Recommended Future Work

Further research is needed in the following areas:

- In this investigation, all the analyses were performed using a zero cut-off angle. Testing the effect of other cut-off angles on the resulting empirical covariance model is recommended.
- It was shown that sampling interval is expected to affect the results of the ambiguity resolution and the accuracy estimation if the physical correlations are neglected. For this reason, tests of the best sampling interval using a sufficient number of baselines so that neglecting the physical correlation may be considered negligible is recommended.
- Further study needs to be done on the effect of varying the correlation time on the accuracy estimation using a sufficient number of baselines.
- In this investigation, the resulting adjustment residuals used to model the temporal physical correlations were based on modelling the tropospheric delay using the Hopfield model. No ionospheric modelling was done. Modelling the ionospheric delay using an empirical model and testing whether the developed empirical covariance model will be affected is recommended.
- In this investigation the unmodelled tropospheric and ionospheric delays were accounted for stochastically through empirical covariance function. The development of an empirical covariance function to account for the multipath effect using short baselines of several meters apart is recommended.

REFERENCES

- Abidin, H. Z. (1992). *Computational and Geometrical Aspects of on-the-Fly Ambiguity Resolution*. Ph.D. dissertation, Department of Surveying Engineering Technical Report No. 164, University of New Brunswick, Fredericton, New Brunswick, Canada, 290 pp.
- Ashtech, Inc. (1993). *GPPS 5.0 Geodetic Postprocessing Software Manual*, Ashtech, Inc., Sunnyvale, California, USA.
- Bendat, J.S. and A.G. Piersol (1986). *Random Data: Analysis and Measurement Procedures*. 2nd Edition. John Wiley & Sons.
- Beutler, G., D. Davidson, R. Langley, R. Santerre, P. Vanicek, and D. Wells (1984). "Some Theoretical and Practical Aspects of the Geodetic Positioning Using Carrier Phase Difference Observations of GPS Satellites." TR # 109, Department of Surveying Engineering, University of New Brunswick, Canada.
- Beutler, G., W. Gurtner, M. Rothacher, U. Wild, and E. Frei (1989). "Relative Static Positioning With the Global Positioning System: Basic Technical Considerations." *Proceedings of the International Association of Geodesy No. 102 Global Positioning System: An Overview*, Edinburgh, Scotland, 7-8 August, Springer Verlag, New York, pp. 17-26.

- Biacs, Z. F., E. J. Krakiwsky, and D. Lapucha (1990). "Reliability Analysis of Phase Observations in GPS Baseline Estimation." *Journal of Surveying Engineering*, Volume 116, No. 4, pp. 204-224.
- Box, G. P. and G. M. Jenkins (1970). *Time Series Analysis Forecasting and Control*. Holden-Day, San Francisco, California.
- Brown, R. and P. Hwang (1983). "A Kalman filter approach to precision GPS geodesy." *Navigation*, vol 30, No. 4.
- Brunner, F. and W. Welsch (1993). "Effect of the Troposphere on GPS Measurements." *GPS World*, Volume , Number , pp. 42-51.
- Craymer, M.R., D.E. Wells, P. Vanicek, and R.L. Devlin (1990). "Specifications for Urban GPS Surveys." *Surveying and Land Information Systems*, Volume 50, Number 4, pp. 251-259.
- Craymer, M.R. and N. Beck (1992). "Session Versus Single-Baseline GPS Processing." *Proceedings of ION GPS-92, Fifth International Technical Meeting of the Satellite Division of the Institute of Navigation*, Albuquerque, New Mexico, 16-18 September.
- Ebner, H., R. Hoessler, and D. Joos (1984). "Random processes and their application to linear problems." *Manuscripta geodaetica*, vol. 9, pp. 21-43.
- El-Rabbany, A. (1991). "Optimal Considerations of the Covariance Matrix in GPS Positioning." Ph.D. Research Proposal, Department of Surveying Engineering, University of New Brunswick, Canada.

- El-Rabbany, A. and A. Kleusberg (1992). "Physical Correlation in GPS Differential Positioning." *Proceedings of the 6th International Geodetic Symposium on Satellite Positioning*, 17-20 March, Columbus, Ohio, USA.
- El-Rabbany, A. and A. Kleusberg (1993a). "Modeling Temporal Correlations in GPS Differential Positioning." Presented at the European Geophysical Society XVIII General Assembly, 3-7 May, Wiesbaden, Germany.
- El-Rabbany, A. and A. Kleusberg (1993b). "Efficient Algorithm for the Inverse of the Fully Populated Covariance Matrix in GPS Differential Positioning." Presented at the European Geophysical Society XVIII General Assembly, 3-7 May, Wiesbaden, Germany.
- El-Rabbany, A. and A. Kleusberg (1993c). "Improved Accuracy Estimation of Differential GPS: Theory and Results." Paper presented at the ION GPS-93, *Sixth International Technical Meeting of the Satellite Division of the Institute of Navigation*, Salt Lake City, Utah, 22-24 September.
- Erickson, C. (1992). "An Analysis of Ambiguity Resolution Techniques for Rapid Static GPS Surveys Using Single Frequency Data." *Proceedings of ION GPS-92, Fifth International Technical Meeting of the Satellite Division of the Institute of Navigation*, Albuquerque, New Mexico, 16-18 September.
- Evans, A. (1986). "Comparison of GPS Pseudorange and Biased Doppler Range Measurements to Demonstrate Signal Multipath Effect." *Proceedings of the Fourth International Geodetic Symposium on Satellite Positioning*, Austin, Tx, 28 April to May 2, pp. 573-587.
- Frei, E. and G. Beutler (1989). "Some considerations concerning an adaptive optimized technique to resolve the initial phase ambiguities for static and kinematic GPS

- surveying techniques." *Proceedings of the 5th International Geodetic Symposium on Satellite Positioning*, Las Cruces, NM, 13-17 March, pp. 671-686.
- Frei, E. and G. Beutler (1990). "Rapid Static Positioning Based on the Fast Ambiguity Resolution Approach "FARA": Theory and Results." *Manuscripta geodaetica*, vol. 15, pp. 325-356.
- Gelb, A. (1974). *Applied Optimal Control*. MIT Press.
- Georgiadou, Y. and A. Kleusberg (1989). "On Carrier Signal Multipath Effects in Relative GPS Positioning." *Manuscripta Geodaetica*, Vol. 14, pp. 143-148.
- Georgiadou, Y, I. Webster, A. El-Rabbany, and A. Kleusberg (1990). "Analysis of the 1989 Vancouver Island GPS Survey Data." Final contract report prepared for Pacific Geoscience Centre of the Geological Survey of Canada. Geodetic Research Laboratory, University of New Brunswick, Fredericton, N.B., Canada.
- Georgiadou, Y. and K. Doucet (1990). "The Issue of Selective Availability." *GPS World*, Volume 1, Number 5, pp. 53-56.
- Hatch, R. (1989). "Ambiguity resolution in the fast lane." *Proceedings of the ION GPS-89, Second International Technical Meeting of the Satellite Division of the Institute of Navigation*, Colorado Springs, CO, 27-29 September, 45-50.
- Hatch, R. (1990). "Instantaneous Ambiguity Resolution." *Proceedings of the International Association of Geodesy No. 107 Kinematic Systems in Geodesy, Surveying, and Remote Sensing*, Banff, Canada, 10-13 September, Springer Verlag, New York.
- Hofmann-Wellenhof, B., H. Lichtenegger, and J. Collins (1992). *Global Positioning System Theory and Practice*. Springer-Verlag.

Jenkins, G. M. and D. G. Watts (1968). *Spectral Analysis and its Applications*.
HOLDEN-DAY.

Jong, C.D. (1991). "GPS - Satellite Orbits and Atmospheric Effects." Faculty of
Geodetic Engineering, Department of Mathematical and Physical Geodesy,
Report No. 91.1, Delft University of Technology, The Netherlands.

Kleusberg, A., and L. Wanninger (1987). "Analysis of the Juan de Fuca GPS Survey
1986." Technical Report No. 127, Department of Surveying Engineering,
University of New Brunswick, Fredericton, N.B., Canada.

Kleusberg, A., Y. Georgiadou, F. van Heuvel and P. Héroux (1989). "Single and Dual
Frequency GPS Data Processing with DIPOP 2.1." Department of Surveying
Engineering Technical Memorandum TM-21, University of New Brunswick,
Fredericton, N.B., Canada.

Kleusberg, A. (1990). "A review of kinematic and static GPS surveying procedures."
*Proceedings of the Second International Symposium on Precise Positioning with
the Global Positioning System*, Ottawa, Canada, 3-7 September.

Kleusberg, A. and R. Langley (1990). "The Limitations of GPS." *GPS World*, Volume ,
Number 2, pp. 50-52.

Kleusberg, A. (1992). "GPS Positioning." Unpublished Lecture Notes, Department of
Surveying Engineering, University of New Brunswick, Fredericton, Canada.

Klobuchar, J. (1991). "Ionospheric Effects on GPS." *GPS World*, Volume 2, Number 4,
pp. 48-51.

Lachapelle, G. (1990). "GPS Observations and Error Sources for Kinematic
Positioning." *Proceedings of the International Association of Geodesy No. 107*

Kinematic Systems in Geodesy, Surveying, and Remote Sensing, Banff, Canada, 10-13 September, Springer Verlag, New York, pp. 17-26.

Langley, R., G. Beutler, D. Delikaraoglou, R. Santerre, P. Vanicek, and D. Wells (1984). Studies in the application of the Global Positioning System. TR # 108, Department of Surveying Engineering, University of New Brunswick, Canada.

Langley, R. (1990). "Why is the GPS Signal So Complex." *GPS World*, Volume 1, Number 3, pp. 56-59.

Langley, R. (1991a). "The GPS Receiver: An Introduction." *GPS World*, Volume 2, Number 1, pp. 50-53.

Langley, R. (1991b). "The Orbits of GPS Satellites." *GPS World*, Volume 2, Number 3, pp. 50-53.

Langley, R. (1991c). "The Mathematics of GPS." *GPS World*, Volume 2, Number 7, pp. 45-50.

Langley, R. (1993). "The GPS Observables." *GPS World*, Volume 4, Number 4, pp. 52-59.

Loomis, P., L. Sheynblat, and T. Mueller (1991). "Differential GPS Network Design." *Proceedings of ION GPS-91, Fourth International Technical Meeting of the Satellite Division of the Institute of Navigation*, Albuquerque, New Mexico, 11-13 September.

Mader, G. (1990). "Ambiguity Function Technique for GPS Phase Initialization and Kinematic Solution." *Proceedings of the Second International Symposium on Precise Positioning with the Global Positioning System*, Ottawa, Canada, 3-7 September.

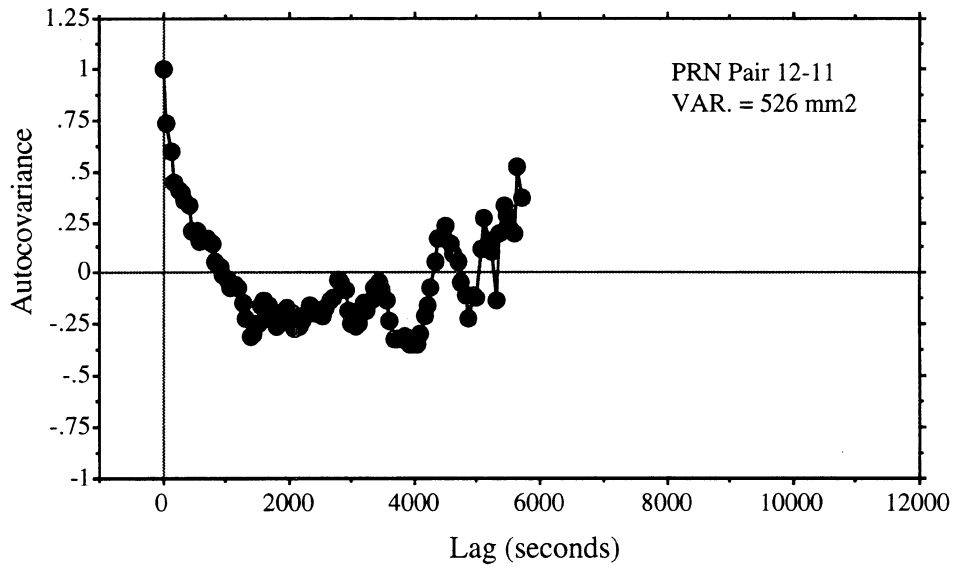
- Marple, S. (1987). *Digital Spectral Analysis*. Prentice-Hall, Inc., Englewood Cliffs, New Jersey 07632.
- Mikhail, E. (1976). *Observations and least squares*. University press of America.
- Montgomery, H. (1993a). "Nonprecision Approaches, GPS in IVHS, and New Federal Policy." *GPS World*, Volume 4, Number 3, pp. 16-20.
- Otens, R. and L. Enochson (1978). *Applied Time Series Analysis*. John Wiley & Sons, Inc.
- Pankratz, A. (1983). *Forecasting with Univariate Box-Jenkins Models, Concept and Cases*. John Wiley & Sons.
- Rothacher, M., G. Beutler, W. Gurtner, D. Schneider, A. Wiget, A. Geiger and H.-G. Kahle (1990). "The Role of the Atmosphere in Small GPS Networks." *Proceedings of the Second International Symposium on Precise Positioning with the Global Positioning System*, Ottawa, Canada, 3-7 September, pp. 581-598.
- Santerre, R. (1989). *GPS Satellite Sky Distribution: Impact on the Propagation of Some Important Errors in Precise Relative Positioning*. Ph.D. dissertation, Department of Surveying Engineering Technical Report No. 145, University of New Brunswick, Fredericton, New Brunswick, Canada, 220 pp.
- Santerre, R., G. Beutler, and A. Geiger (1990). "GPS Error Analysis and Modelling." *Proceedings of the Second International Symposium on Precise Positioning with the Global Positioning System*, Ottawa, Canada, 3-7 September, pp. 356-372.
- Seeber, G. and G. Wubbena (1989). "Kinematic positioning with carrier phases and 'on the fly' ambiguity solution." *Proceedings of the 5th International Geodetic Symposium on Satellite Positioning*, Las Cruces, NM, 13-17 March, pp. 600-610.

- Tralli, D. and S. Lichten (1990). "Stochastic Estimation of Tropospheric Path Delays in Global Positioning System Geodetic measurements." *Bulletin Géodésique* , Volume 64, pp. 127-159.
- Vanicek, P., G. Beutler, A. Kleusberg, R. Langley, R. Santerre, and D. Wells (1985). "'DIPOP' Differential Positioning Program Package for the Global Positioning System." TR # 115, Department of Surveying Engineering, University of New Brunswick, Fredericton, Canada.
- Vanicek, P., and E.J. Krakiwsky (1986). *Geodesy: The Concepts*. Second Edition, North Holland, Amsterdam.
- Webster, I. and A. Kleusberg (1992). "Regional Modelling of the Ionosphere for Single Frequency Users of the Global Positioning System." *Proceedings of the 6th International Geodetic Symposium on Satellite Positioning*, 17-20 March, Columbus, Ohio, USA.
- Wells, D.E. and E.J. Krakiwsky (1971). "The Method of Least Squares." LN # 18, Department of Surveying Engineering, University of New Brunswick, Fredericton, Canada.
- Wells, D.E., P. Vanicek , and S. Pagiatakis (1985). "Least Squares Spectral Analysis Revisited." TR # 84, Department of Surveying Engineering, University of New Brunswick, Fredericton, Canada.
- Wells, D.E., N. Beck, D. Delikaraoglou, A. Kleusberg, E.J. Krakiwsky, G. Lachapelle, R.B. Langley, N. Nakiboglu, K.P. Schwarz, J.M. Tranquilla, and P. Vanicek (1987). *Guide to GPS Positioning.*, 2nd corrected printing. Canadian GPS Associates, Fredericton, N.B., Canada.

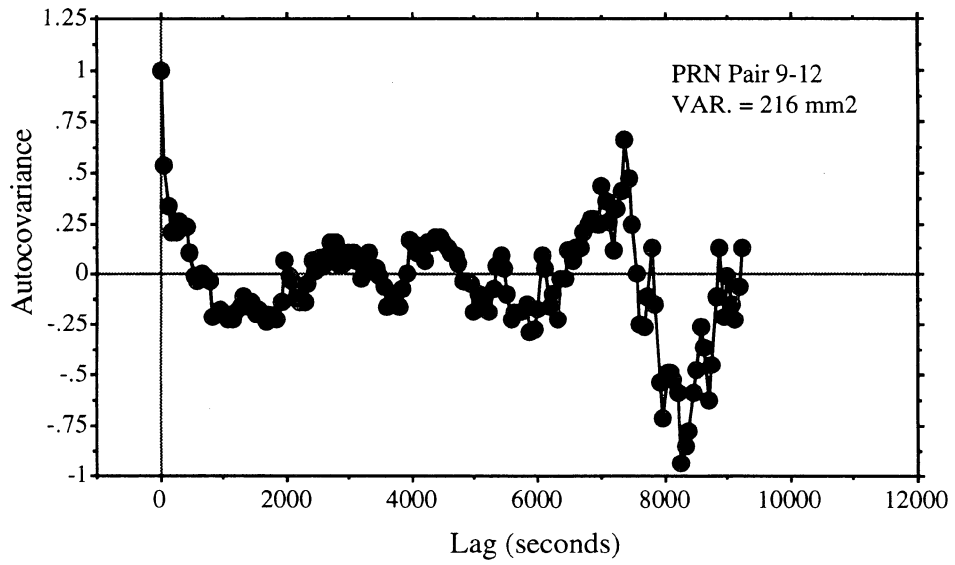
- Wells, D.E. (1990). "Functional Analysis and Adjustments." Unpublished Lecture Notes, Department of Surveying Engineering, University of New Brunswick, Fredericton, Canada.
- Wild, U., G. Beutler, S. Fankhauser, and W. Gurtner (1990). "Stochastic Properties of the Ionosphere Estimated From GPS Observations." *Proceedings of the Second International Symposium on Precise Positioning with the Global Positioning System*, Ottawa, Canada, 3-7 September, pp. 411-428.
- Wubben, G. (1989). "The GPS adjustment software package GEONAP, concepts and models." *Proceedings of the 5th International Geodetic Symposium on Satellite Positioning*, Las Cruces, NM, 13-17 March, pp. 452-461.

APPENDIX I

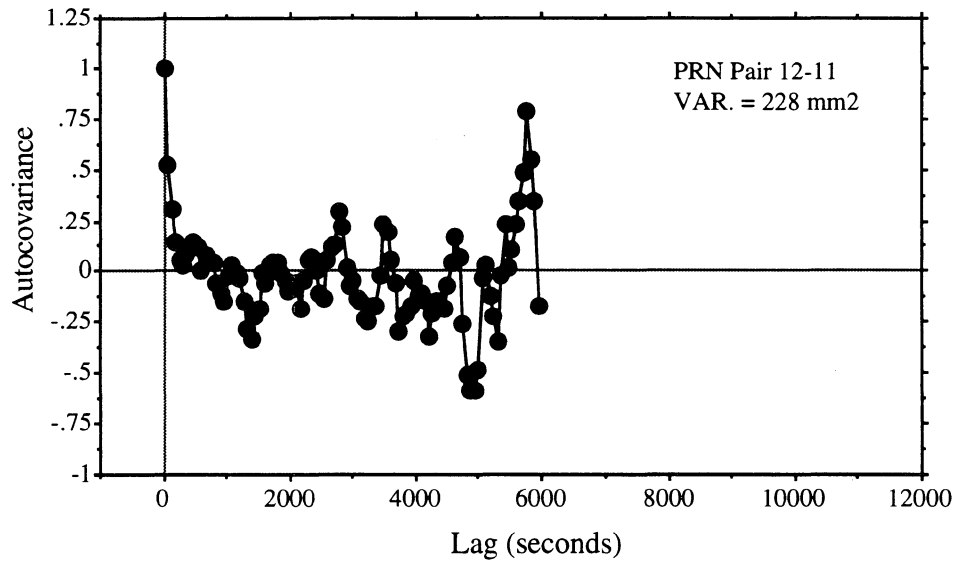
ESTIMATED AUTOCOVARANCE FUNCTIONS DUE TO RESIDUAL TROPOSPHERIC DELAYS



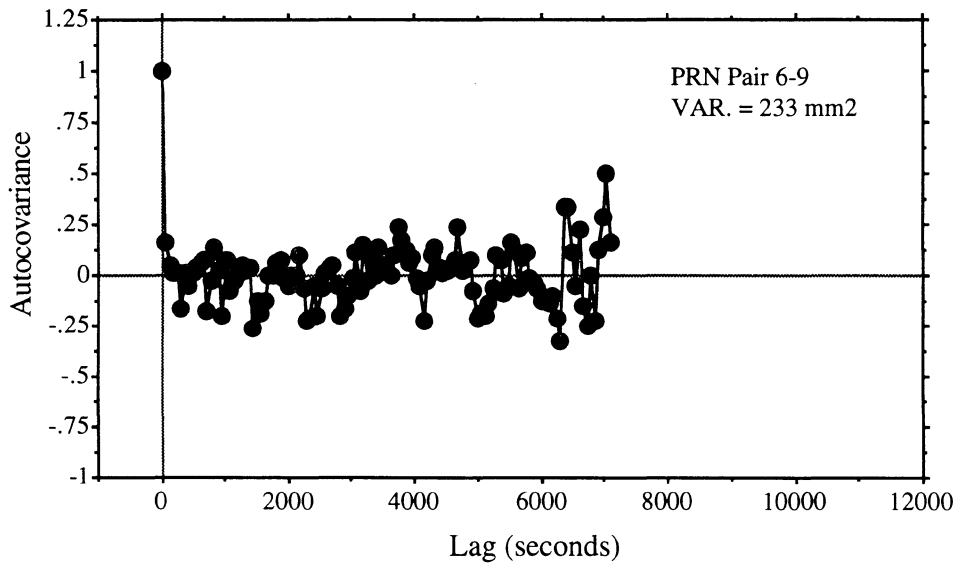
Estimated Autocovariance Function of the Nonlinear Residual
Tropospheric Delay for a 12 km Baseline



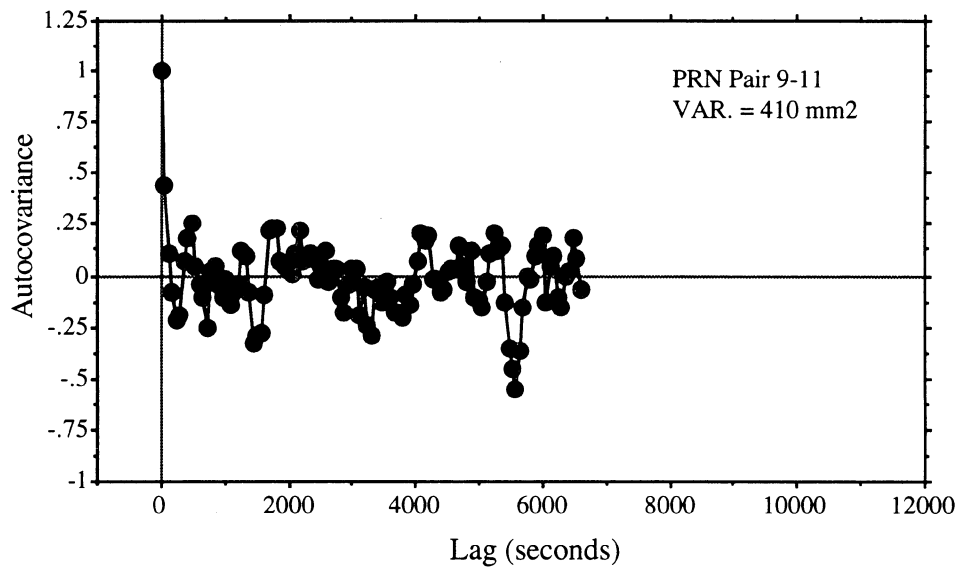
Estimated Autocovariance Function of the Nonlinear Residual
Tropospheric Delay for a 12 km Baseline



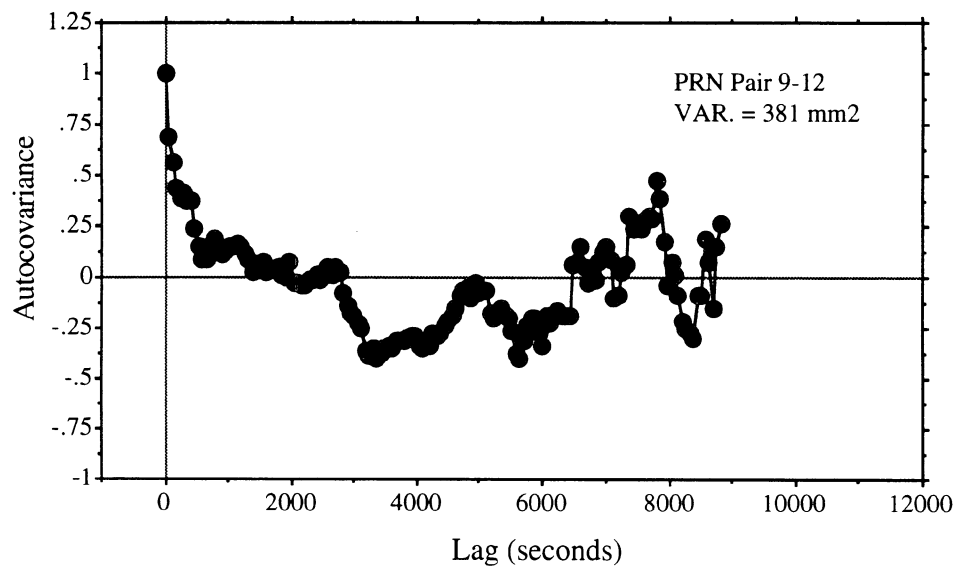
Estimated Autocovariance Function of the Nonlinear Residual
Tropospheric Delay for a 29 km Baseline



Estimated Autocovariance Function of the Nonlinear Residual
Tropospheric Delay for a 29 km Baseline



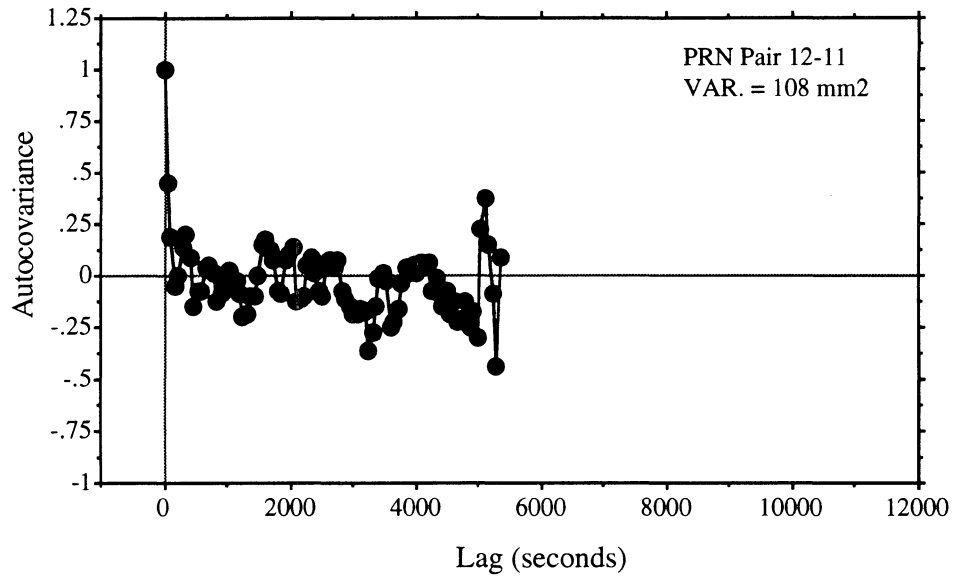
Estimated Autocovariance Function of the Nonlinear Residual
Tropospheric Delay for a 29 km Baseline



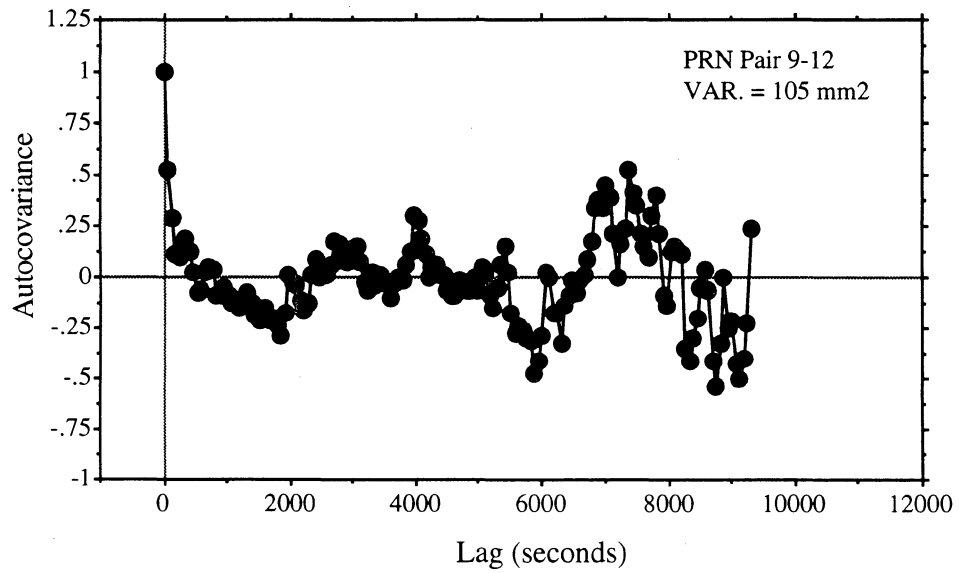
Estimated Autocovariance Function of the Nonlinear Residual
Tropospheric Delay for a 29 km Baseline

APPENDIX II

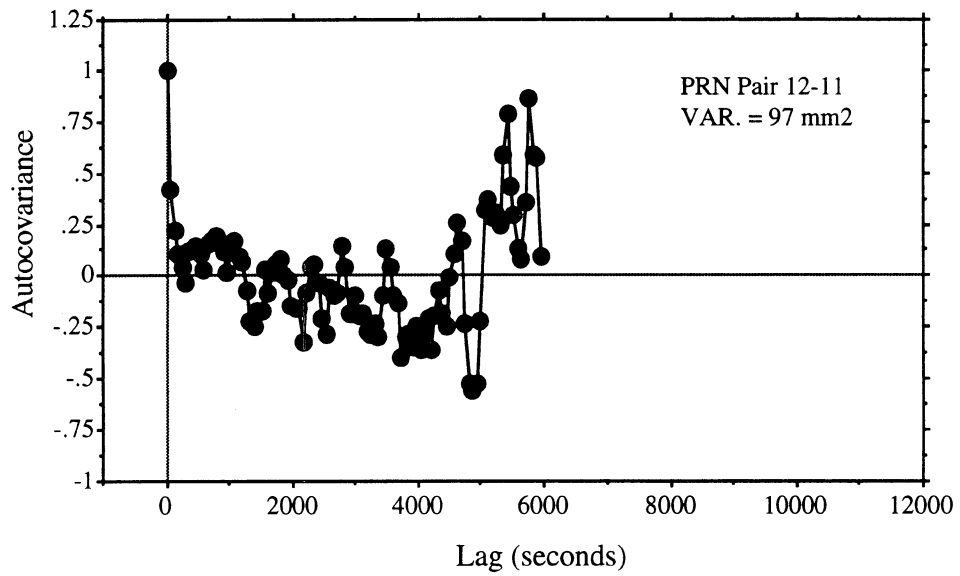
ESTIMATED AUTOCOVARIANCE FUNCTIONS DUE TO IONOSPHERIC DELAYS



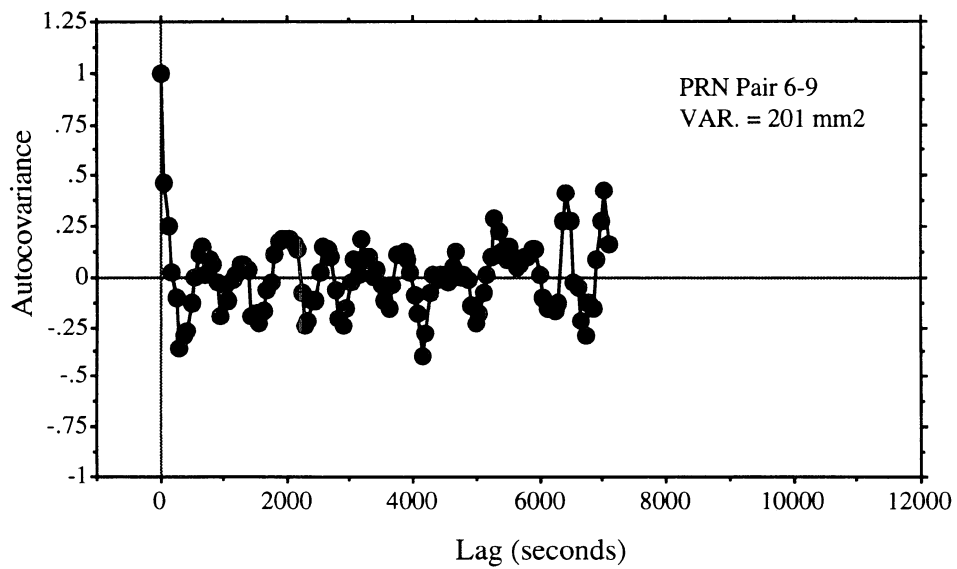
Estimated Autocovariance Function of the Nonlinear
Ionospheric Delay for a 12 km Baseline



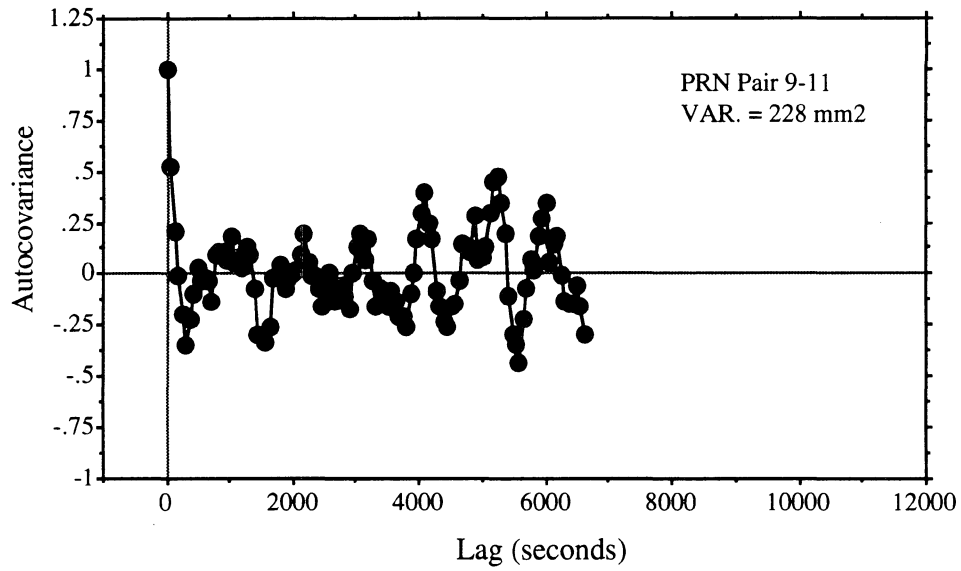
Estimated Autocovariance Function of the Nonlinear
Ionospheric Delay for a 12 km Baseline



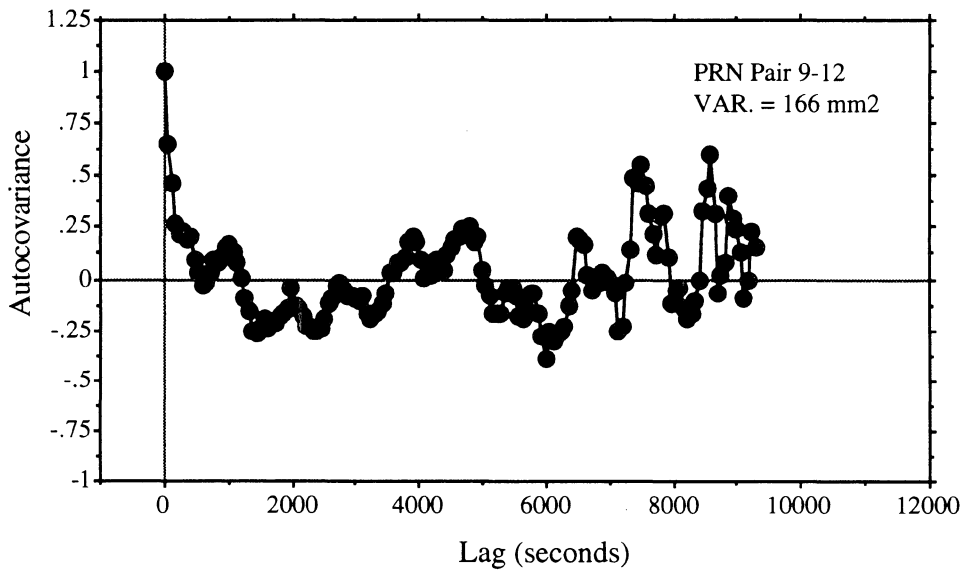
Estimated Autocovariance Function of the Nonlinear
Ionospheric Delay for a 29 km Baseline



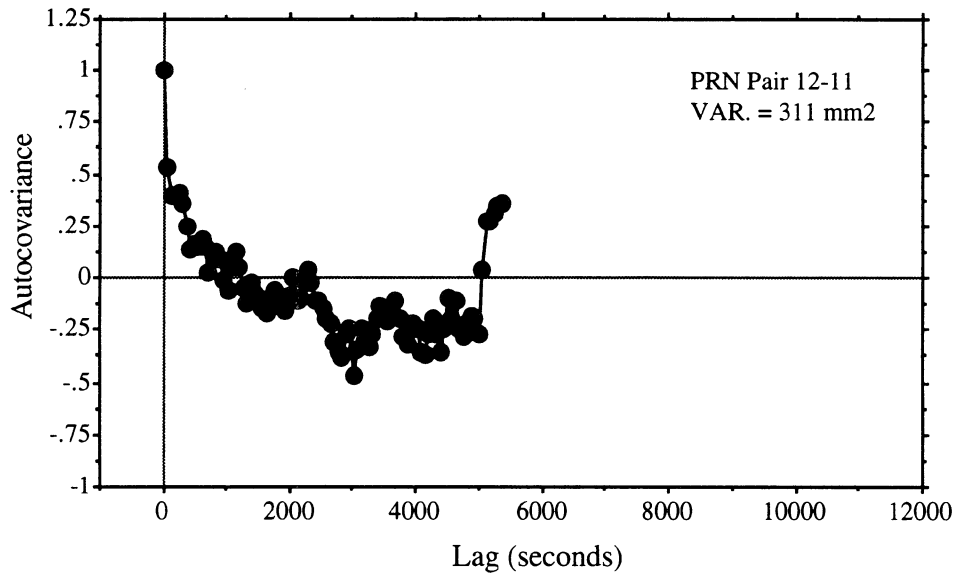
Estimated Autocovariance Function of the Nonlinear
Ionospheric Delay for a 29 km Baseline



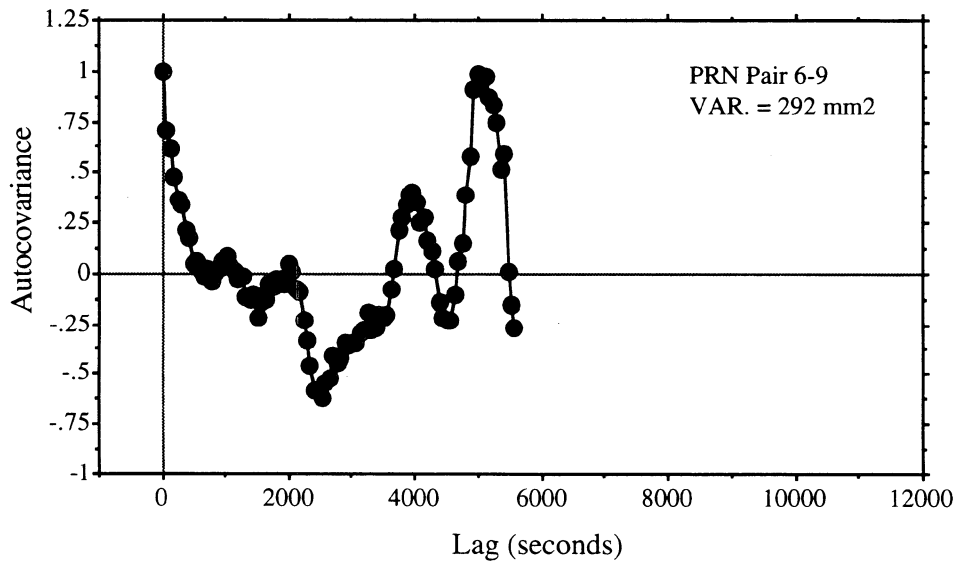
Estimated Autocovariance Function of the Nonlinear
Ionospheric Delay for a 29 km Baseline



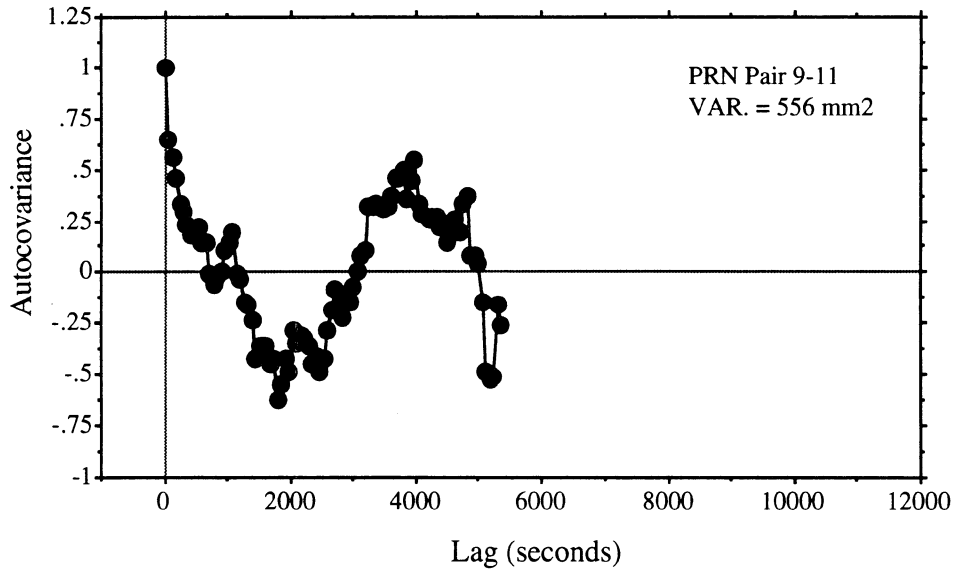
Estimated Autocovariance Function of the Nonlinear
Ionospheric Delay for a 29 km Baseline



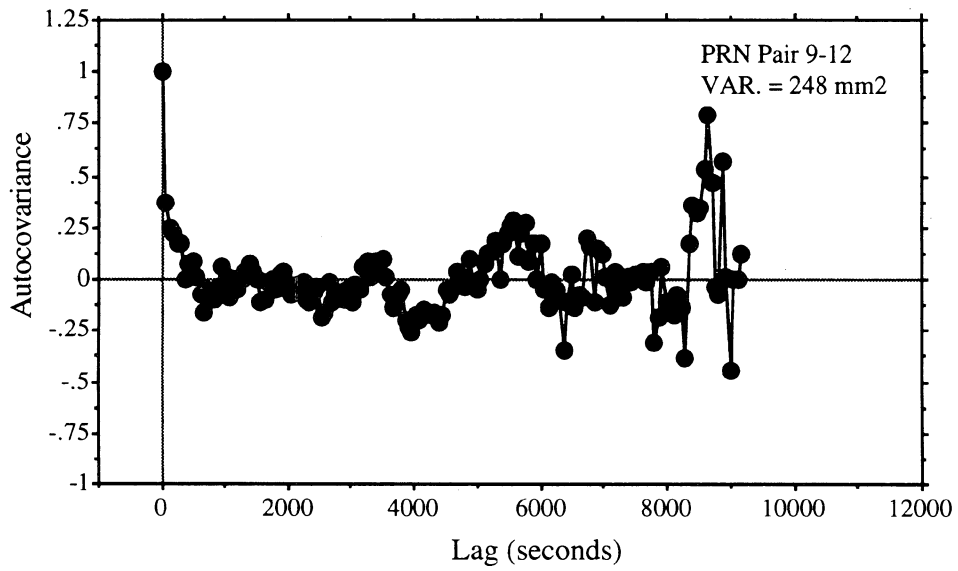
Estimated Autocovariance Function of the Nonlinear
Ionospheric Delay for an 81 km Baseline



Estimated Autocovariance Function of the Nonlinear
Ionospheric Delay for an 81 km Baseline



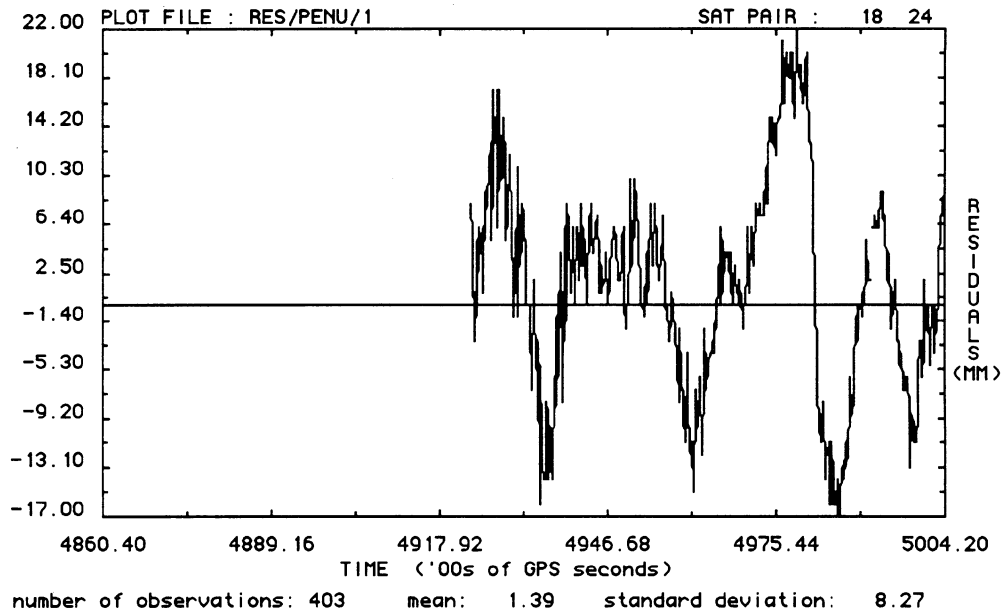
Estimated Autocovariance Function of the Nonlinear
Ionospheric Delay for an 81 km Baseline



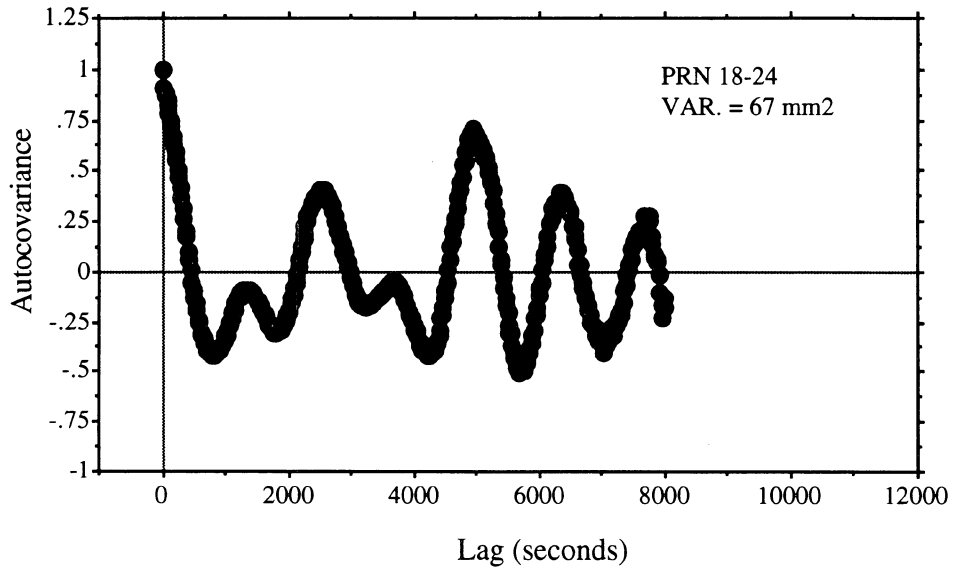
Estimated Autocovariance Function of the Nonlinear
Ionospheric Delay for an 81 km Baseline

APPENDIX III

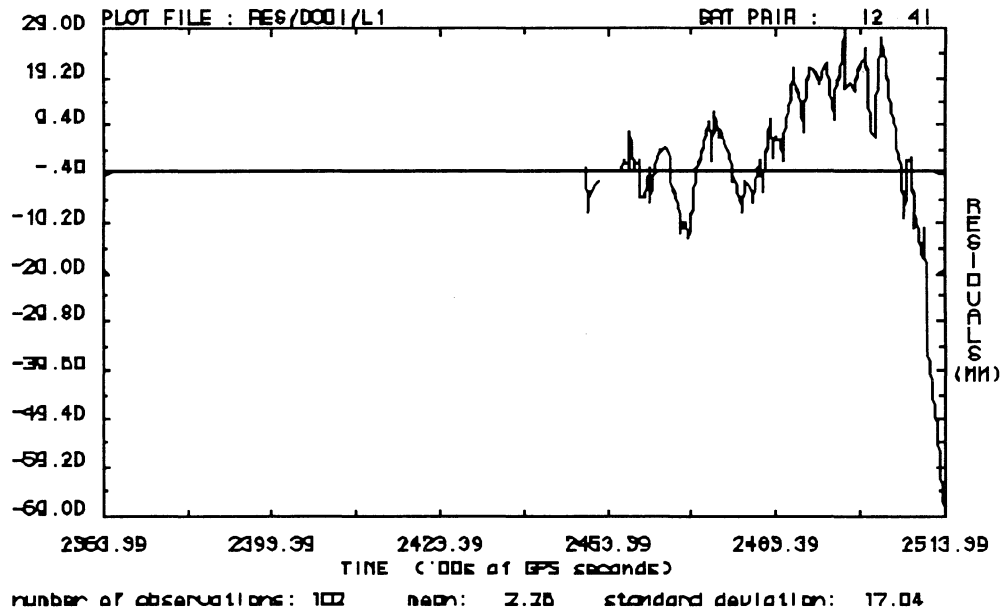
**ESTIMATED AUTOCOVARANCE FUNCTIONS FOR THE
ADJUSTMENT RESIDUALS**



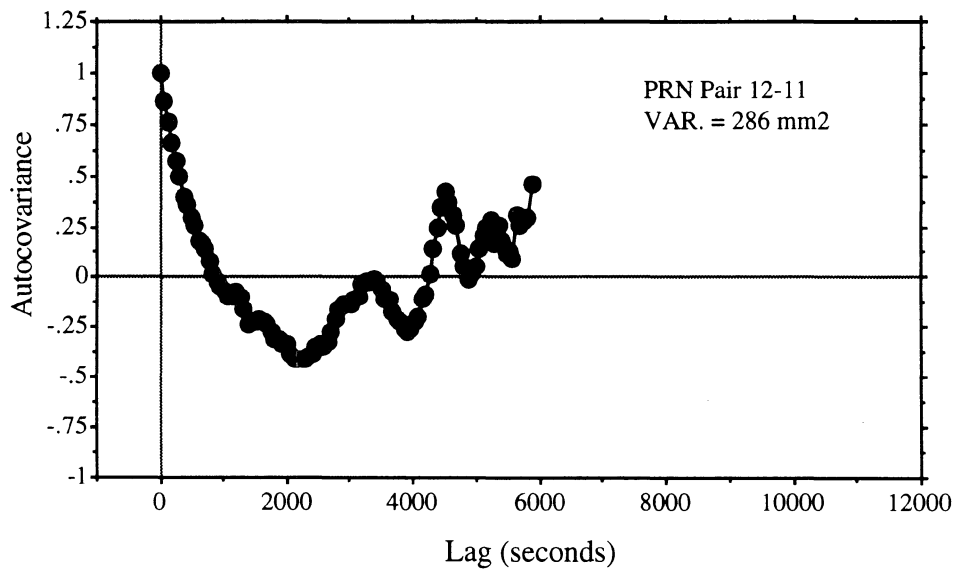
Carrier Phase Double Difference Residuals for a 4 km Baseline (L1)



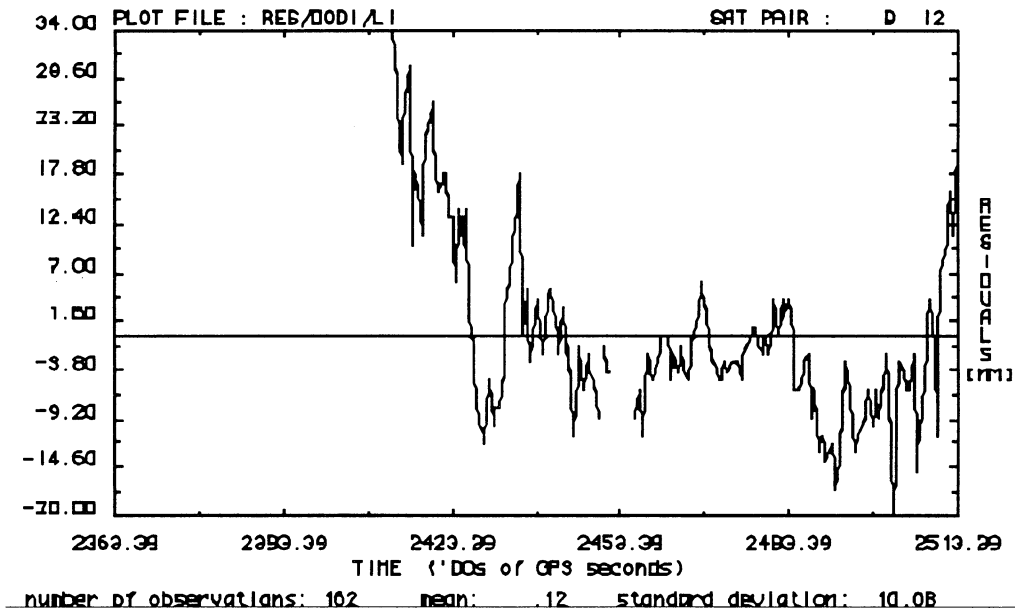
Estimated Autocovariance Function of the Carrier Phase Double Difference Residuals for a 4 km Baseline (L1)



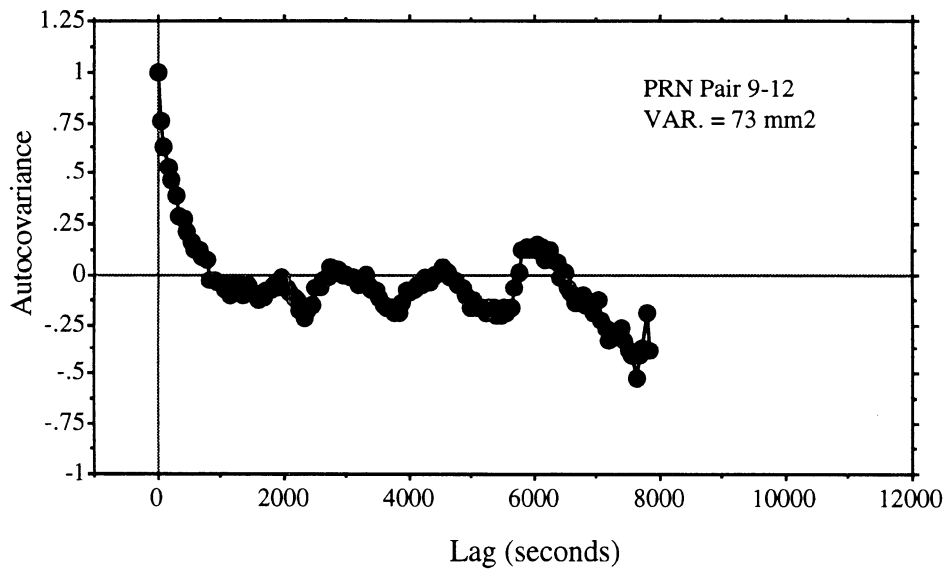
Carrier Phase Double Difference Residuals for a 12 km Baseline (L1)



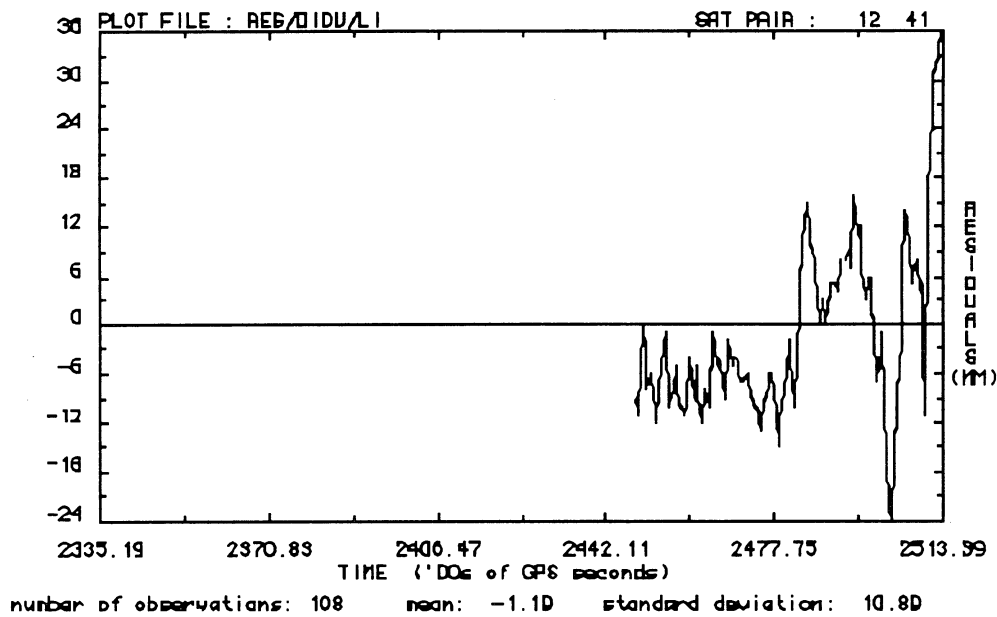
Estimated Autocovariance Function of the Carrier Phase Double Difference Residuals for a 12 km Baseline (L1)



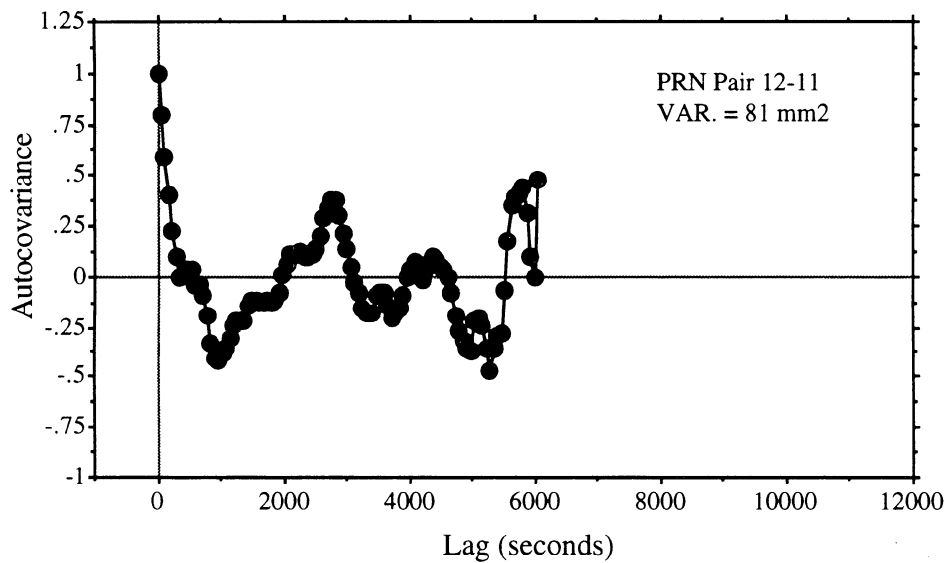
Carrier Phase Double Difference Residuals for a 12 km Baseline (L1)



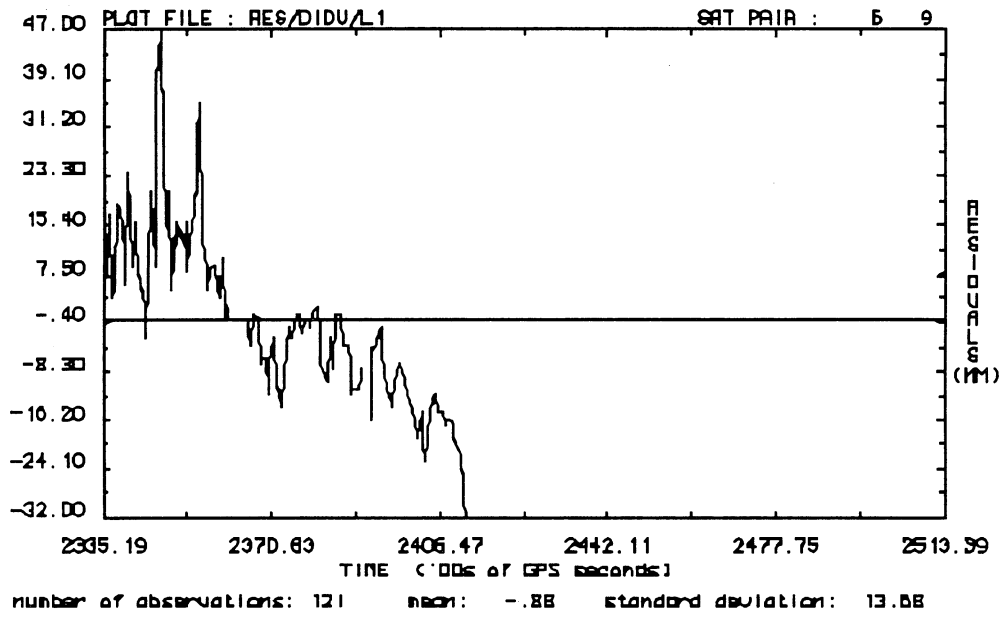
Estimated Autocovariance Function of the Carrier Phase Double Difference Residuals for a 12 km Baseline (L1)



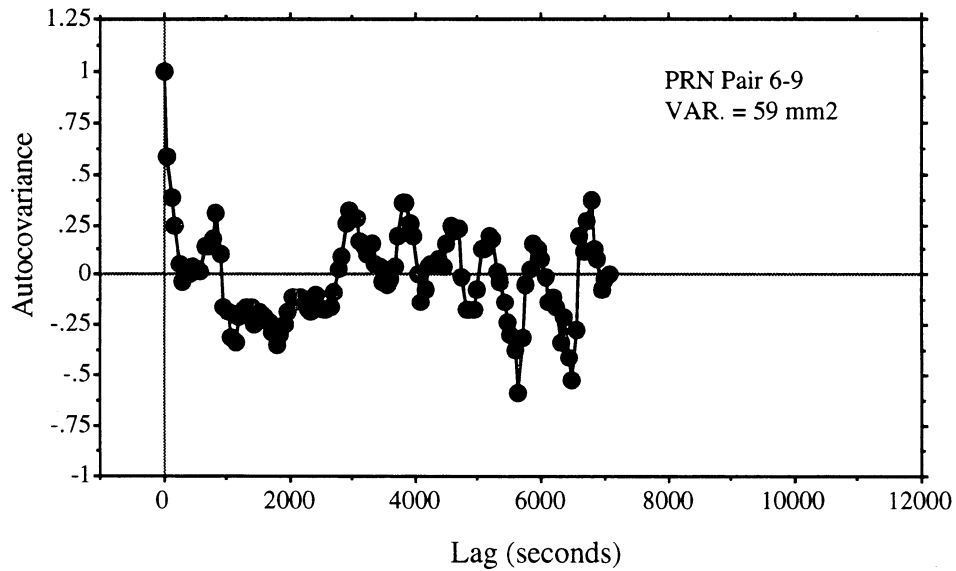
Carrier Phase Double Difference Residuals for a 29 km Baseline (L1)



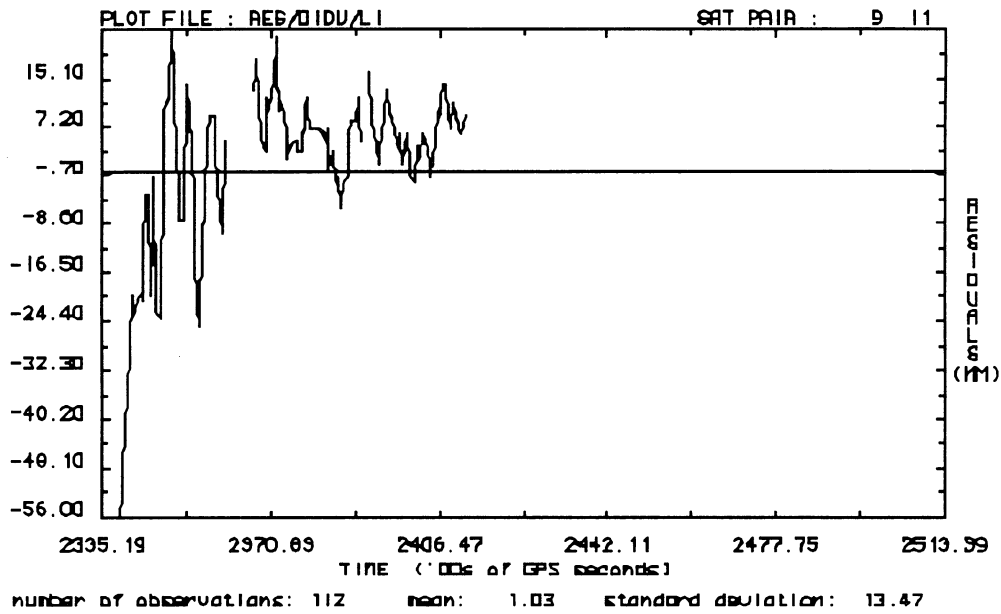
Estimated Autocovariance Function of the Carrier Phase Double Difference Residuals for a 29 km Baseline (L1)



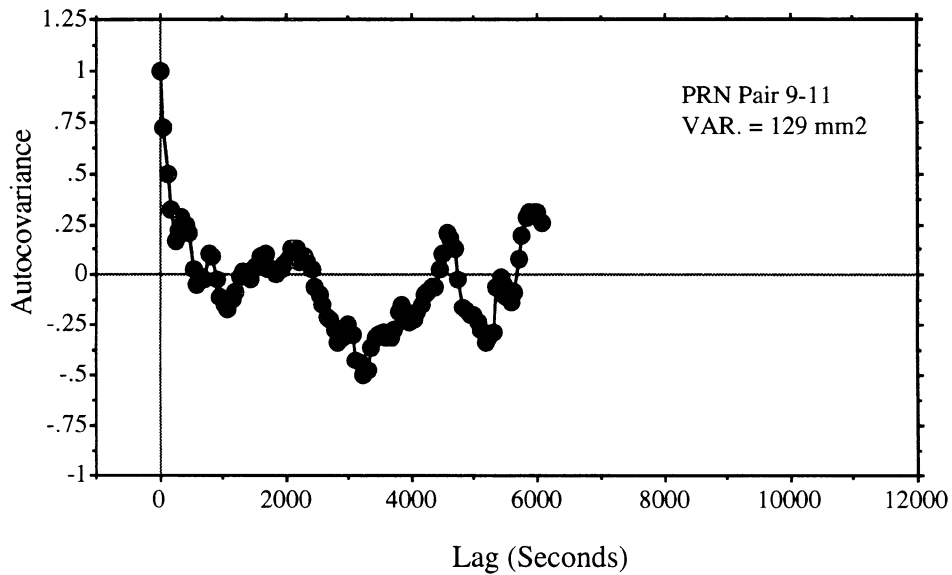
Carrier Phase Double Difference Residuals for a 29 km Baseline (L1)



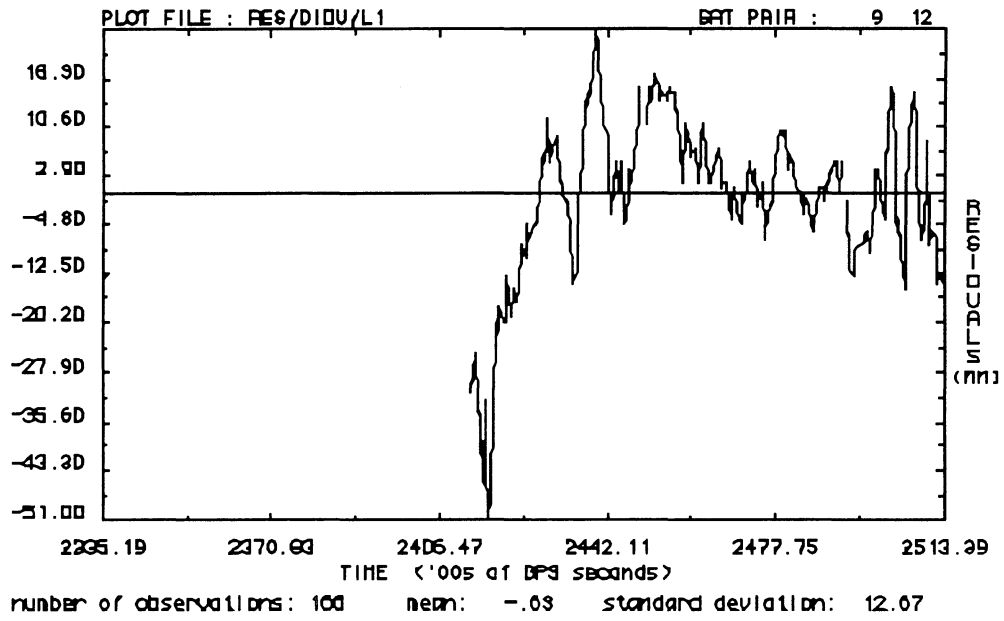
Estimated Autocovariance Function of the Carrier Phase Double Difference Residuals for a 29 km Baseline (L1)



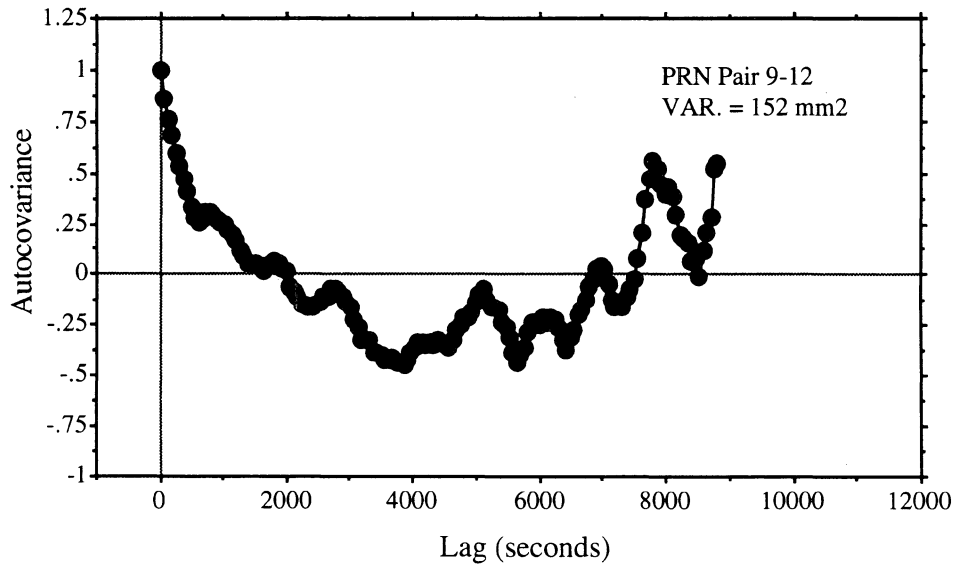
Carrier Phase Double Difference Residuals for a 29 km Baseline (L1)



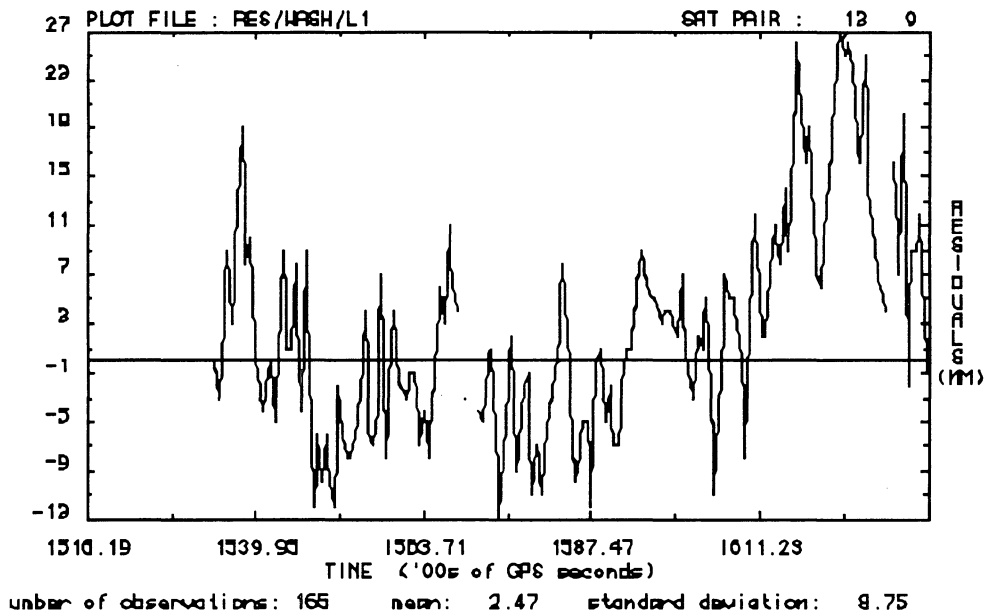
Estimated Autocovariance Function of the Carrier Phase Double Difference Residuals for a 29 km Baseline (L1)



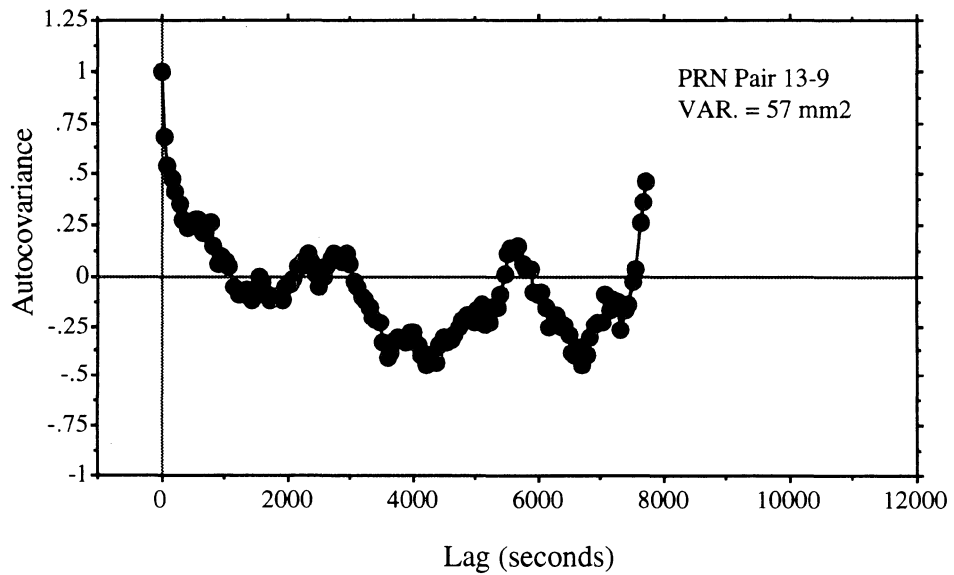
Carrier Phase Double Difference Residuals for a 29 km Baseline (L1)



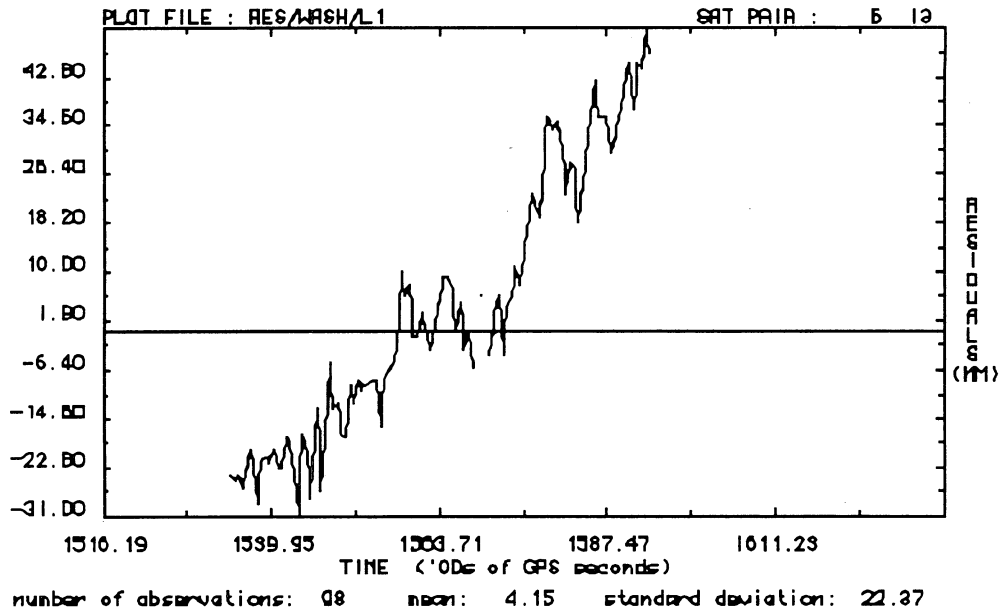
Estimated Autocovariance Function of the Carrier Phase Double Difference Residuals for a 29 km Baseline (L1)



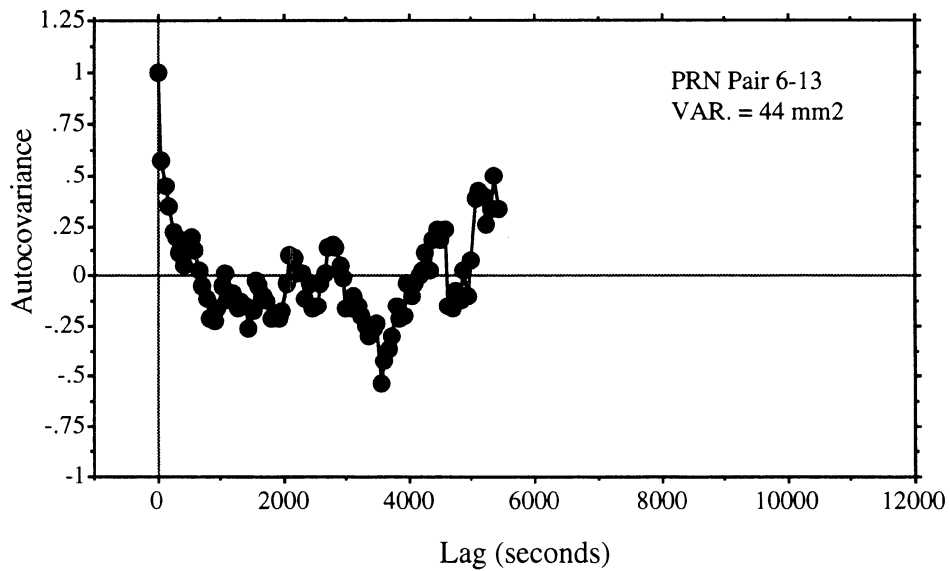
Carrier Phase Double Difference Residuals for a 50 km Baseline (L1)



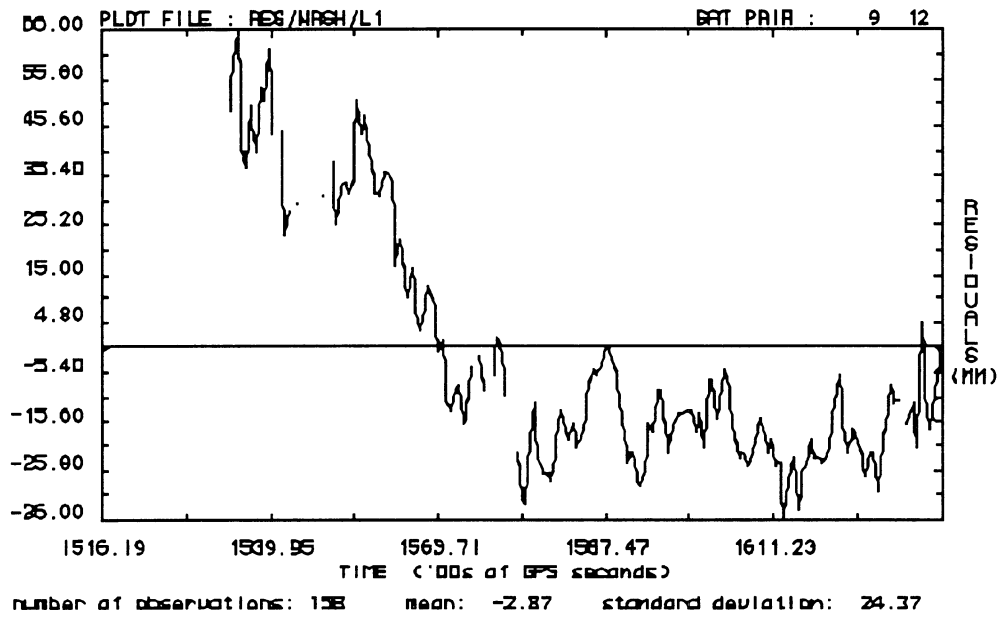
Estimated Autocovariance Function of the Carrier Phase Double Difference Residuals for a 50 km Baseline (L1)



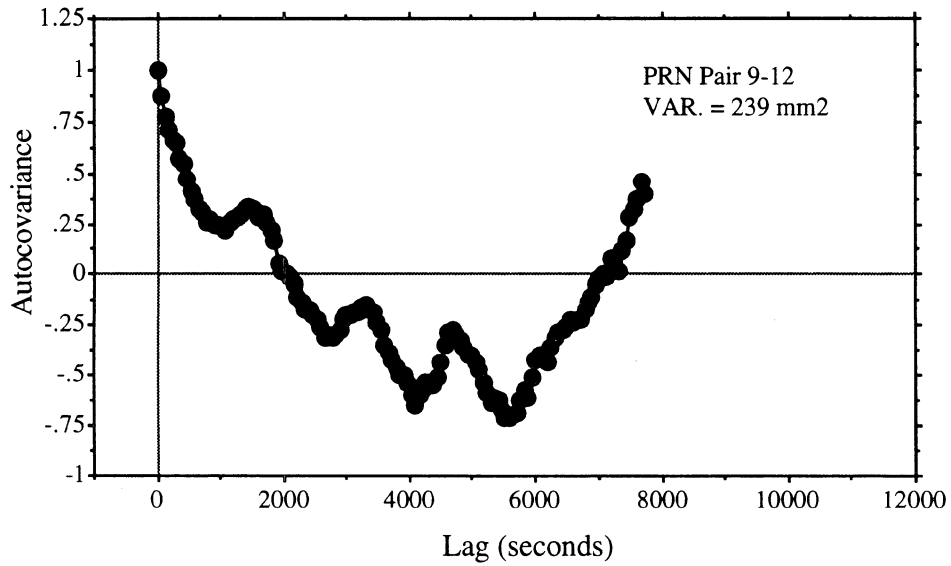
Carrier Phase Double Difference Residuals for a 50 km Baseline (L1)



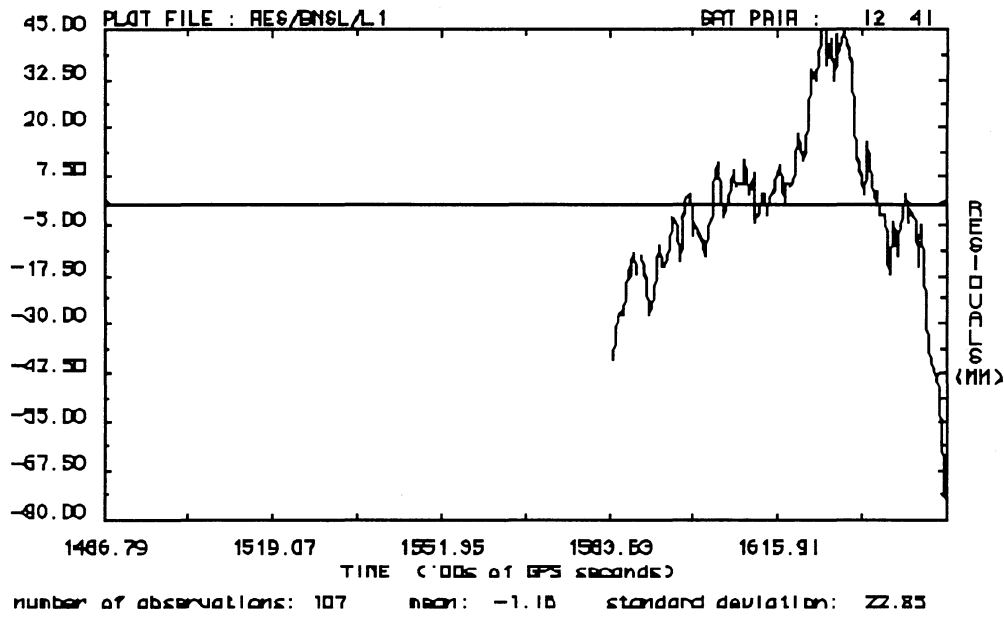
Estimated Autocovariance Function of the Carrier Phase Double Difference Residuals for a 50 km Baseline (L1)



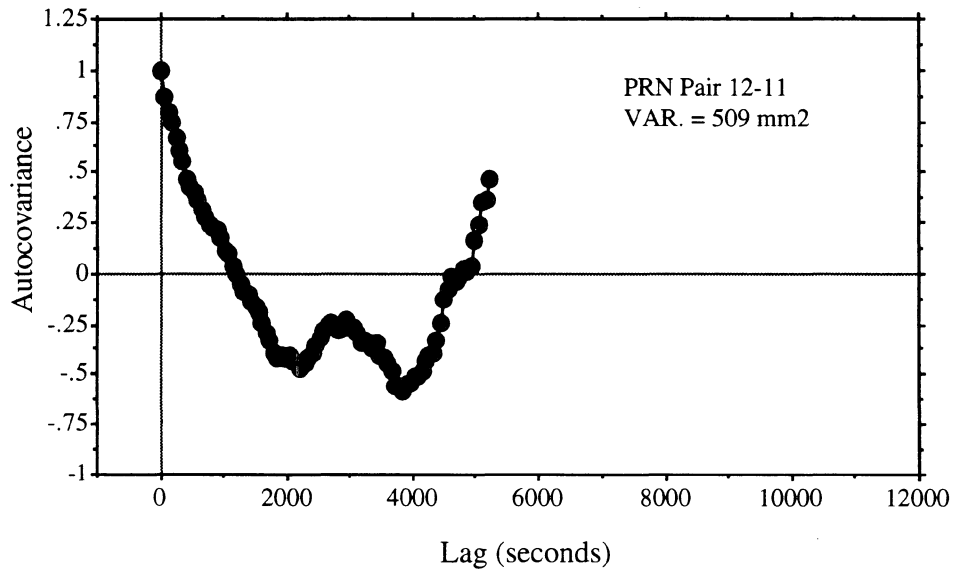
Carrier Phase Double Difference Residuals for a 50 km Baseline (L1)



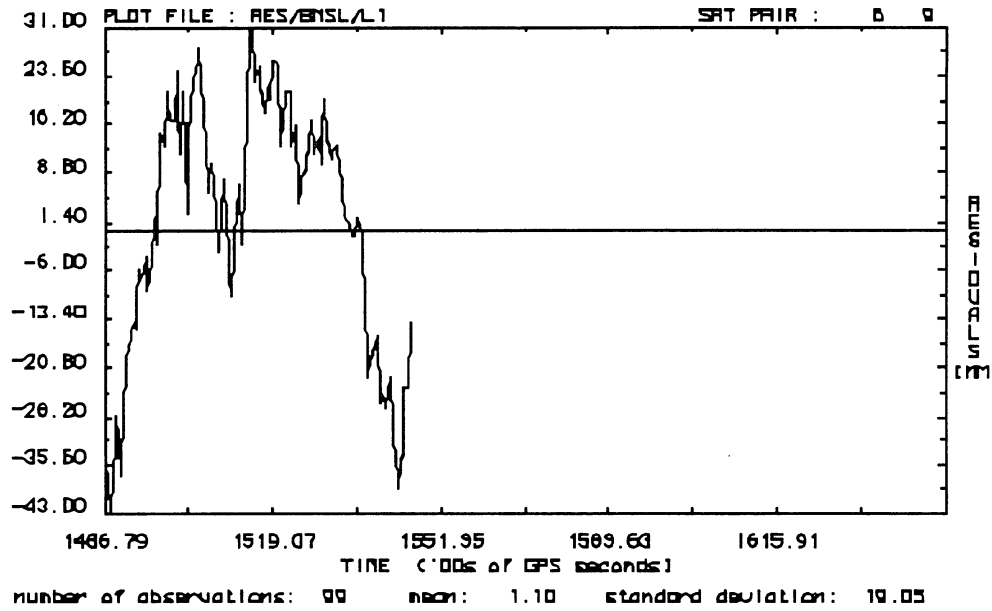
Estimated Autocovariance Function of the Carrier Phase Double Difference Residuals for a 50 km Baseline (L1)



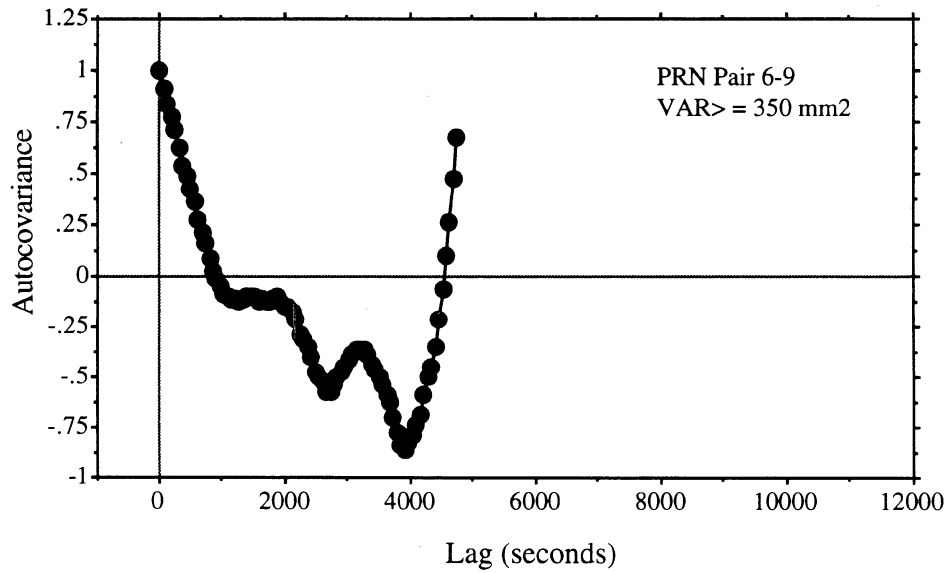
Carrier Phase Double Difference Residuals for an 81 km Baseline (L1)



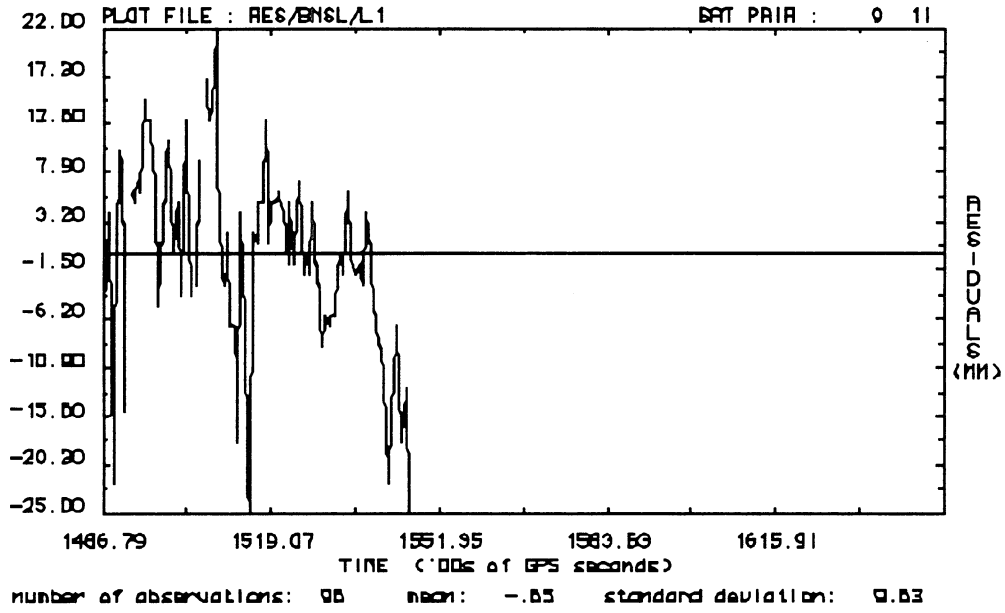
Estimated Autocovariance Function of the Carrier Phase Double Difference Residuals for an 81 km Baseline (L1)



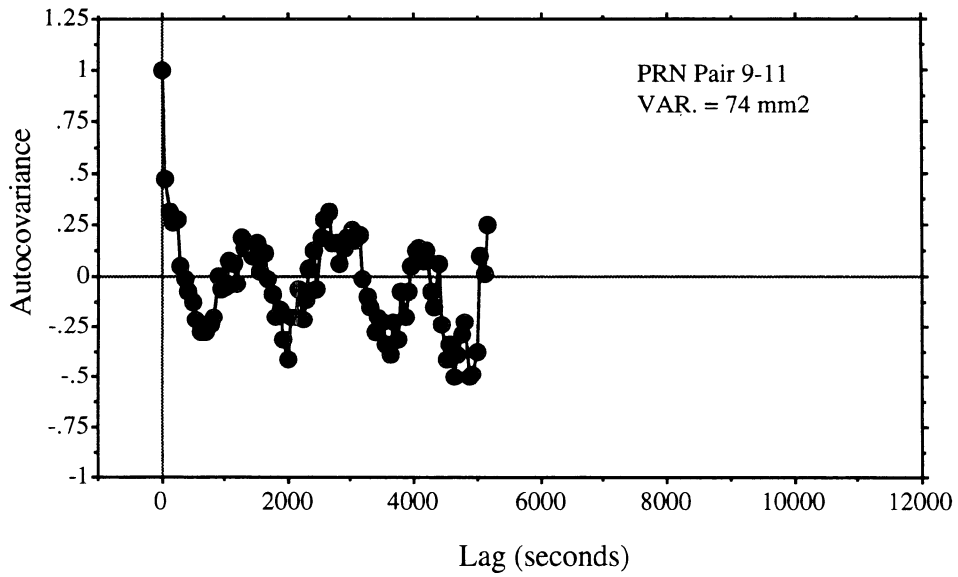
Carrier Phase Double Difference Residuals for an 81 km Baseline (L1)



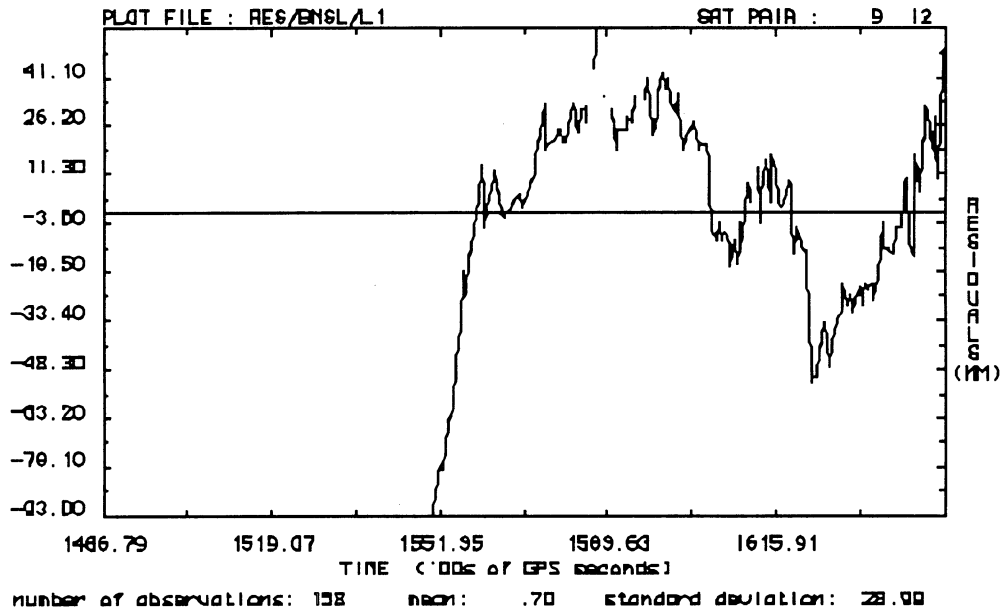
Estimated Autocovariance Function of the Carrier Phase Double Difference Residuals for an 81 km Baseline (L1)



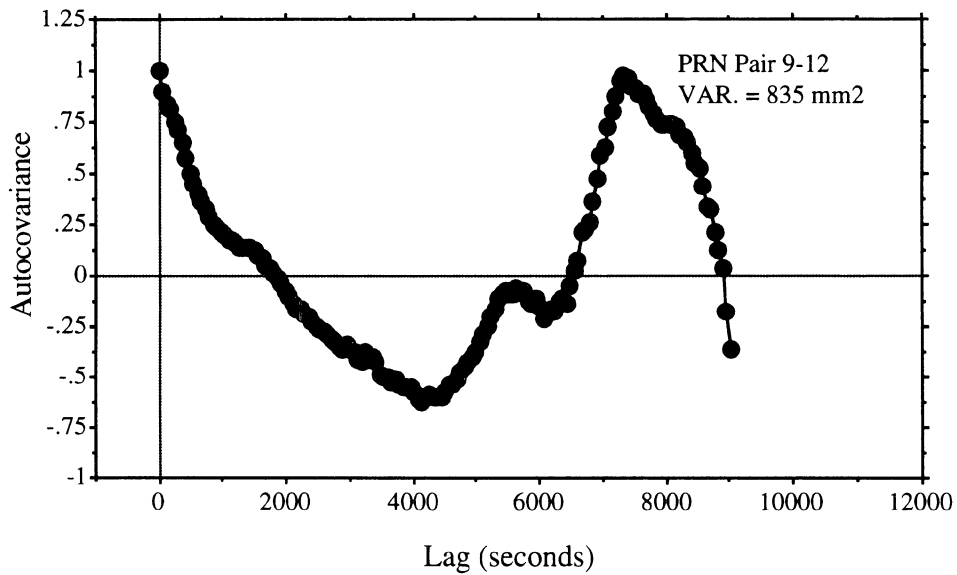
Carrier Phase Double Difference Residuals for an 81 km Baseline (L1)



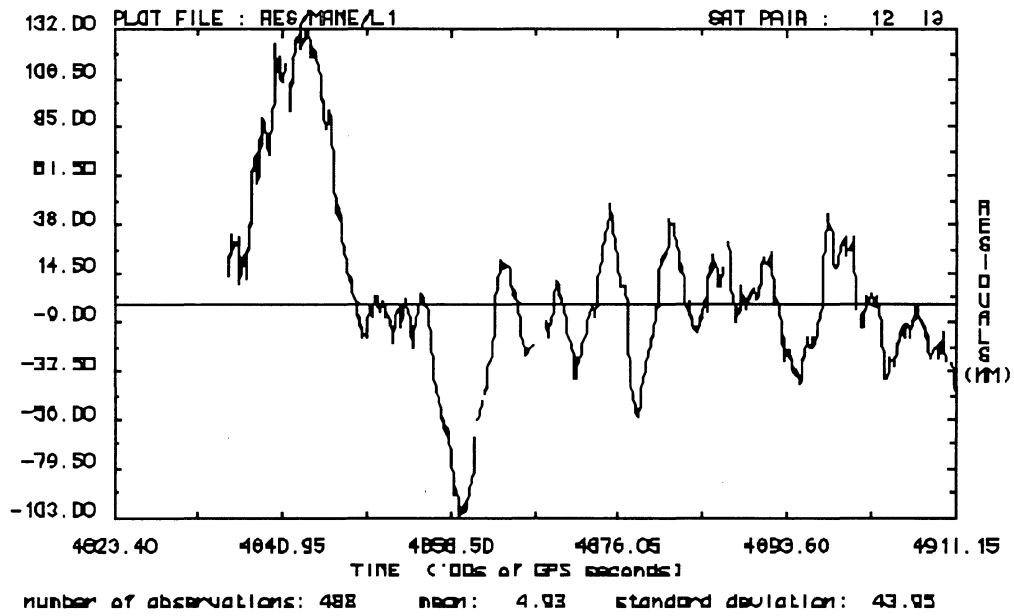
Estimated Autocovariance Function of the Carrier Phase Double Difference Residuals for an 81 km Baseline (L1)



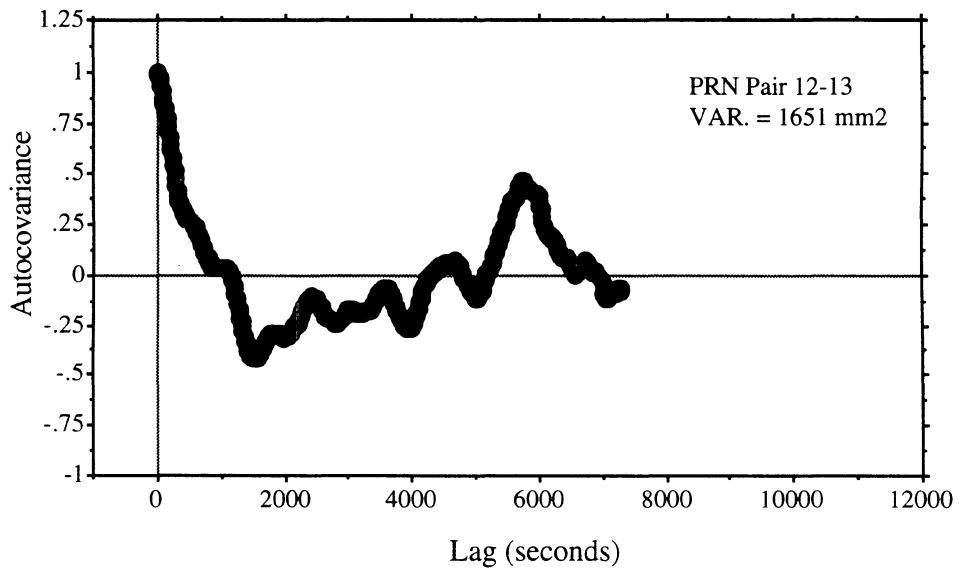
Carrier Phase Double Difference Residuals for an 81 km Baseline (L1)



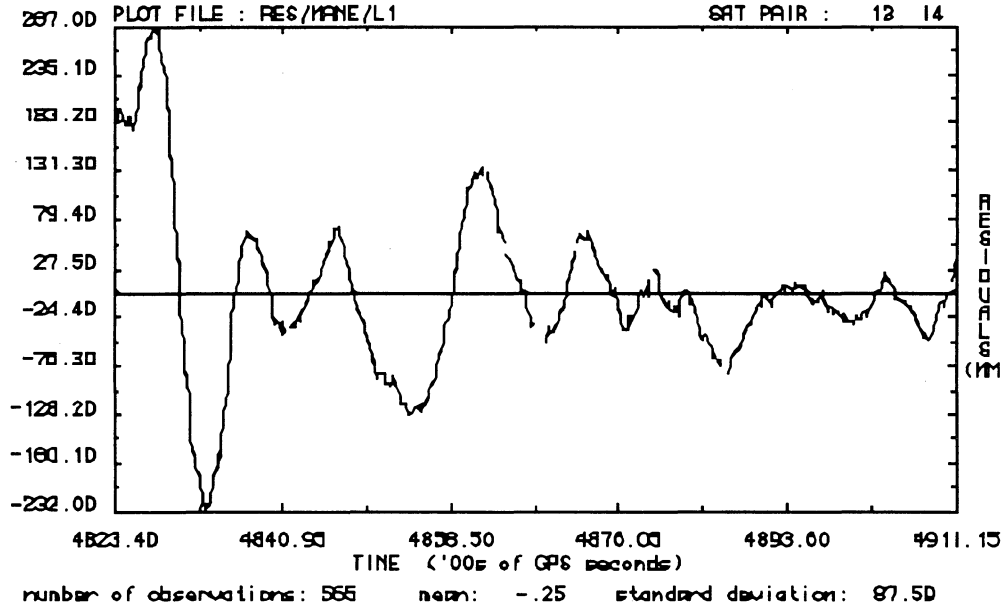
Estimated Autocovariance Function of the Carrier Phase Double Difference Residuals for an 81 km Baseline (L1)



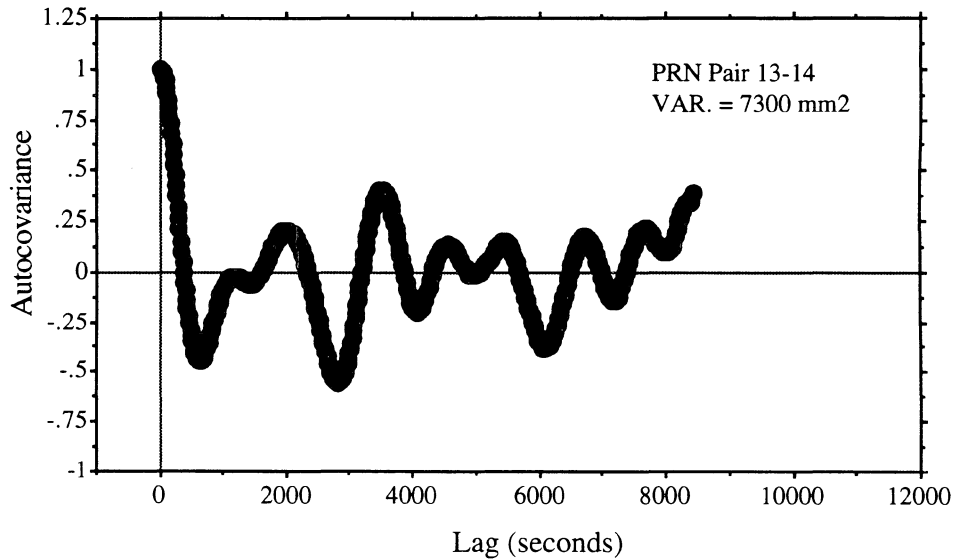
Carrier Phase Double Difference Residuals for a 92 km Baseline (L1)



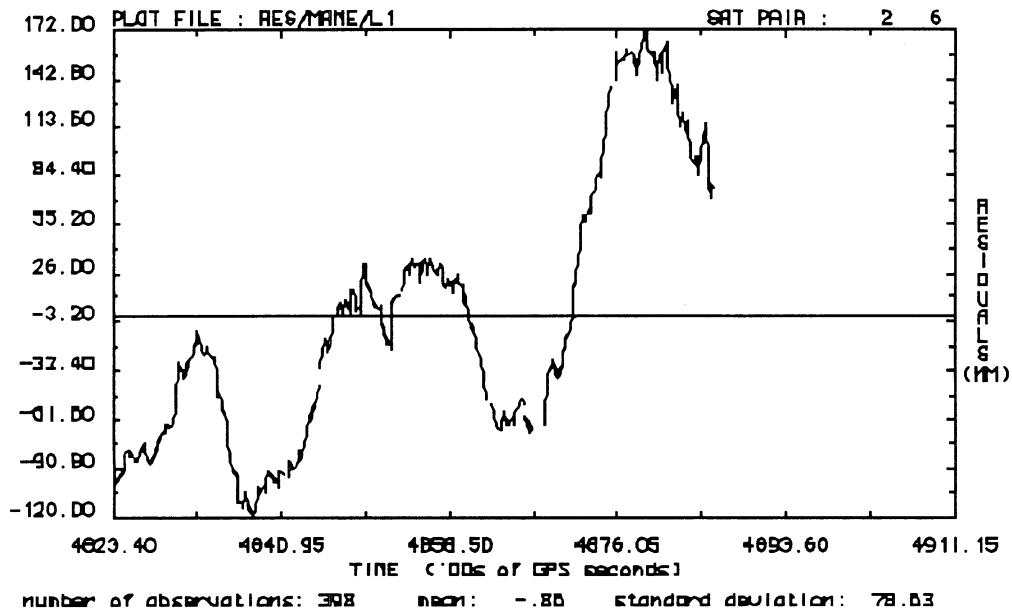
Estimated Autocovariance Function of the Carrier Phase Double Difference Residuals for a 92 km Baseline (L1)



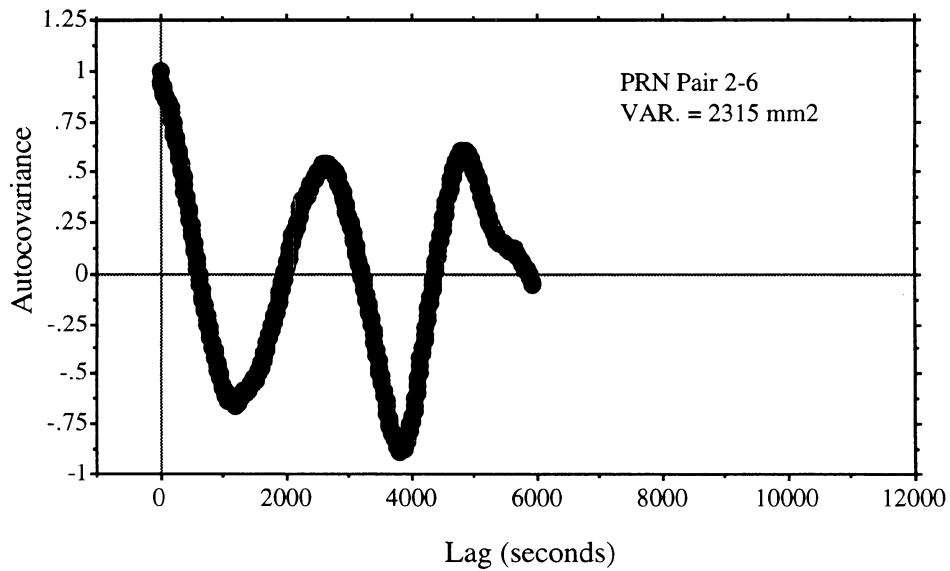
Carrier Phase Double Difference Residuals for a 92 km Baseline (L1)



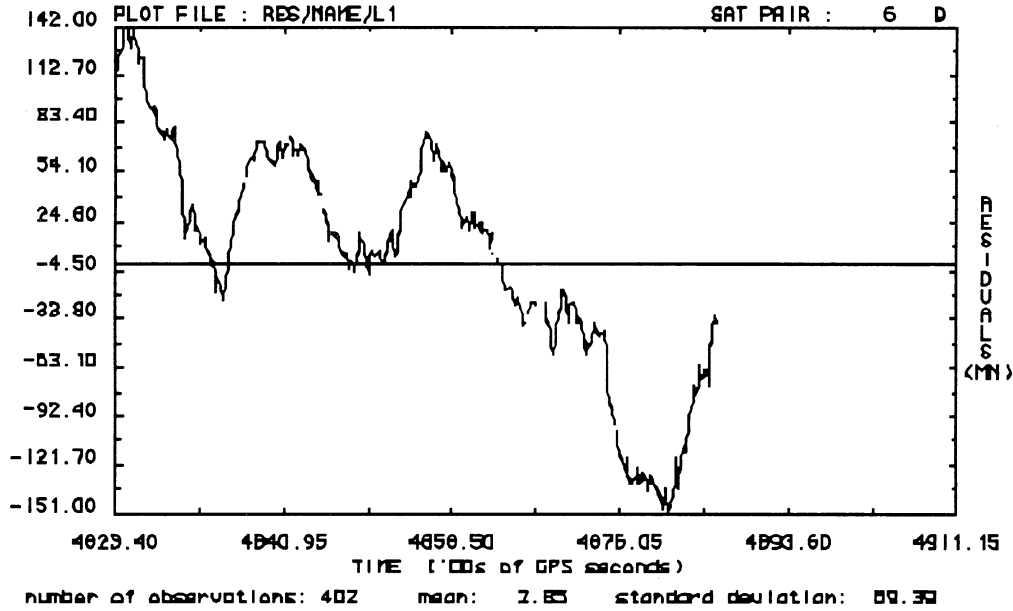
Estimated Autocovariance Function of the Carrier Phase Double Difference Residuals for a 92 km Baseline (L1)



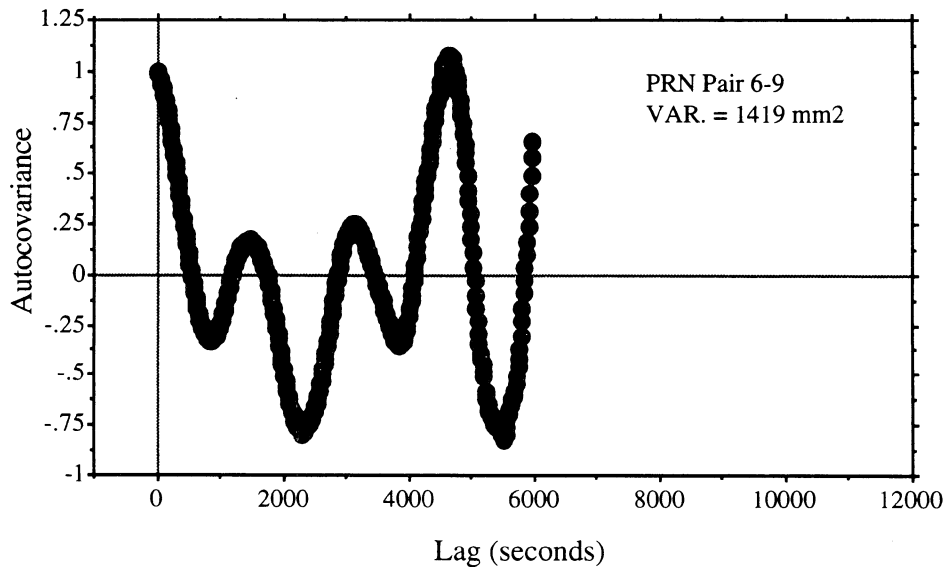
Carrier Phase Double Difference Residuals for a 92 km Baseline (L1)



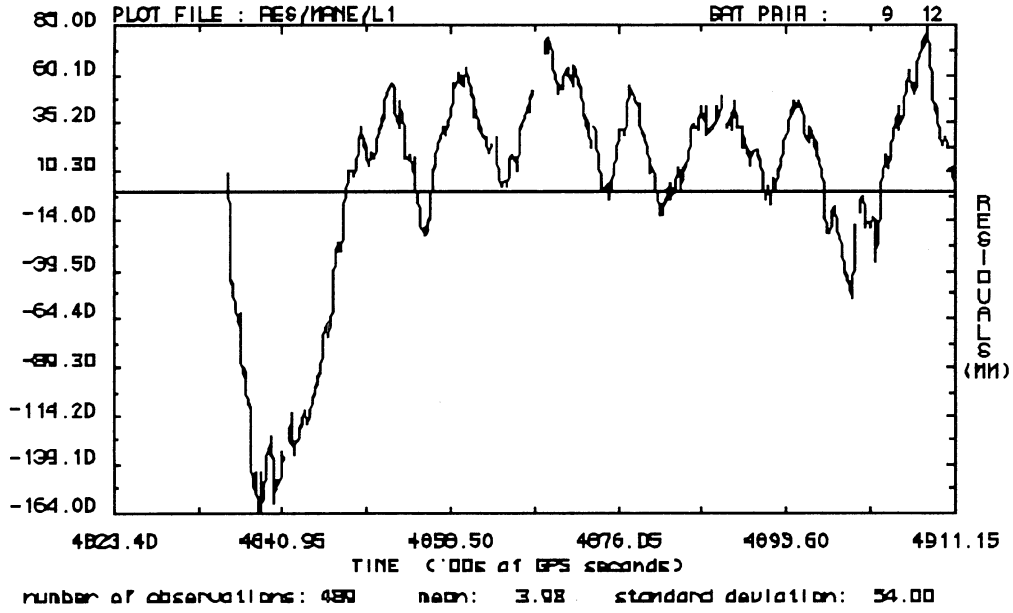
Estimated Autocovariance Function of the Carrier Phase Double Difference Residuals for a 92 km Baseline (L1)



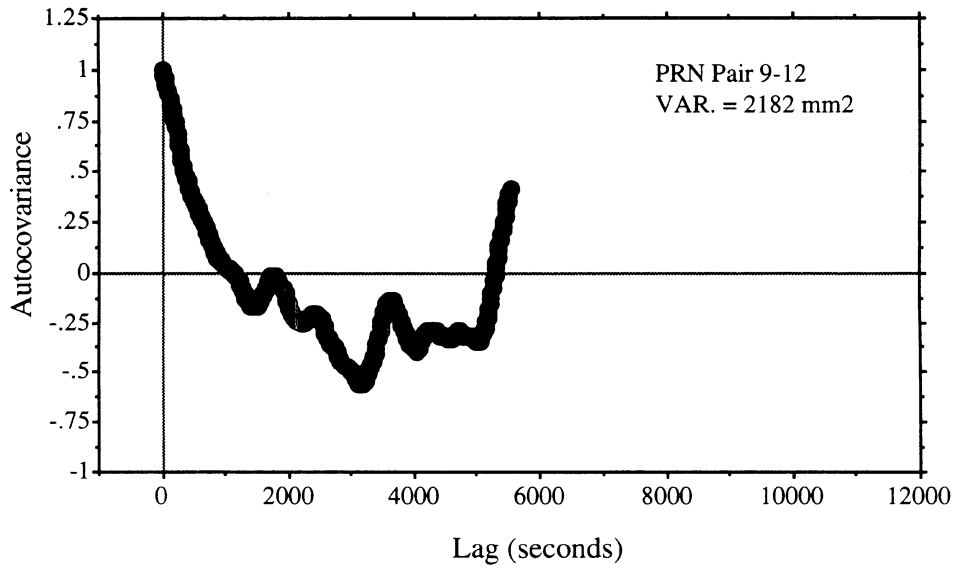
Carrier Phase Double Difference Residuals for a 92 km Baseline (L1)



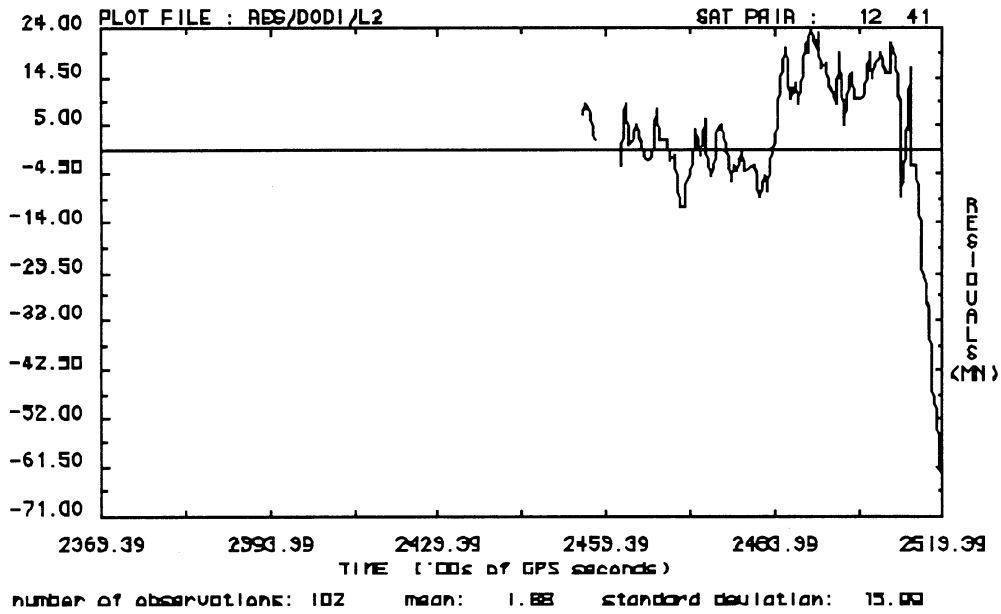
Estimated Autocovariance Function of the Carrier Phase Double Difference Residuals for a 92 km Baseline (L1)



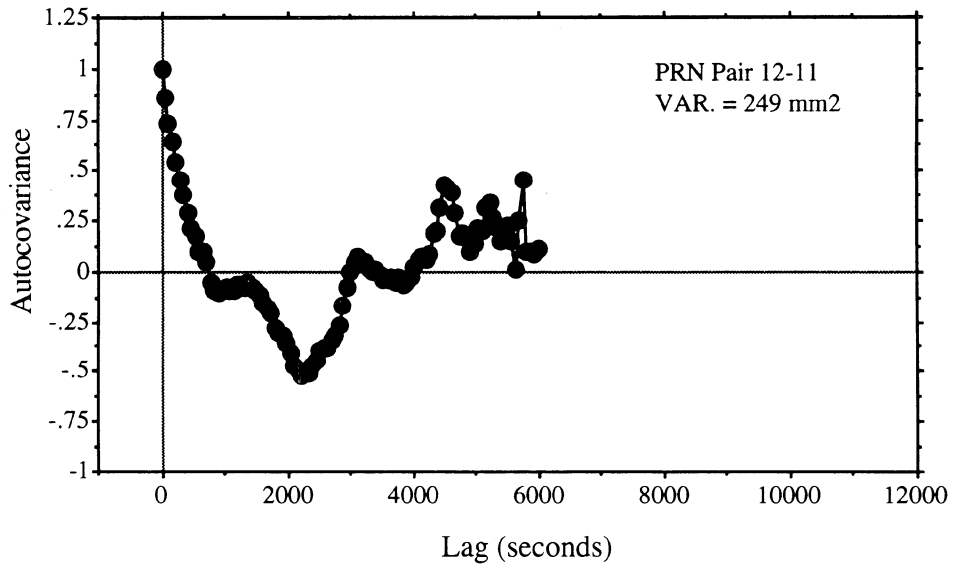
Carrier Phase Double Difference Residuals for a 92 km Baseline (L1)



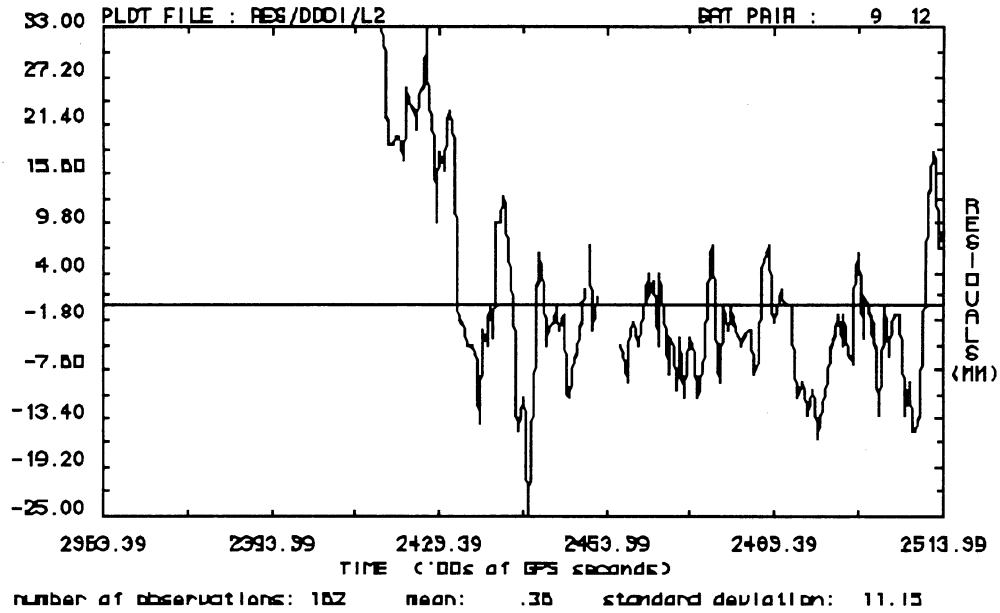
Estimated Autocovariance Function of the Carrier Phase Double Difference Residuals for a 92 km Baseline (L1)



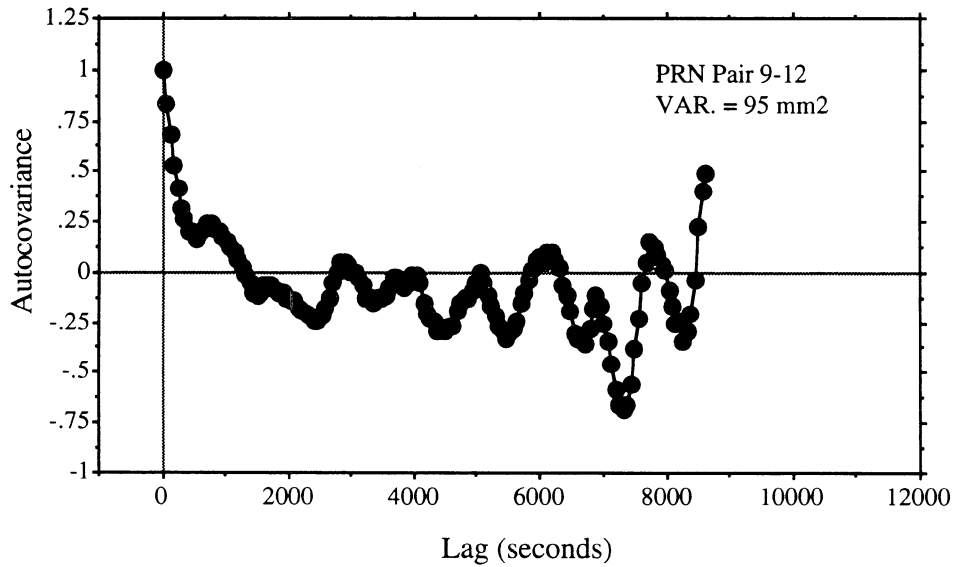
Carrier Phase Double Difference Residuals for a 12 km Baseline (L2)



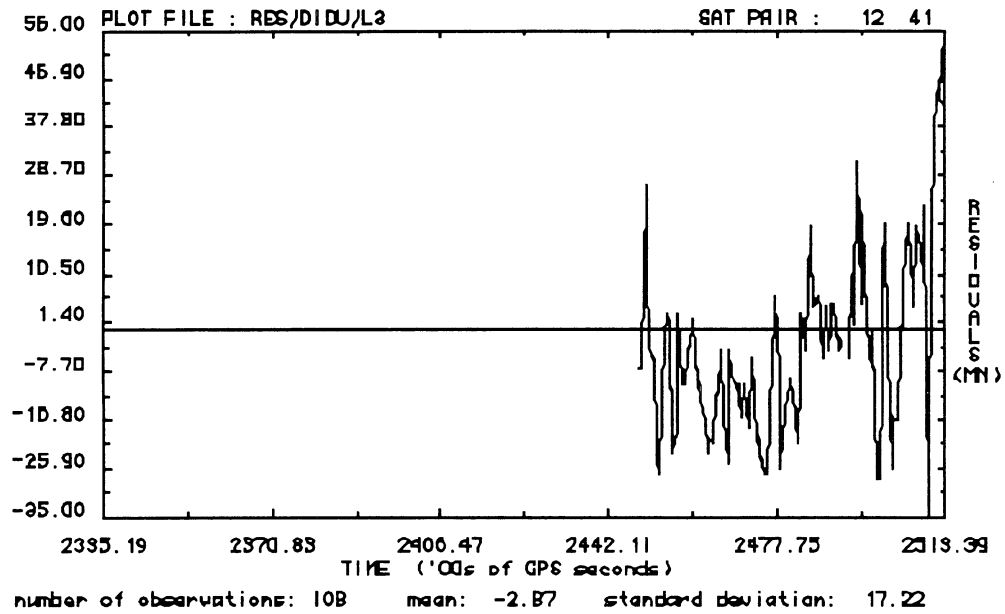
Estimated Autocovariance Function of the Carrier Phase Double Difference Residuals for a 12 km Baseline (L2)



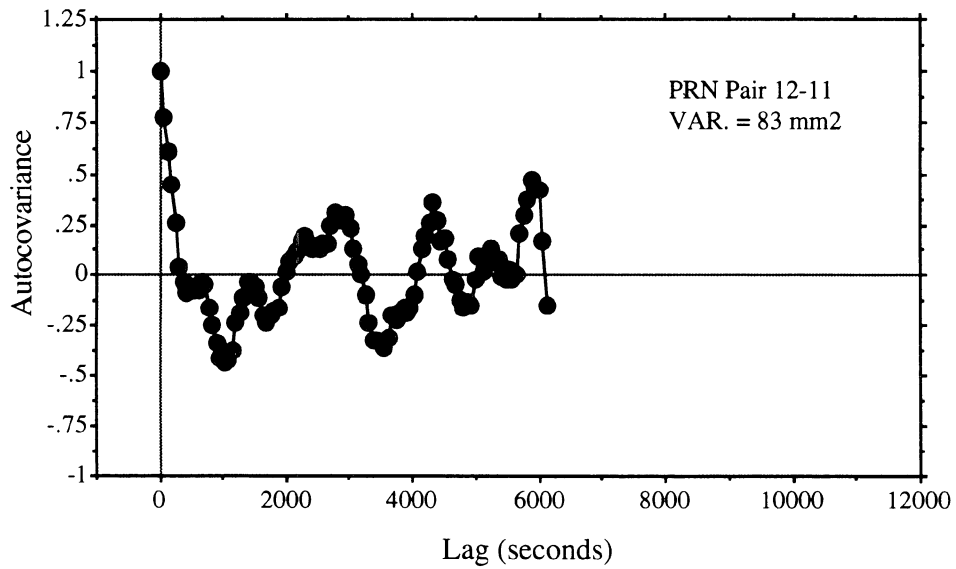
Carrier Phase Double Difference Residuals for a 12 km Baseline (L2)



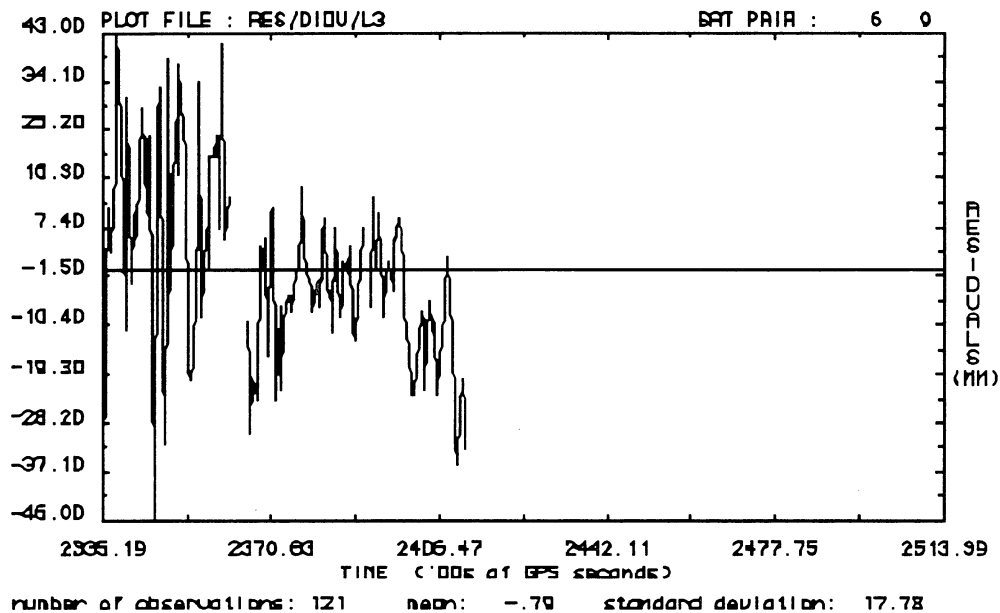
Estimated Autocovariance Function of the Carrier Phase Double Difference Residuals for a 12 km Baseline (L2)



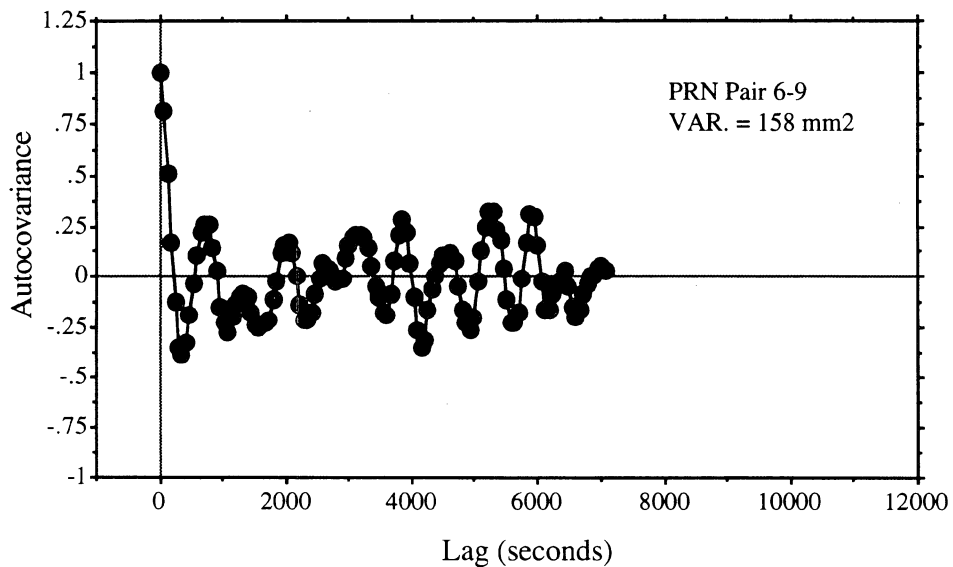
Carrier Phase Double Difference Residuals for a 29 km Baseline (L2)



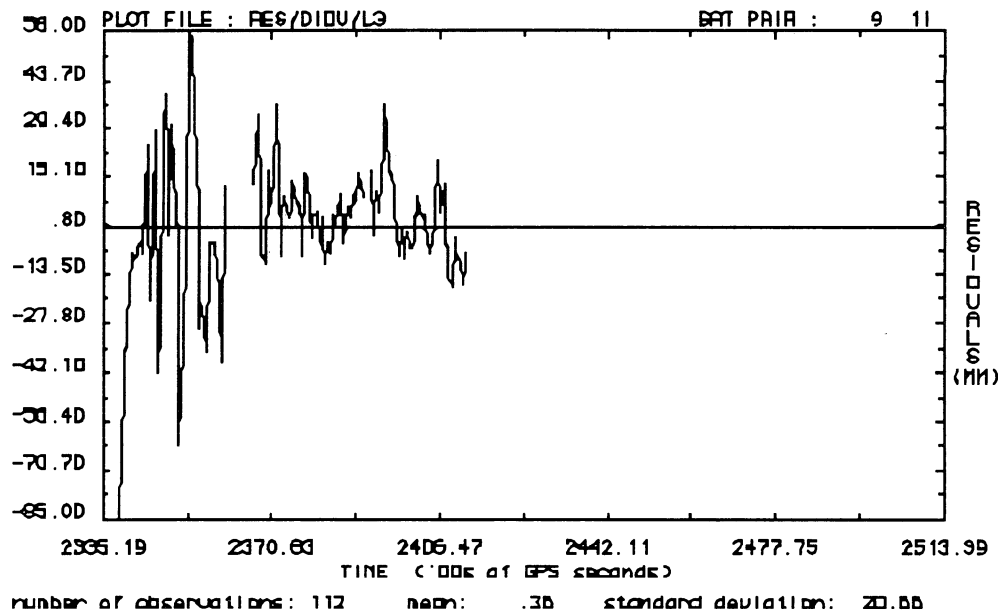
Estimated Autocovariance Function of the Carrier Phase Double Difference Residuals for a 29 km Baseline (L2)



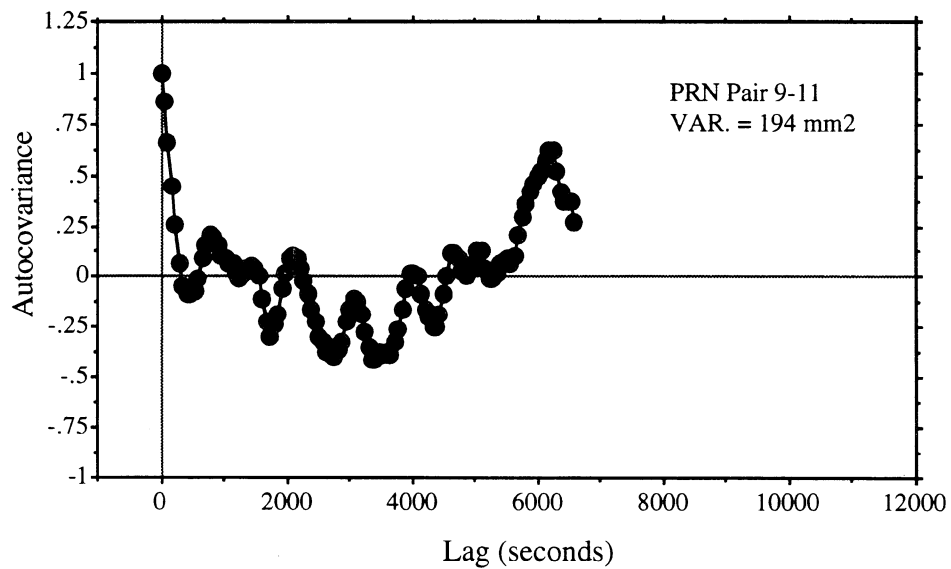
Carrier Phase Double Difference Residuals for a 29 km Baseline (L2)



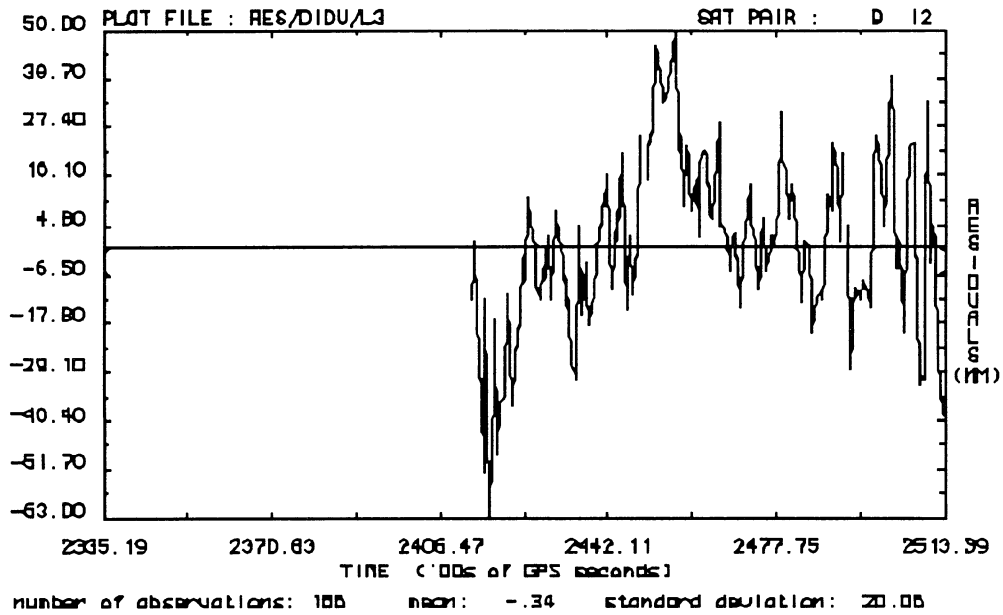
Estimated Autocovariance Function of the Carrier Phase Double Difference Residuals for a 29 km Baseline (L2)



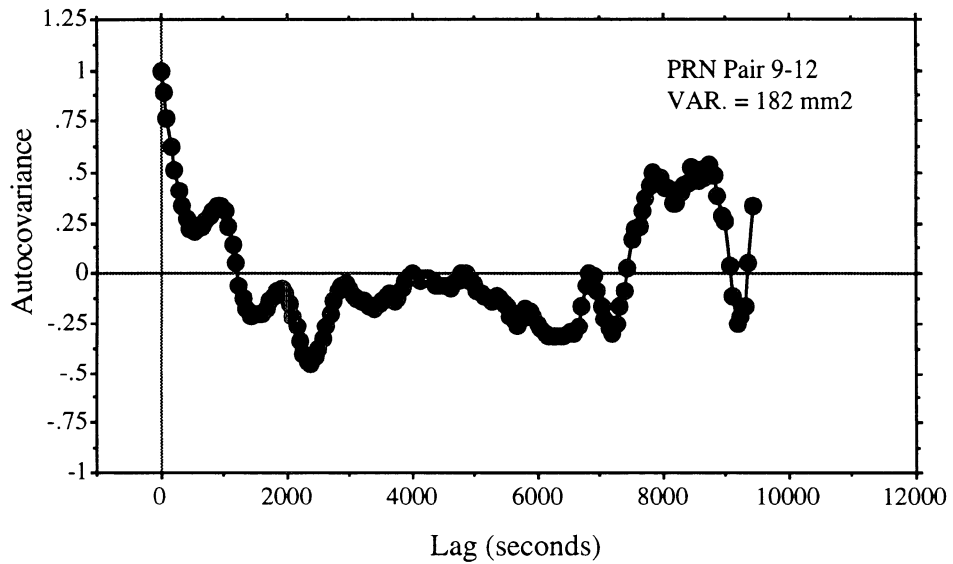
Carrier Phase Double Difference Residuals for a 29 km Baseline (L2)



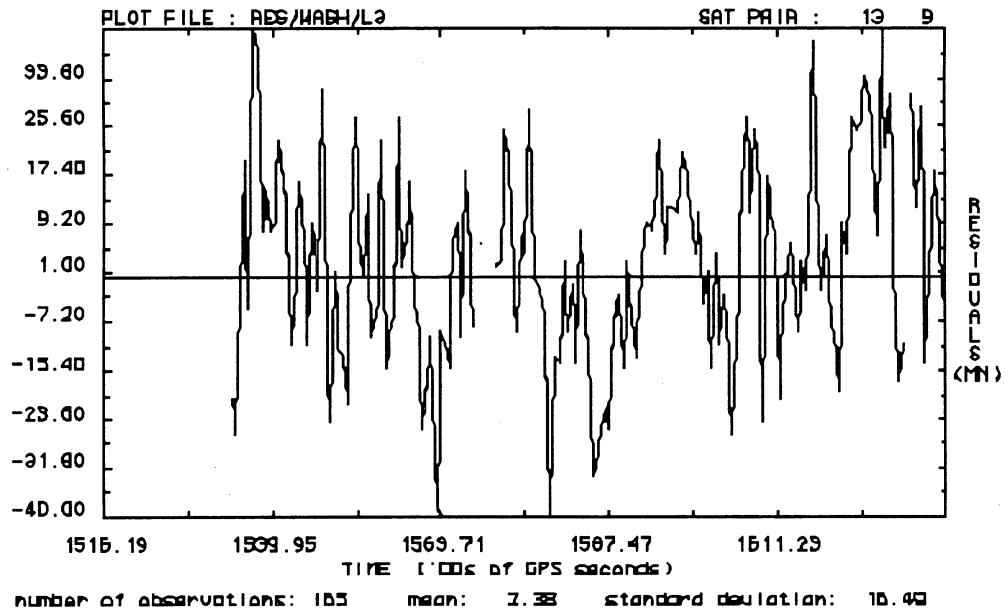
Estimated Autocovariance Function of the Carrier Phase Double Difference Residuals for a 29 km Baseline (L2)



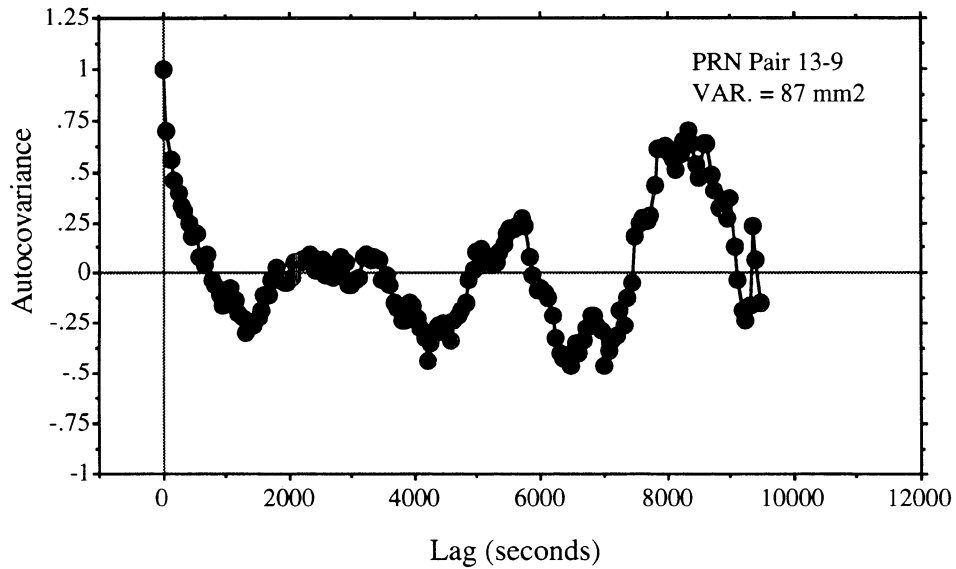
Carrier Phase Double Difference Residuals for a 29 km Baseline (L2)



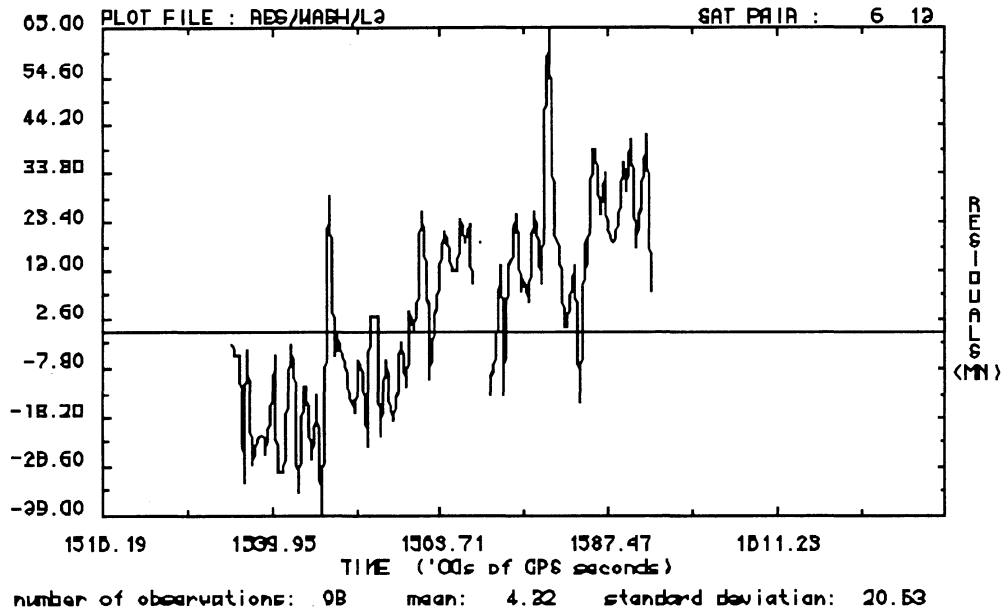
Estimated Autocovariance Function of the Carrier Phase Double Difference Residuals for a 29 km Baseline (L2)



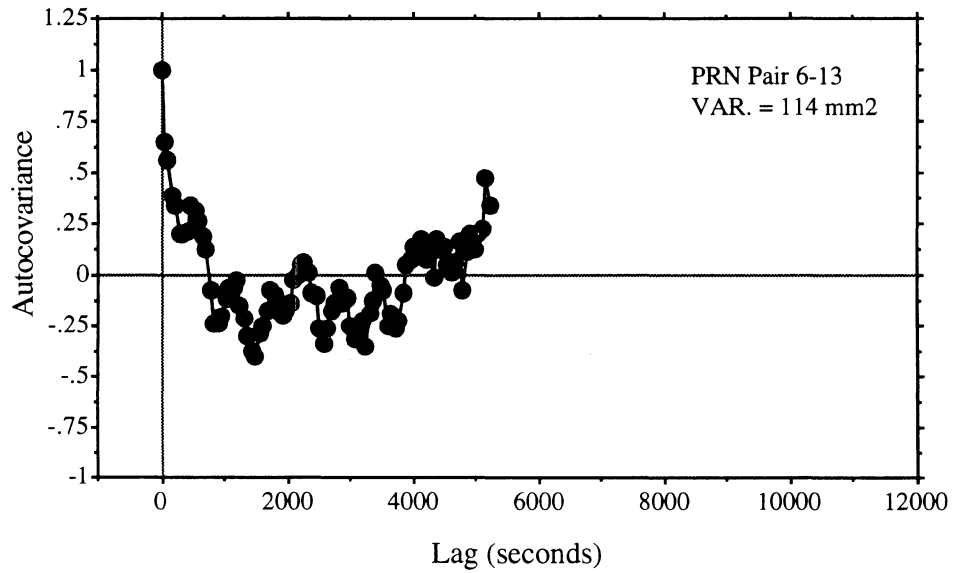
Carrier Phase Double Difference Residuals for a 50 km Baseline (L2)



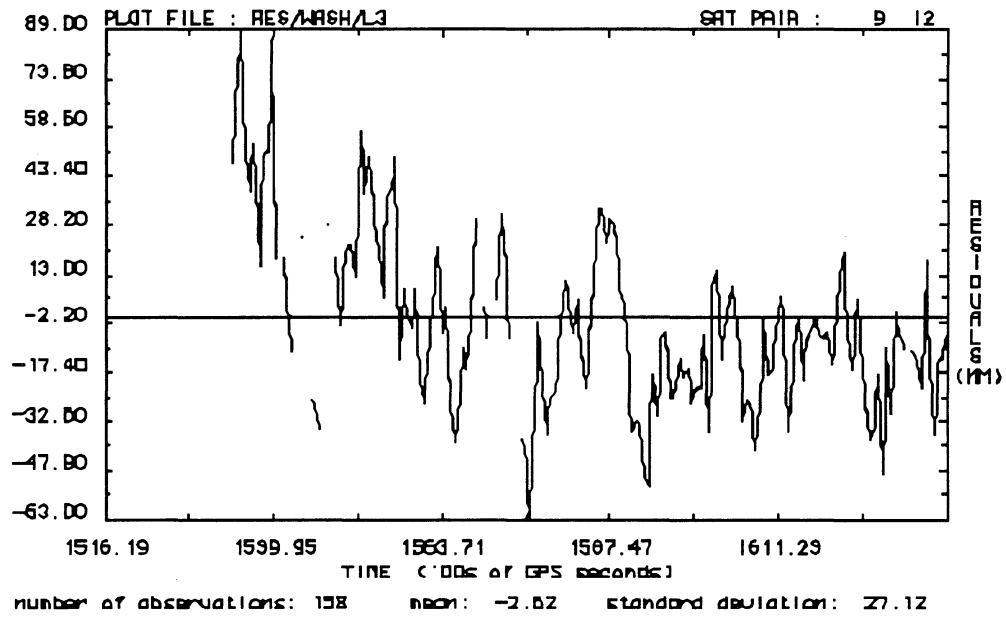
Estimated Autocovariance Function of the Carrier Phase Double Difference Residuals for a 50 km Baseline (L2)



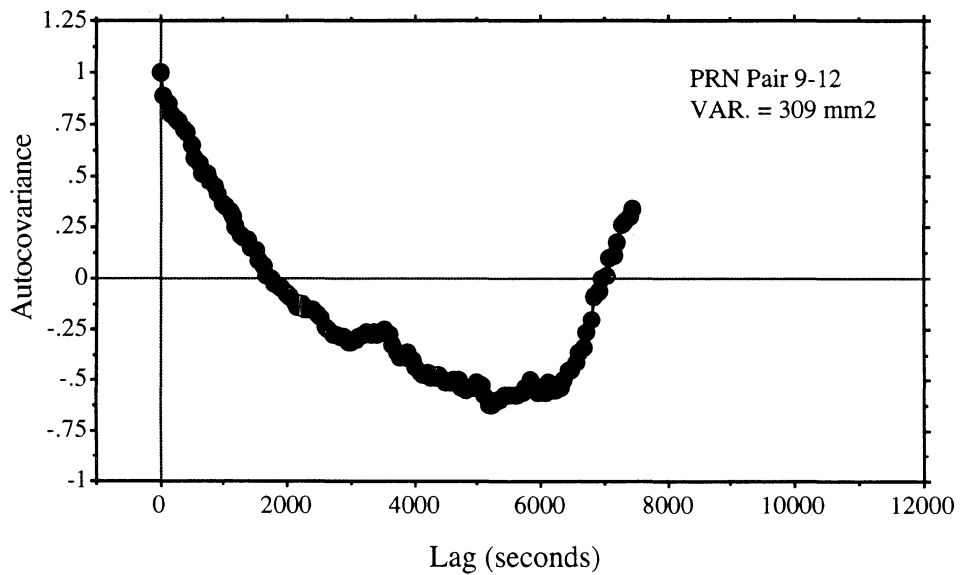
Carrier Phase Double Difference Residuals for a 60 km Baseline (L2)



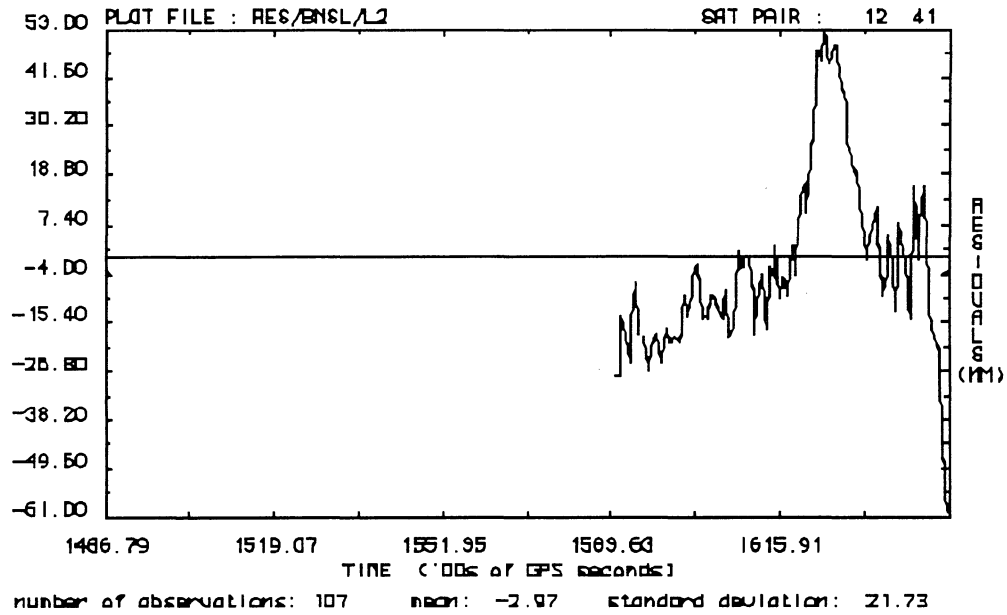
Estimated Autocovariance Function of the Carrier Phase Double Difference Residuals for a 50 km Baseline (L2)



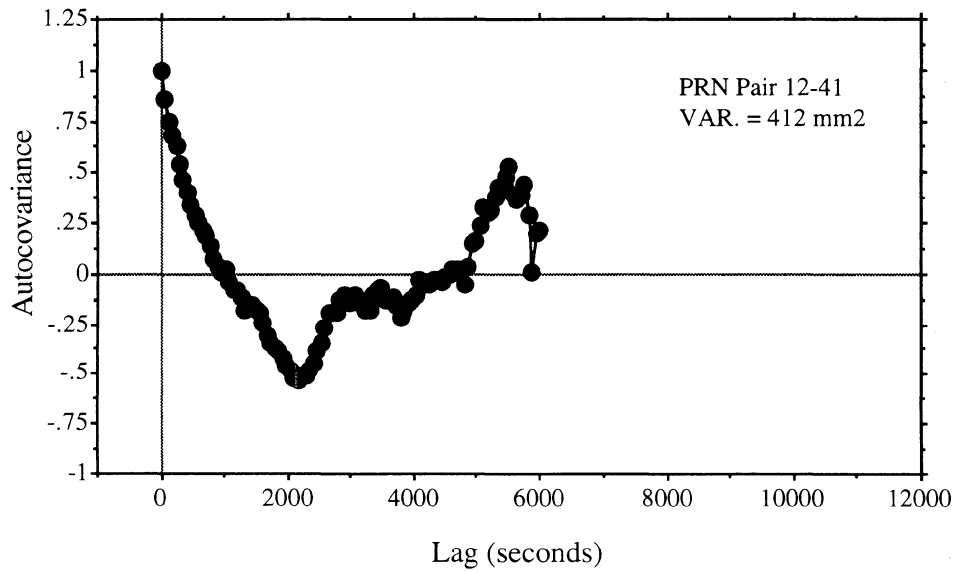
Carrier Phase Double Difference Residuals for a 50 km Baseline (L2)



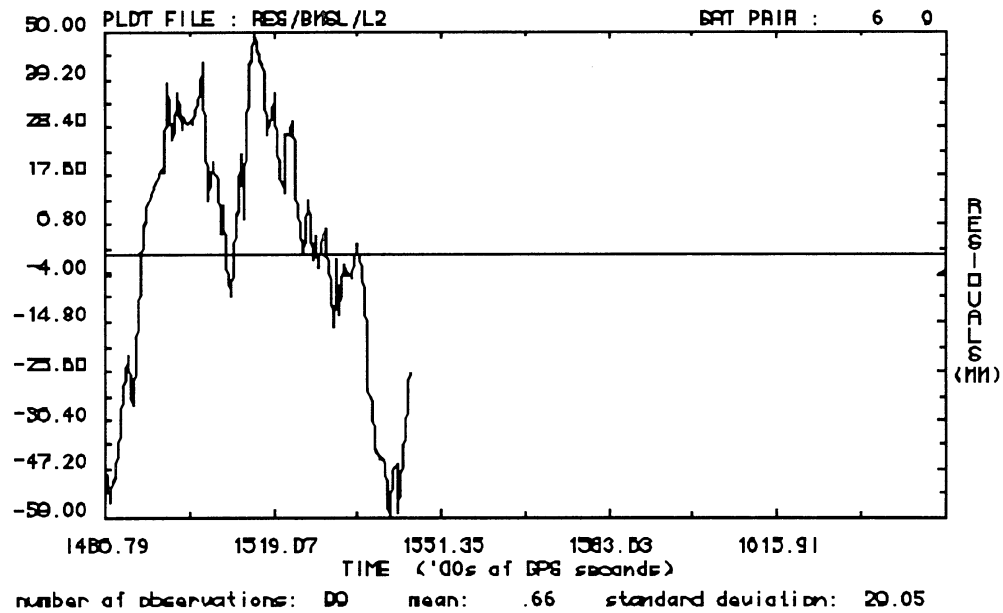
Estimated Autocovariance Function of the Carrier Phase Double Difference Residuals for a 50 km Baseline (L2)



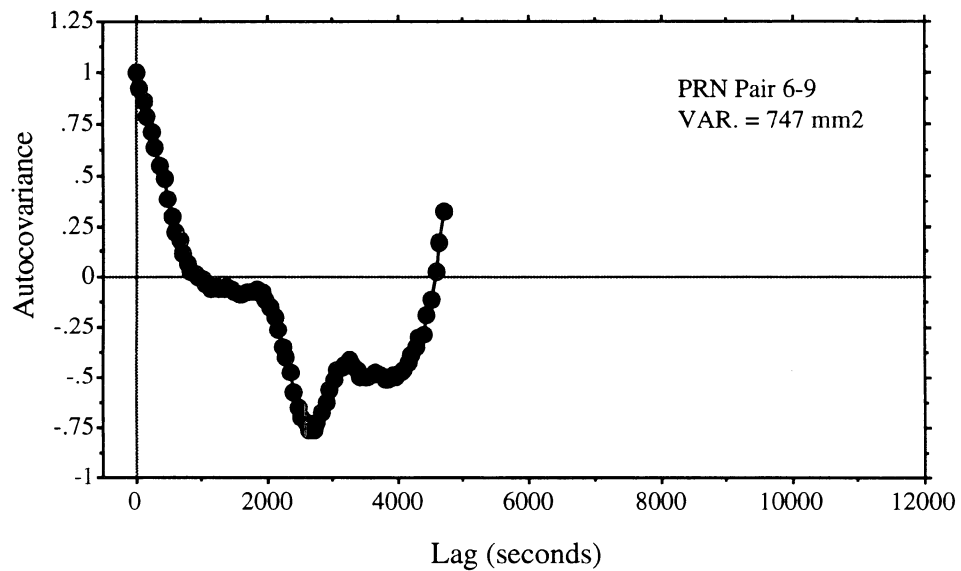
Carrier Phase Double Difference Residuals for an 81 km Baseline (L2)



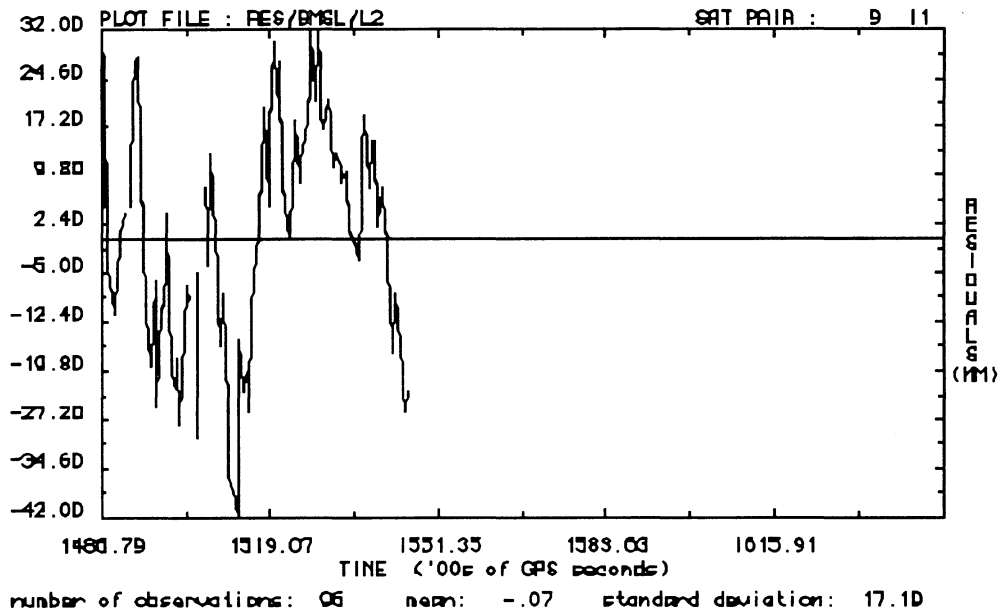
Estimated Autocovariance Function of the Carrier Phase Double Difference Residuals for an 81 km Baseline (L2)



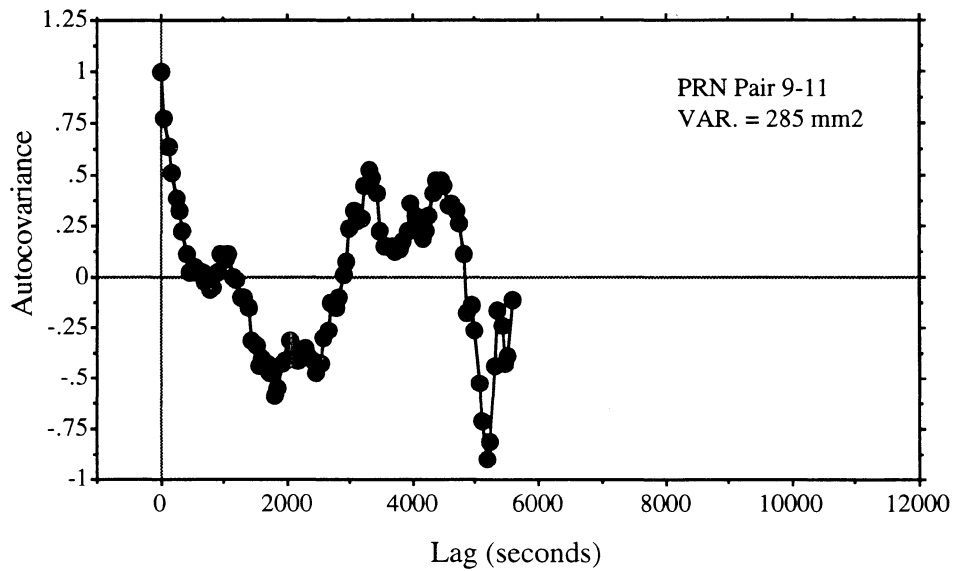
Carrier Phase Double Difference Residuals for an 81 km Baseline (L2)



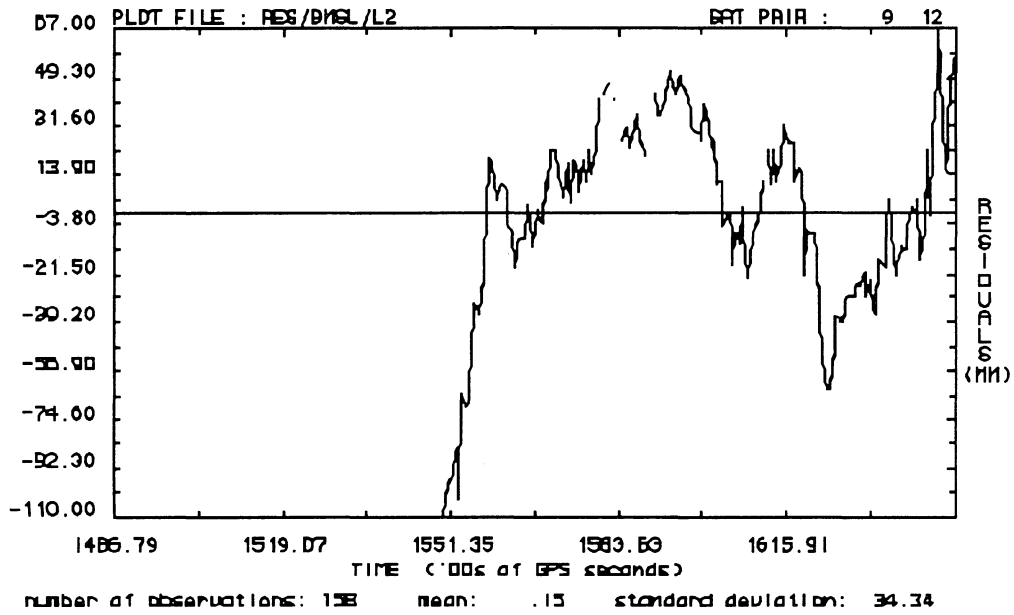
Estimated Autocovariance Function of the Carrier Phase Double Difference Residuals for an 81 km Baseline (L2)



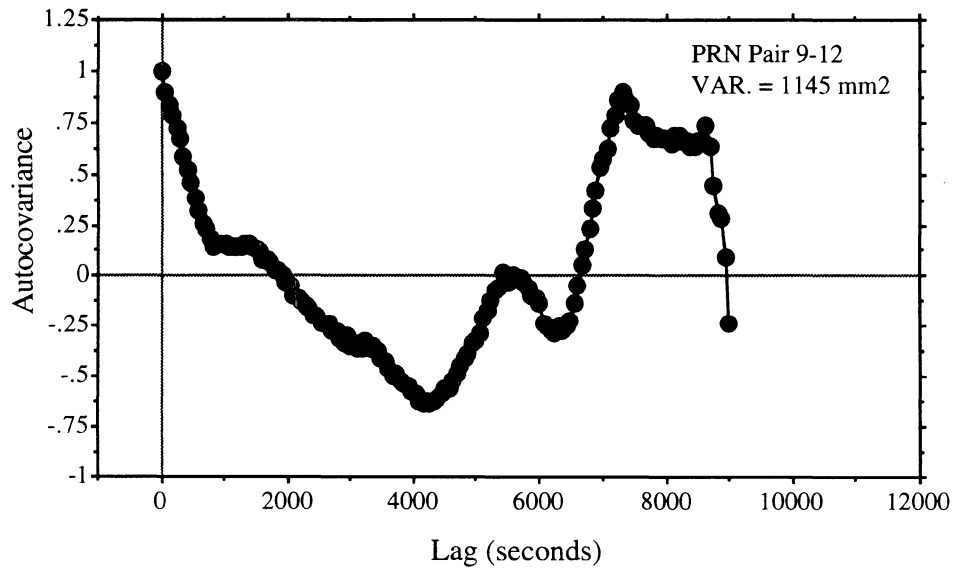
Carrier Phase Double Difference Residuals for an 81 km Baseline (L2)



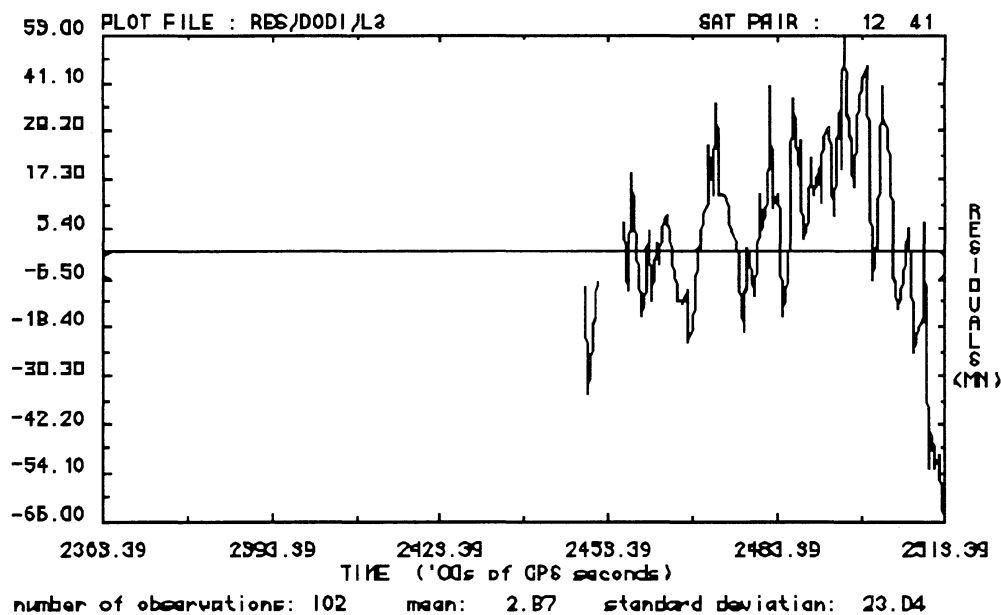
Estimated Autocovariance Function of the Carrier Phase Double Difference Residuals for an 81 km Baseline (L2)



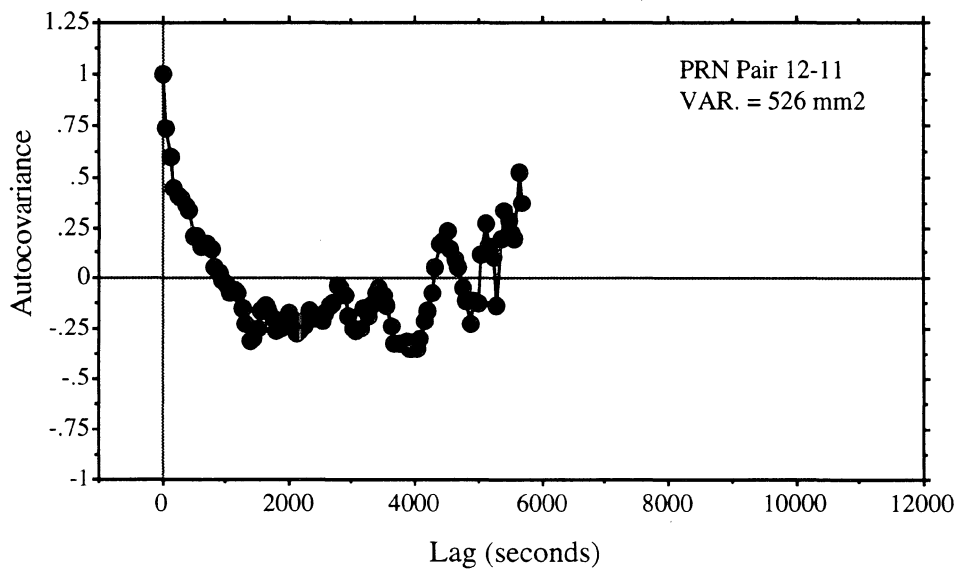
Carrier Phase Double Difference Residuals for an 81 km Baseline (L2)



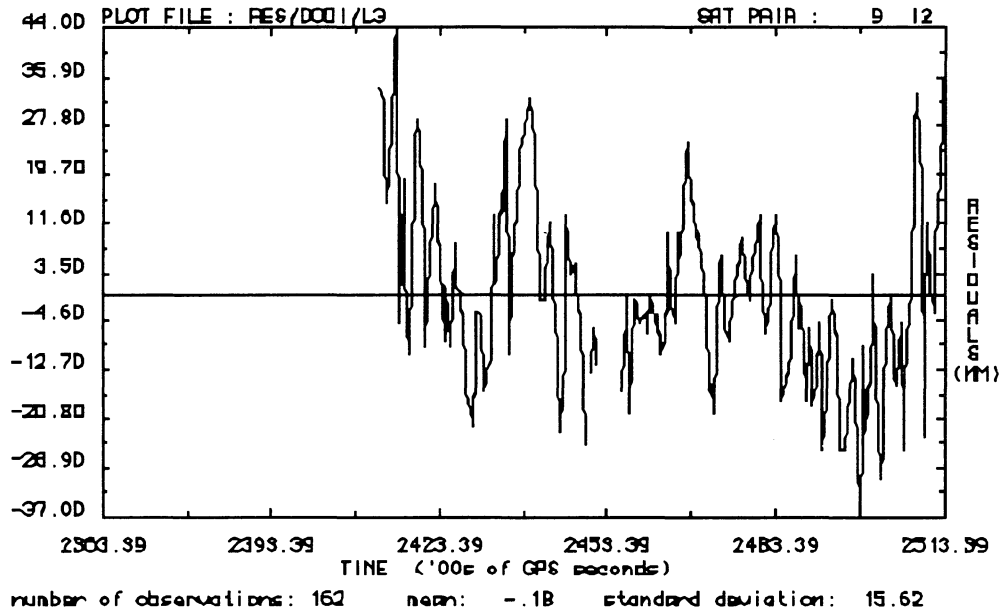
Estimated Autocovariance Function of the Carrier Phase Double Difference Residuals for an 81 km Baseline (L2)



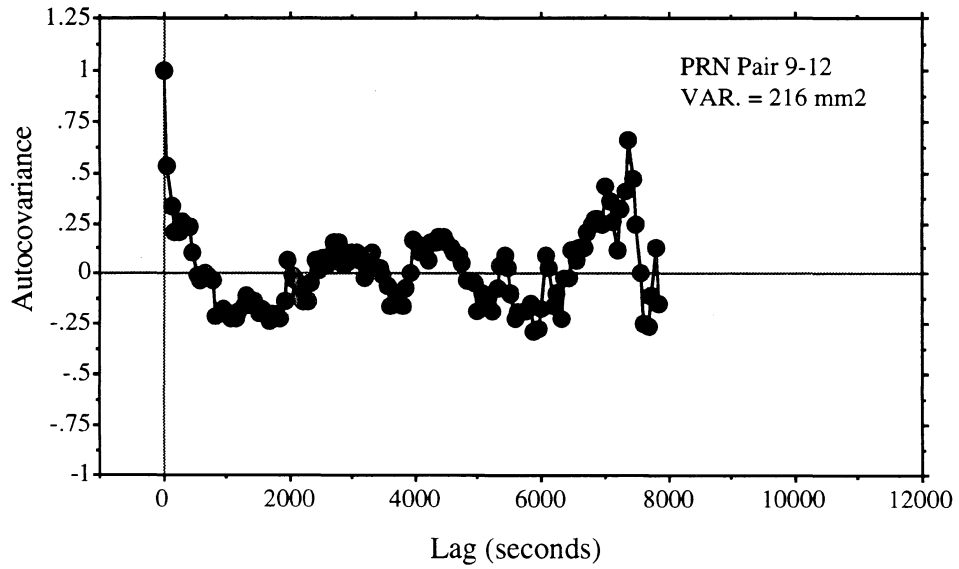
Carrier Phase Double Difference Residuals for a 12 km Baseline (L3)



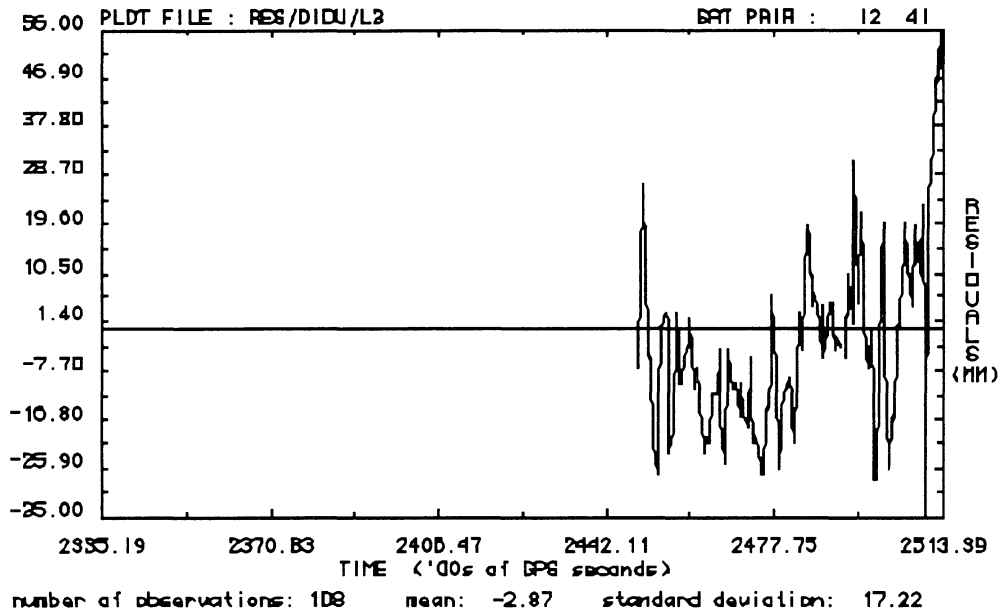
Estimated Autocovariance Function of the Carrier Phase Double Difference Residuals for a 12 km Baseline (L3)



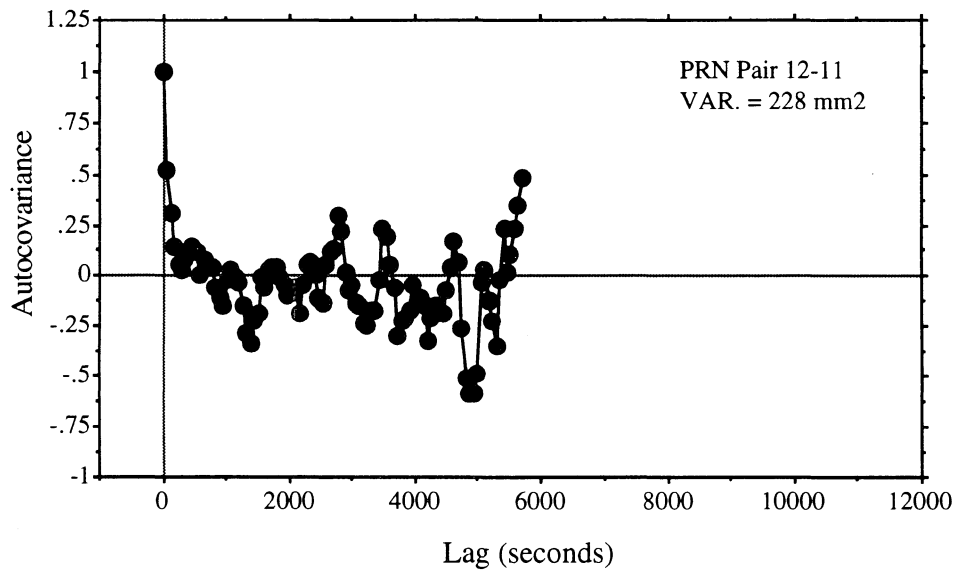
Carrier Phase Double Difference Residuals for a 12 km Baseline (L3)



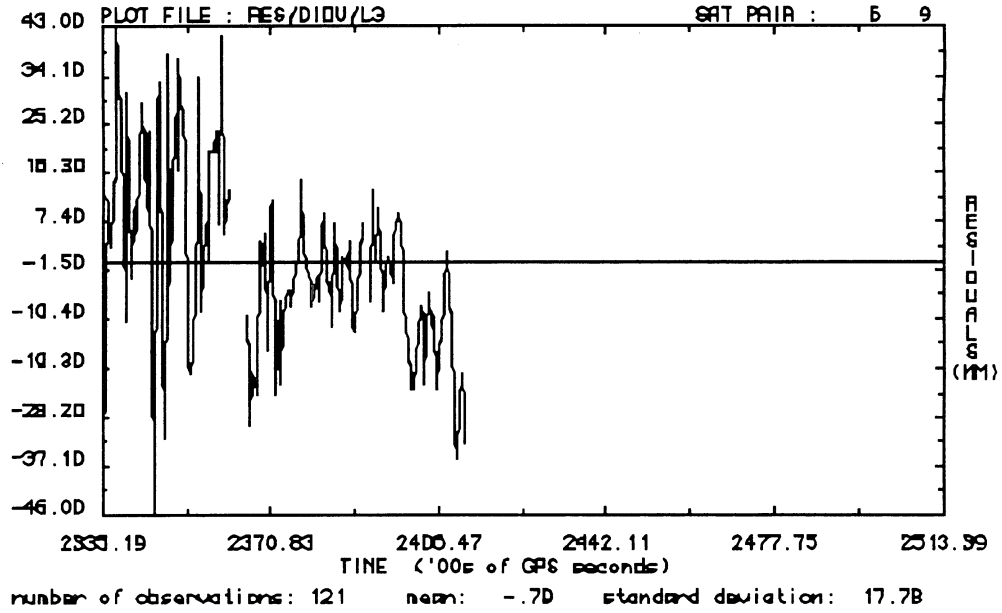
Estimated Autocovariance Function of the Carrier Phase Double Difference Residuals for a 12 km Baseline (L3)



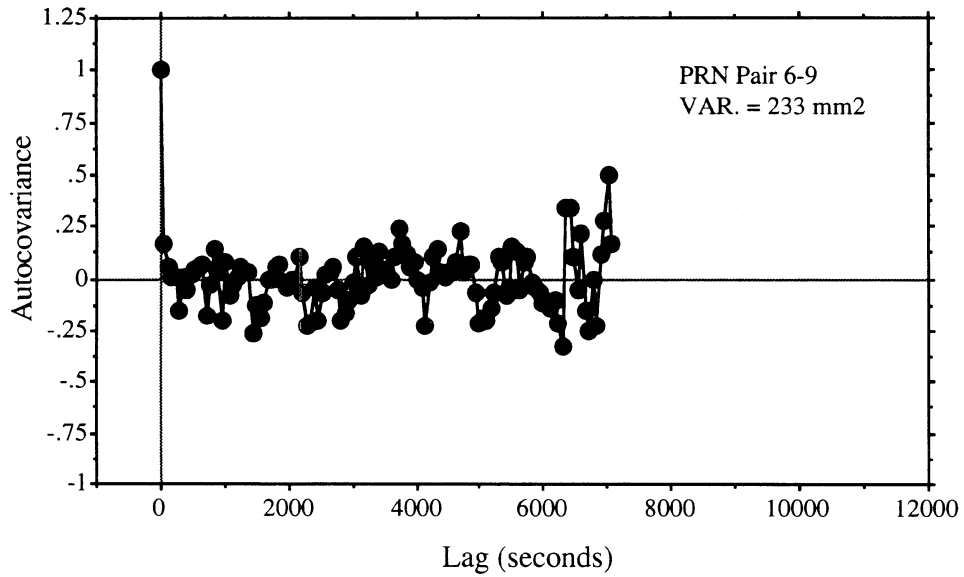
Carrier Phase Double Difference Residuals for a 29 km Baseline (L3)



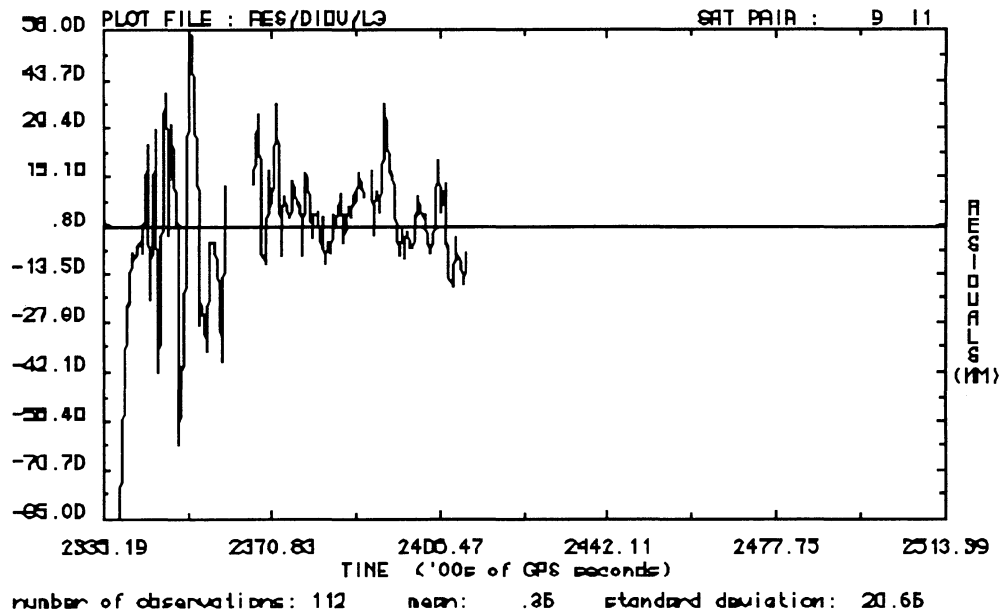
Estimated Autocovariance Function of the Carrier Phase Double Difference Residuals for a 29 km Baseline (L3)



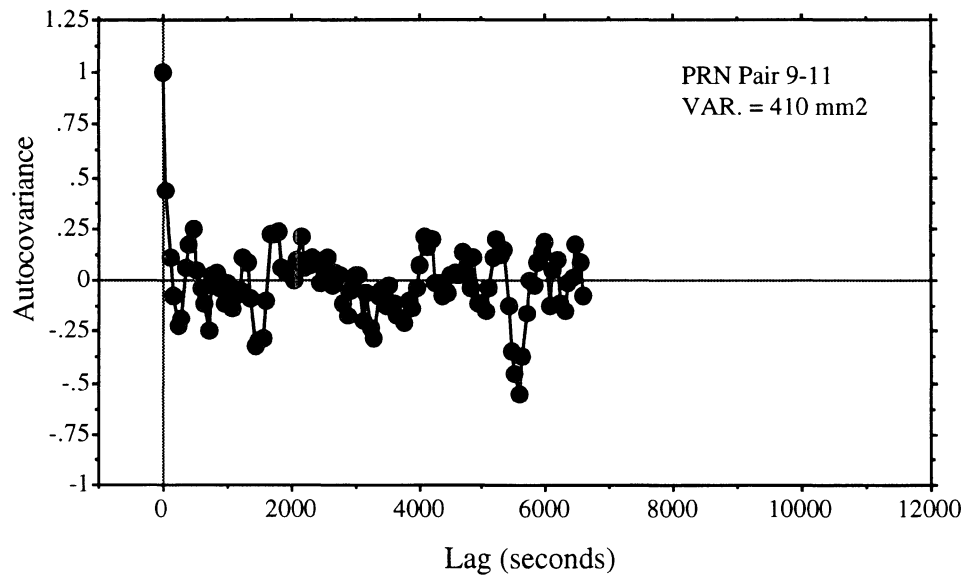
Carrier Phase Double Difference Residuals for a 29 km Baseline (L3)



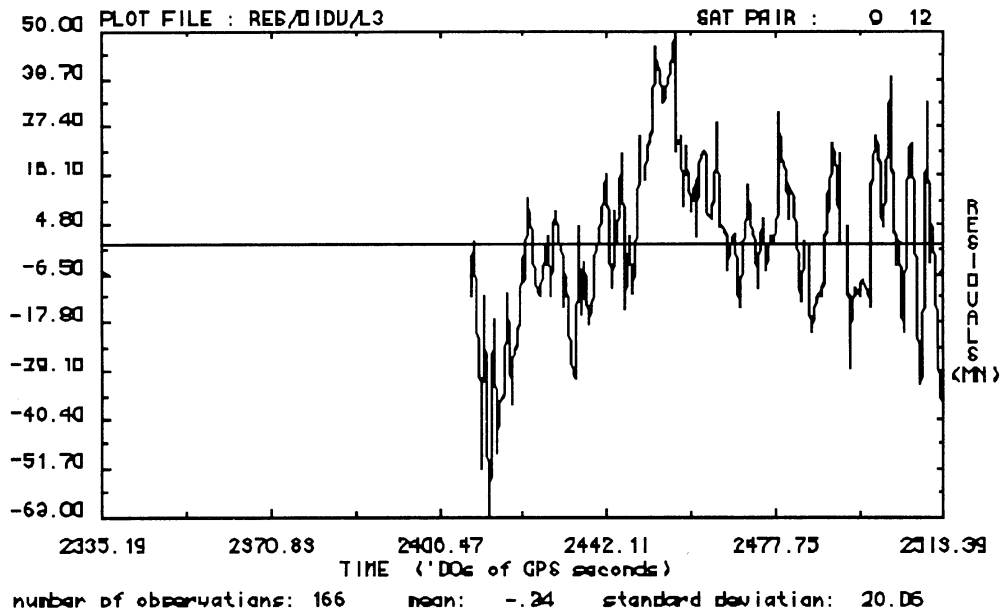
Estimated Autocovariance Function of the Carrier Phase Double Difference Residuals for a 29 km Baseline (L3)



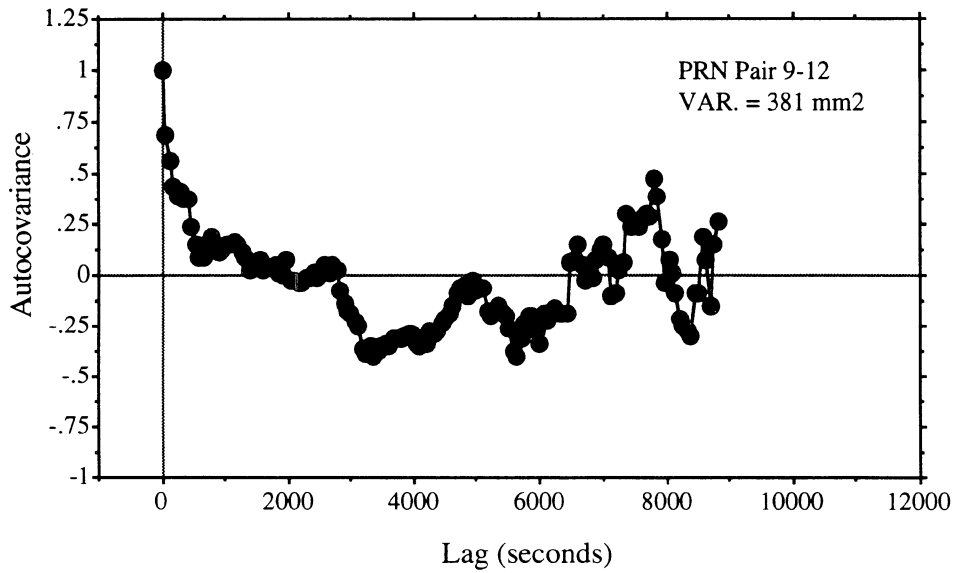
Carrier Phase Double Difference Residuals for a 29 km Baseline (L3)



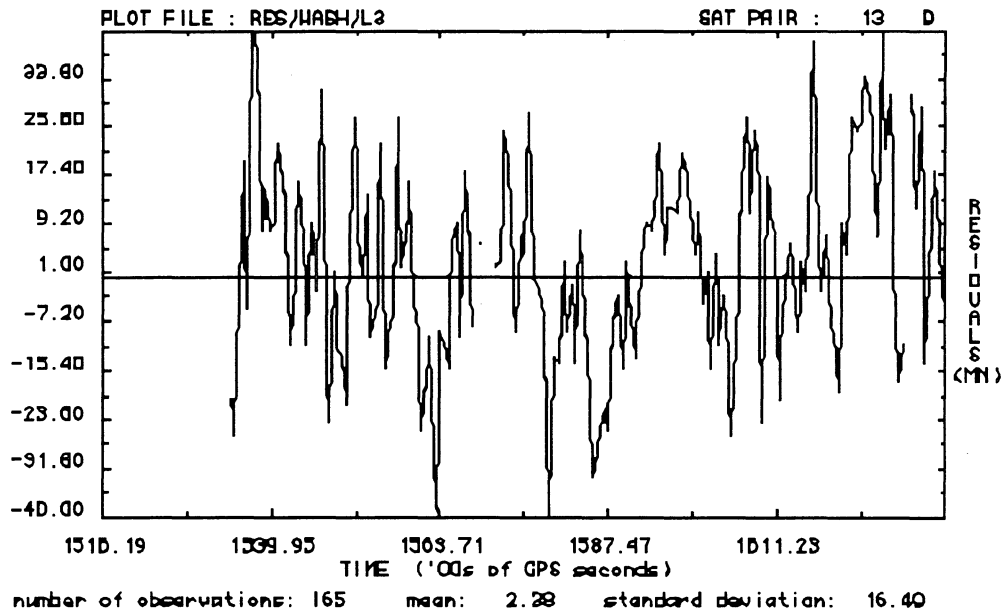
Estimated Autocovariance Function of the Carrier Phase Double Difference Residuals for a 29 km Baseline (L3)



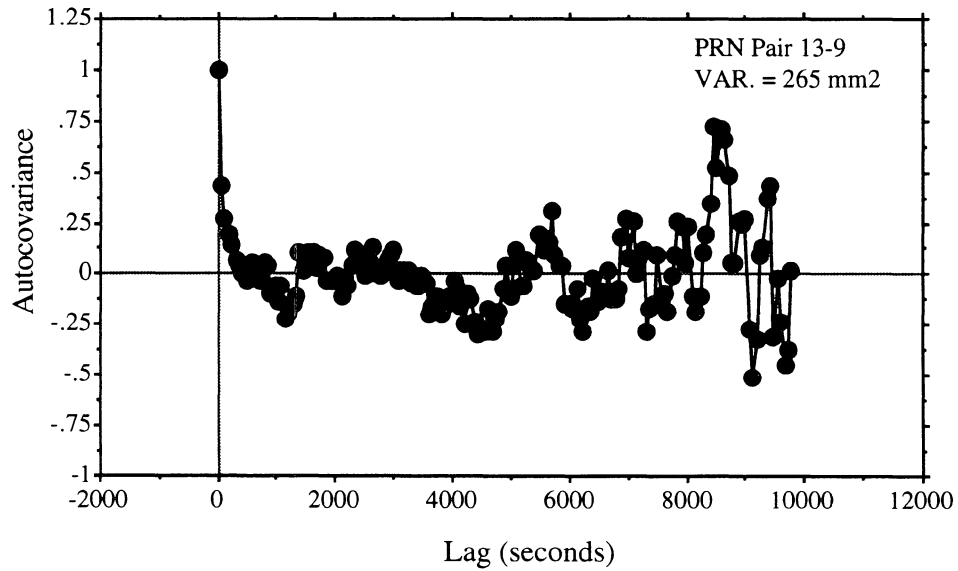
Carrier Phase Double Difference Residuals for a 29 km Baseline (L3)



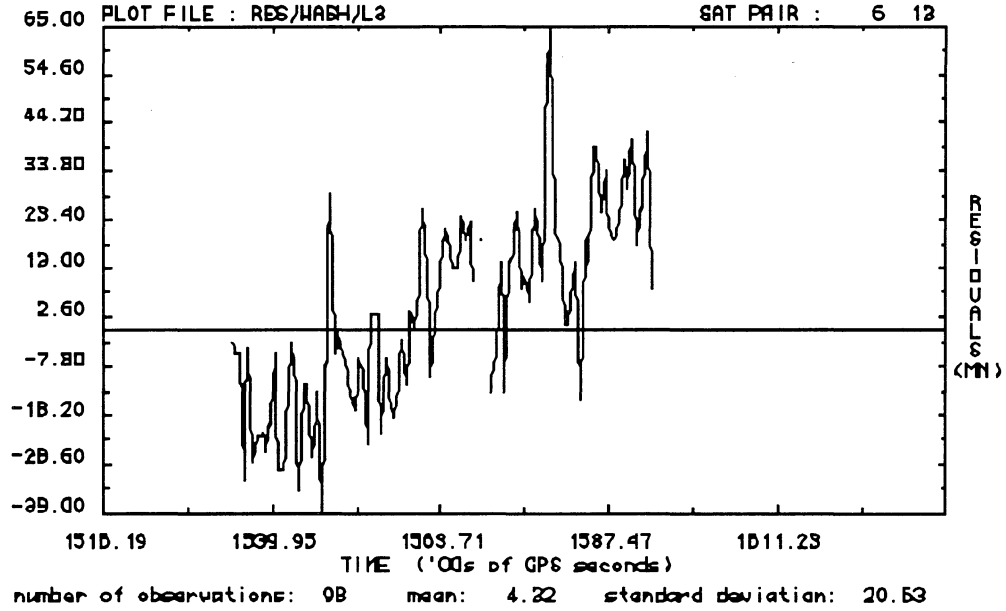
Estimated Autocovariance Function of the Carrier Phase Double Difference Residuals for a 29 km Baseline (L3)



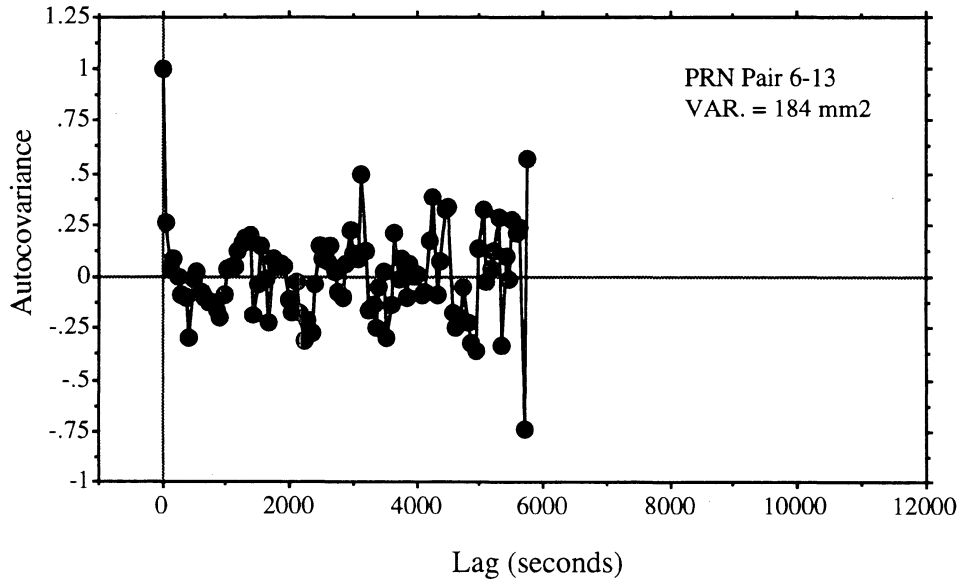
Carrier Phase Double Difference Residuals for a 50 km Baseline (L3)



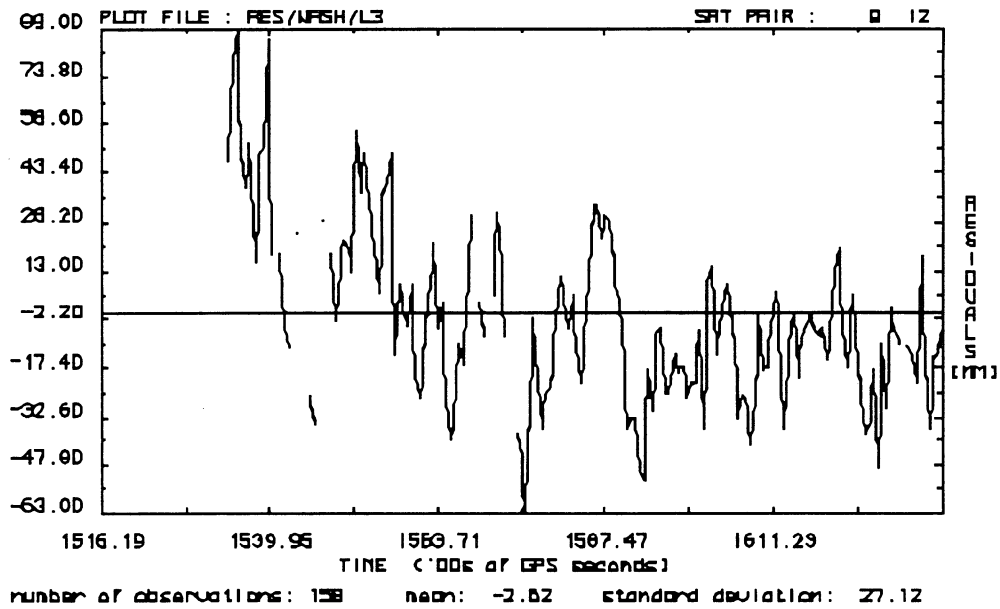
Estimated Autocovariance Function of the Carrier Phase Double Difference Residuals for a 50 km Baseline (L3)



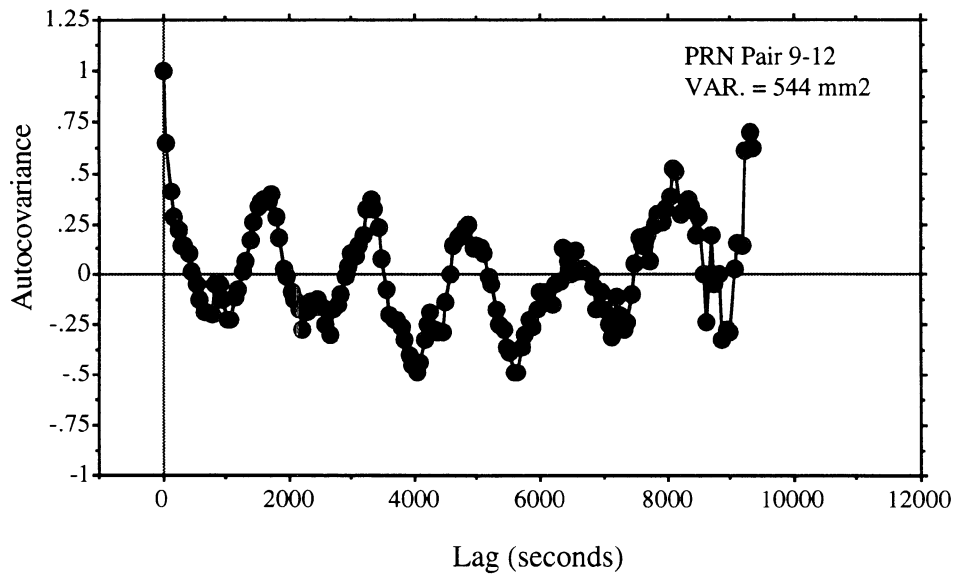
Carrier Phase Double Difference Residuals for a 50 km Baseline (L3)



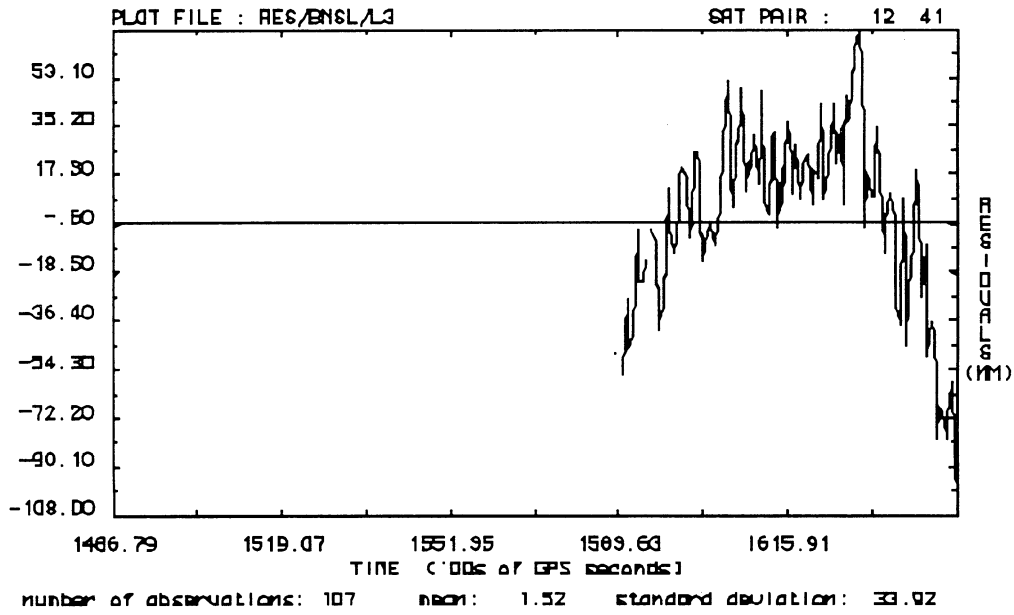
Estimated Autocovariance Function of the Carrier Phase Double Difference Residuals for a 50 km Baseline (L3)



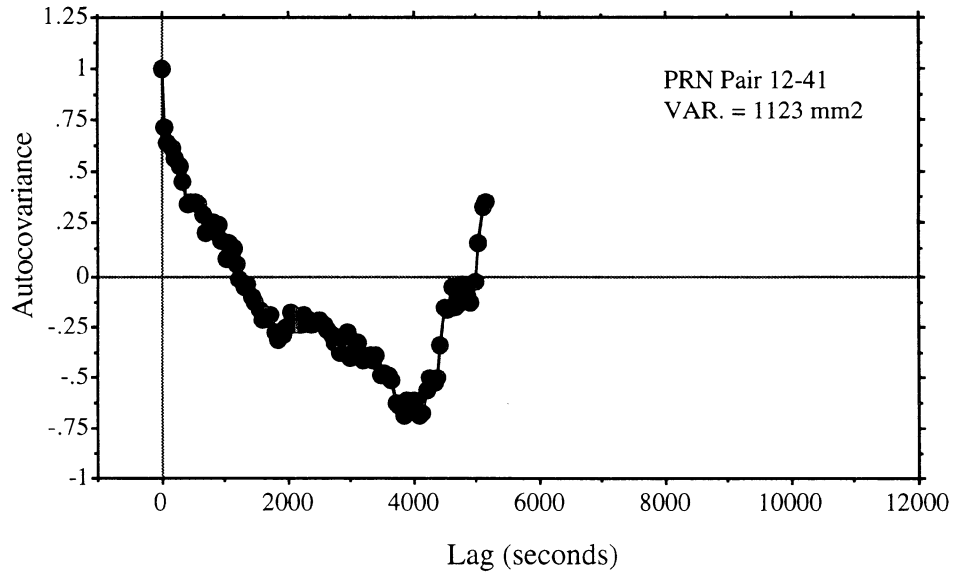
Carrier Phase Double Difference Residuals for a 50 km Baseline (L3)



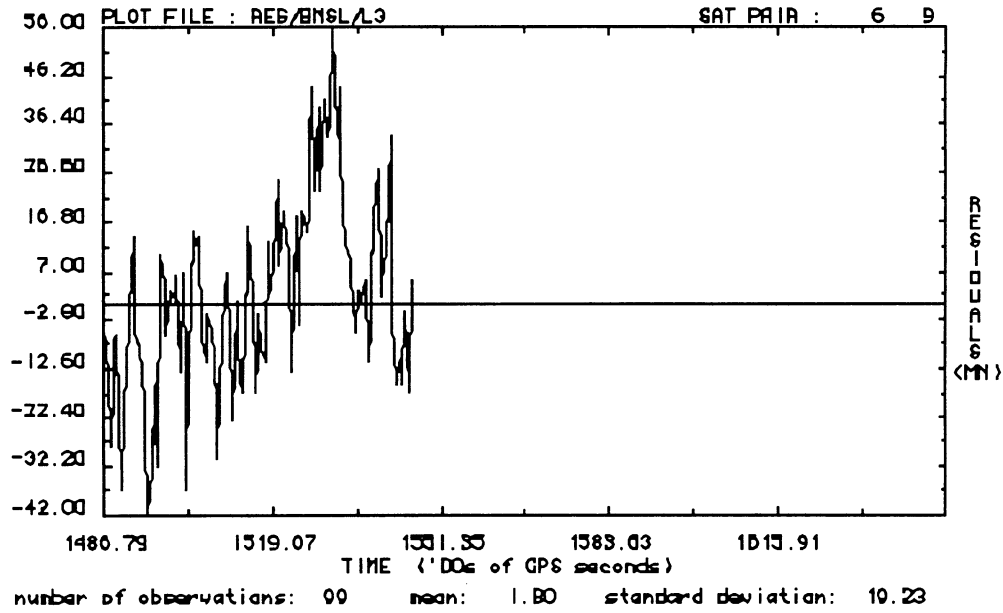
Estimated Autocovariance Function of the Carrier Phase Double Difference Residuals for a 50 km Baseline (L3)



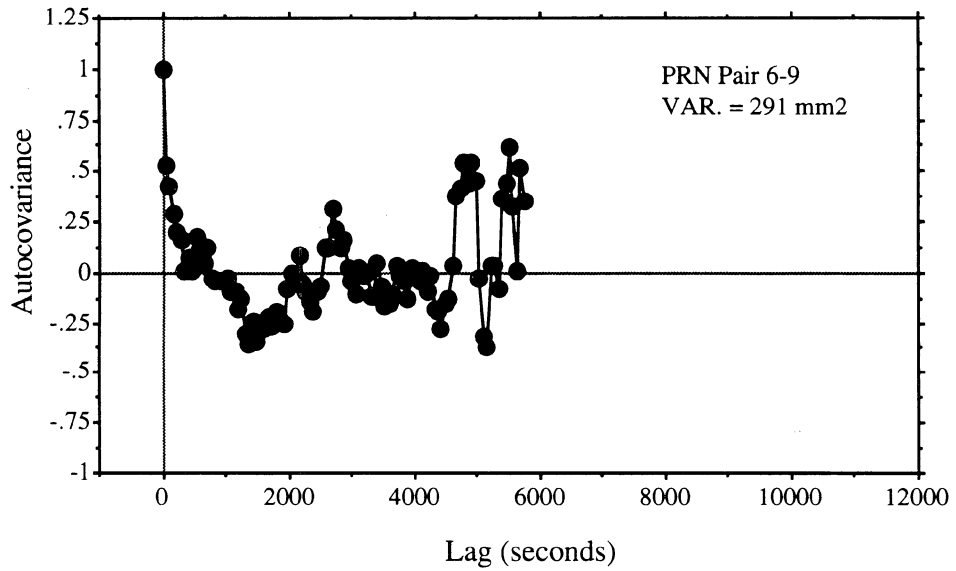
Carrier Phase Double Difference Residuals for an 81 km Baseline (L3)



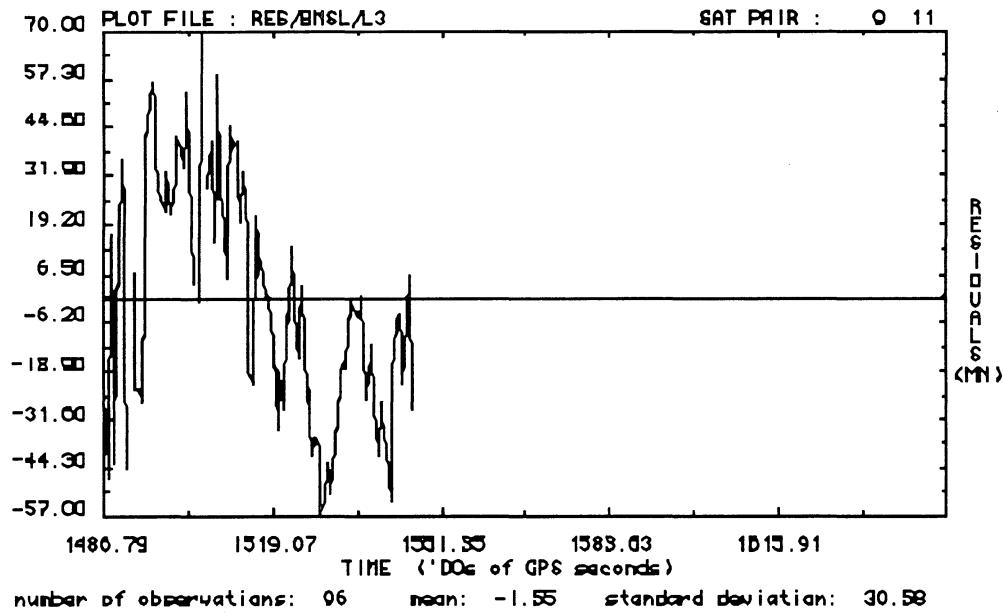
Estimated Autocovariance Function of the Carrier Phase Double Difference Residuals for an 81 km Baseline (L3)



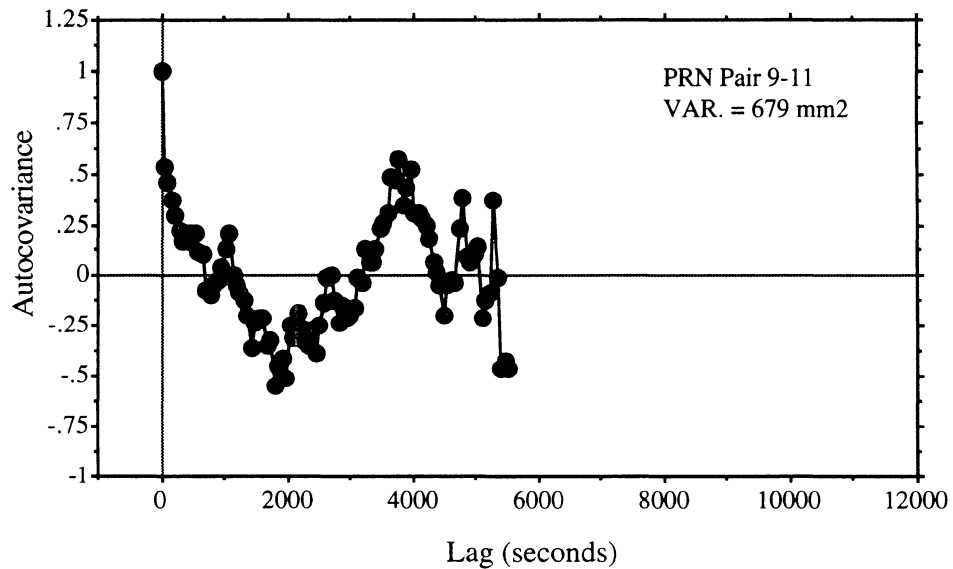
Carrier Phase Double Difference Residuals for an 81 km Baseline (L3)



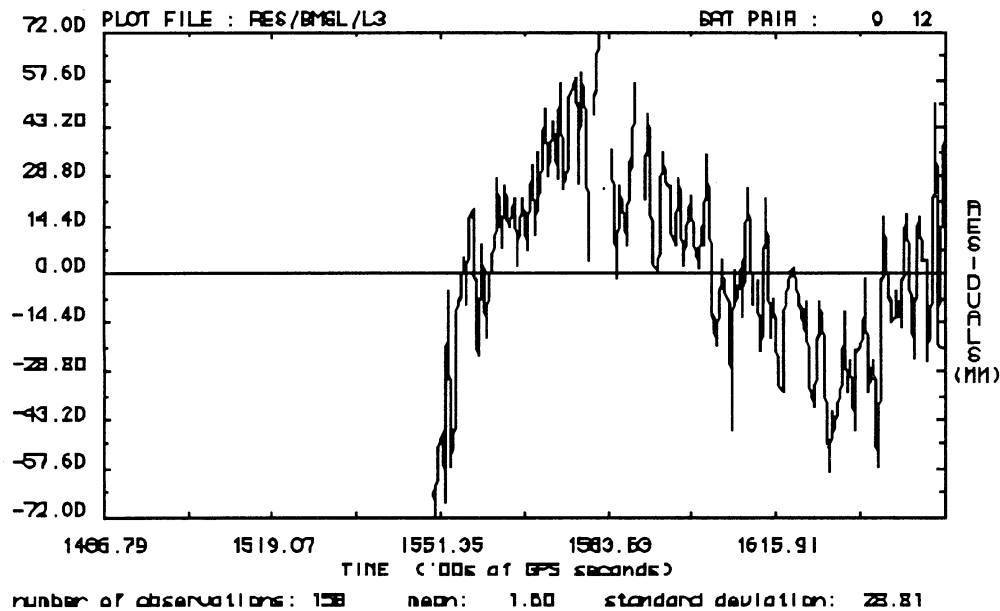
Estimated Autocovariance Function of the Carrier Phase Double Difference Residuals for an 81 km Baseline (L3)



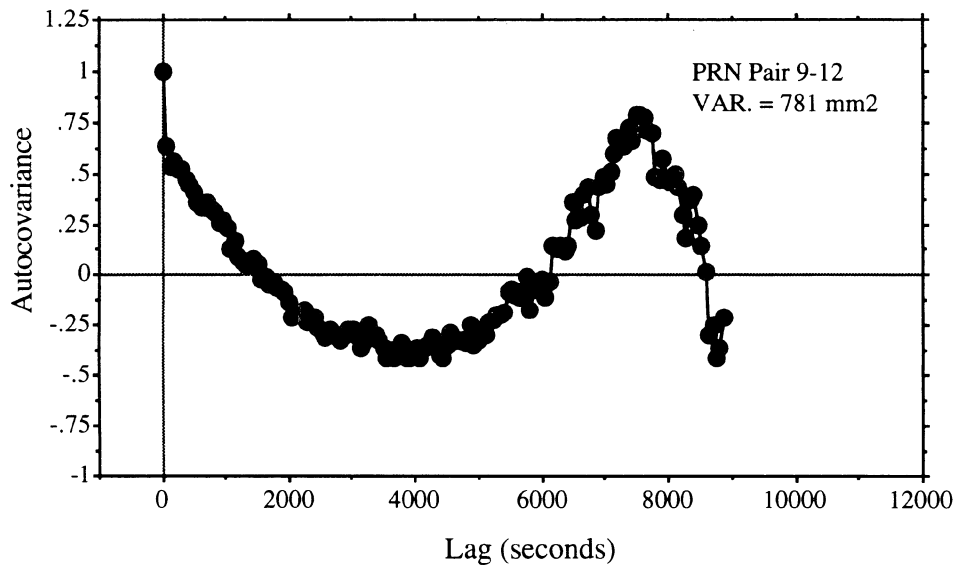
Carrier Phase Double Difference Residuals for an 81 km Baseline (L3)



Estimated Autocovariance Function of the Carrier Phase Double Difference Residuals for an 81 km Baseline (L3)



Carrier Phase Double Difference Residuals for an 81 km Baseline (L3)



Estimated Autocovariance Function of the Carrier Phase Double Difference Residuals for an 81 km Baseline (L3)

APPENDIX IV

DERIVATION OF THE INVERSE OF THE FULLY POPULATED COVARIANCE MATRIX

To find the inverse of the matrix (4.35), let us rewrite it again as

$$C_{\ell} = \begin{bmatrix} \mathbf{M} & f_1 \mathbf{M} & \cdots & f_1^{n-1} \mathbf{M} & f_1^n \mathbf{M}_{n+1,1}^T & f_1^{n+1} \mathbf{M} & f_1^{n+2} \mathbf{M} \\ f_1 \mathbf{M} & \mathbf{M} & \cdots & f_1^{n-2} \mathbf{M} & f_1^{n-1} \mathbf{M}_{n+1,2}^T & f_1^n \mathbf{M} & f_1^{n+1} \mathbf{M} \\ \vdots & \vdots & \vdots & \vdots & \vdots & \vdots & \vdots \\ f_1^{n-1} \mathbf{M} & f_1^{n-2} \mathbf{M} & \cdots & \mathbf{M} & f_1 \mathbf{M}_{n+1,n}^T & f_1^2 \mathbf{M} & f_1^3 \mathbf{M} \\ f_1^n \mathbf{M}_{n+1,1} & f_1^{n-1} \mathbf{M}_{n+1,2} & \cdots & f_1 \mathbf{M}_{n+1,n} & \mathbf{M}_{n+1,n+1} & f_1 \mathbf{M}_{n+1,n} & f_1^2 \mathbf{M}_{n+1,n} \\ f_1^{n+1} \mathbf{M} & f_1^n \mathbf{M} & \cdots & f_1^2 \mathbf{M} & f_1 \mathbf{M}_{n+1,n}^T & \mathbf{M} & f_1 \mathbf{M} \\ f_1^{n+2} \mathbf{M} & f_1^{n+1} \mathbf{M} & \cdots & f_1^3 \mathbf{M} & f_1^2 \mathbf{M}_{n+1,n}^T & f_1 \mathbf{M} & \mathbf{M} \end{bmatrix} \quad (\text{IV.1})$$

Comparing (IV.1) with (4.7), we can denote the upper left corner of (IV.1) by C_{11} , the lower left corner by C_{21} , and the lower right corner by C_{22} . The inverse of the upper left corner is given by (4.26). The inverse of (IV.1) may be written in a similar way to (4.8) using (4.9) through (4.12). First the lower right part can be obtained as

$$P_{22} = \{ \mathbf{M} - [f_1^{n+2} \mathbf{M} \ f_1^{n+1} \mathbf{M} \ \cdots \ f_1^3 \mathbf{M} \ f_1^2 \mathbf{M}_{n+1,n}^T \ f_1 \mathbf{M}] \times$$

$$\times \begin{bmatrix} \mathbf{M} & f_1 \mathbf{M} & \cdots & f_1^{n-1} \mathbf{M} & f_1^n \mathbf{M}_{n+1,1}^T & f_1^{n+1} \mathbf{M} \\ f_1 \mathbf{M} & \mathbf{M} & \cdots & f_1^{n-2} \mathbf{M} & f_1^{n-1} \mathbf{M}_{n+1,2}^T & f_1^n \mathbf{M} \\ \vdots & \vdots & \vdots & \vdots & \vdots & \vdots \\ f_1^{n-1} \mathbf{M} & f_1^{n-2} \mathbf{M} & \cdots & \mathbf{M} & f_1 \mathbf{M}_{n+1,n}^T & f_1^2 \mathbf{M} \\ f_1^n \mathbf{M}_{n+1,1} & f_1^{n-1} \mathbf{M}_{n+1,2} & \cdots & f_1 \mathbf{M}_{n+1,n} & \mathbf{M}_{n+1,n+1} & f_1 \mathbf{M}_{n+1,n} \\ f_1^{n+1} \mathbf{M} & f_1^n \mathbf{M} & \cdots & f_1^2 \mathbf{M} & f_1 \mathbf{M}_{n+1,n}^T & \mathbf{M} \end{bmatrix}^{-1} \begin{bmatrix} f_1^{n+2} \mathbf{M} \\ f_1^{n+1} \mathbf{M} \\ \vdots \\ f_1^3 \mathbf{M} \\ f_1^2 \mathbf{M}_{n+1,n} \\ f_1 \mathbf{M} \end{bmatrix} \}^{-1} \quad (\text{IV.2})$$

Performing the multiplication of the first two matrices, we get

$$P_{22} = \{ \mathbf{M} - [\mathbf{0} \ \cdots \ \mathbf{0} \ G_1 \ G_2 \ G_3] [f_1^{n+2} \mathbf{M} \ f_1^{n+1} \mathbf{M} \ \cdots \ f_1^3 \mathbf{M} \ f_1^2 \mathbf{M}_{n+1,n}^T \ f_1 \mathbf{M}]^T \}^{-1} \quad (\text{IV.3})$$

where,

$$\mathbf{G}_1 = \begin{bmatrix} f_1^{n+2} \mathbf{M} & f_1^{n+1} \mathbf{M} & \cdots & f_1^3 \mathbf{M} & f_1^2 \mathbf{M}_{n+1,n}^T & f_1 \mathbf{M} \end{bmatrix} \begin{bmatrix} \mathbf{0} & \cdots & -f_1 \mathbf{P} & \mathbf{R}_{11}^T & \mathbf{R}_{21}^T & \mathbf{R}_{31}^T \end{bmatrix}^T, \quad (\text{IV.4})$$

$$\mathbf{G}_2 = \begin{bmatrix} f_1^{n+2} \mathbf{M} & f_1^{n+1} \mathbf{M} & \cdots & f_1^3 \mathbf{M} & f_1^2 \mathbf{M}_{n+1,n}^T & f_1 \mathbf{M} \end{bmatrix} \begin{bmatrix} \mathbf{0} & \cdots & \mathbf{0} & \mathbf{R}_{21} & \mathbf{R}_{22}^T & \mathbf{R}_{32}^T \end{bmatrix}^T, \quad (\text{IV.5})$$

$$\mathbf{G}_3 = \begin{bmatrix} f_1^{n+2} \mathbf{M} & f_1^{n+1} \mathbf{M} & \cdots & f_1^3 \mathbf{M} & f_1^2 \mathbf{M}_{n+1,n}^T & f_1 \mathbf{M} \end{bmatrix} \begin{bmatrix} \mathbf{0} & \cdots & \mathbf{0} & \mathbf{R}_{31} & \mathbf{R}_{32} & \mathbf{R}_{33}^T \end{bmatrix}^T \quad (\text{IV.6})$$

The elements \mathbf{G}_1 , \mathbf{G}_2 and \mathbf{G}_3 can be computed as follows

$$\begin{aligned} \mathbf{G}_1 &= -f_1^5 \mathbf{M} \mathbf{P} + f_1^3 \mathbf{M} (\mathbf{Q}_{11} + \mathbf{E}_1^T \mathbf{R}_{33} \mathbf{E}_1) + f_1^2 \mathbf{M}_{n+1,n}^T (\mathbf{Q}_{21} + \mathbf{E}_2^T \mathbf{R}_{33} \mathbf{E}_1) \\ &\quad - f_1 \mathbf{M} \mathbf{R}_{33} \mathbf{E}_1 \\ &= -f_1^5 \mathbf{M} \mathbf{P} + f_1^3 \mathbf{M} (\mathbf{P} + f_1^2 \mathbf{M}^{-1} \mathbf{M}_{n+1,n}^T \mathbf{Q}_{22} \mathbf{M}_{n+1,n} \mathbf{M}^{-1}) + f_1^3 \mathbf{M} [f_1^2 (1 - f_1^2) (\mathbf{M} \mathbf{P} \\ &\quad - \mathbf{M}_{n+1,n}^T \mathbf{Q}_2 \mathbf{M}_{n+1,n} \mathbf{M}^{-1})^T] \mathbf{R}_{33} \mathbf{E}_1 - f_1^3 \mathbf{M}_{n+1,n}^T \mathbf{Q}_{22} \mathbf{M}_{n+1,n} \mathbf{M}^{-1} \\ &\quad + f_1^3 (1 - f_1^2) \mathbf{M}_{n+1,n}^T \mathbf{Q}_{22} \mathbf{M}_{n+1,n} \mathbf{R}_{33} \mathbf{E}_1 - f_1 \mathbf{M} \mathbf{R}_{33} \mathbf{E}_1 \\ &= f_1^3 (1 - f_1^2) \mathbf{M} \mathbf{P} + f_1^5 \mathbf{M}_{n+1,n}^T \mathbf{Q}_{22} \mathbf{M}_{n+1,n} \mathbf{M}^{-1} + f_1^5 (\mathbf{M} - f_1^3 \mathbf{M}_{n+1,n}^T \mathbf{Q}_{22} \mathbf{M}_{n+1,n} \mathbf{M}^{-1} \\ &\quad - (1 - f_1^2) \mathbf{M}_{n+1,n}^T \mathbf{Q}_2 \mathbf{M}_{n+1,n}) \mathbf{R}_{33} \mathbf{E}_1 + f_1^3 (1 - f_1^2) \mathbf{M}_{n+1,n}^T \mathbf{Q}_{22} \mathbf{M}_{n+1,n} \mathbf{R}_{33} \mathbf{E}_1 \\ &\quad - f_1 \mathbf{M} \mathbf{R}_{33} \mathbf{E}_1 \\ &= f_1^3 (1 - f_1^2) \mathbf{M} \mathbf{P} + f_1^3 (1 - f_1^2) \mathbf{M}_{n+1,n}^T \mathbf{Q}_{22} \mathbf{M}_{n+1,n} \mathbf{M}^{-1} \\ &\quad + f_1^3 (1 - f_1^2)^2 \mathbf{M}_{n+1,n}^T \mathbf{Q}_{22} \mathbf{M}_{n+1,n} \mathbf{R}_{33} \mathbf{E}_1 - f_1 (1 - f_1^4) \mathbf{M} \mathbf{R}_{33} \mathbf{E}_1 \\ &= f_1 [f_1^2 (1 - f_1^2) (\mathbf{M} \mathbf{P} - \mathbf{M}_{n+1,n}^T \mathbf{Q}_{22} \mathbf{M}_{n+1,n} \mathbf{M}^{-1})] \\ &\quad + f_1 [f_1^2 (1 - f_1^2)^2 \mathbf{M}_{n+1,n}^T \mathbf{Q}_{22} \mathbf{M}_{n+1,n} - (1 - f_1^4) \mathbf{M}] \mathbf{R}_{33} \mathbf{E}_1 \\ &= f_1 \mathbf{E}_1 - f_1 [(1 - f_1^4) \mathbf{M} - f_1^2 (1 - f_1^2)^2 \mathbf{M}_{n+1,n}^T \mathbf{Q}_{22} \mathbf{M}_{n+1,n}] \mathbf{R}_{33} \mathbf{E}_1 \end{aligned}$$

Substituting \mathbf{E}_1 and \mathbf{E}_2 in (4.32), it is not difficult to prove that the term between brackets equals \mathbf{R}_{33}^{-1} , i.e.

$$\mathbf{G}_1 = f_1 \mathbf{E}_1 - f_1 \mathbf{E}_1 = \mathbf{0}, \quad (\text{IV.7})$$

$$\begin{aligned}
G_2 &= f_1^3 \mathbf{M}(Q_{21} + E_2^T R_{33} E_1)^T + f_1^2 \mathbf{M}_{n+1,n}^T (Q_{22} + E_2^T R_{33} E_2) - f_1 \mathbf{M} R_{33} E_2 \\
&= f_1^3 \mathbf{M}(-f_1 \mathbf{M}^{-1} \mathbf{M}_{n+1,n}^T Q_{22}) + f_1^2 \mathbf{M}_{n+1,n}^T Q_{22} - f_1 \mathbf{M} R_{33} E_2 \\
&\quad + f_1^3 \mathbf{M}[f_1^2 (1 - f_1^2)(\mathbf{M} P - \mathbf{M}_{n+1,n}^T Q_{22} \mathbf{M}_{n+1,n} \mathbf{M}^{-1})]^T R_{33} E_2 \\
&\quad + f_1^2 \mathbf{M}_{n+1,n}^T Q_{22} + f_1^2 \mathbf{M}_{n+1,n}^T [f_1 (1 - f_1^2) \mathbf{M}_{n+1,n}^T Q_{22}]^T R_{33} E_2 \\
&= f_1^2 (1 - f_1^2) \mathbf{M}_{n+1,n}^T Q_{22} - f_1 (1 - f_1^4) \mathbf{M} R_{33} E_2 \\
&\quad + f_1^3 (1 - f_1^2)^2 \mathbf{M}_{n+1,n}^T Q_{22} \mathbf{M}_{n+1,n} R_{33} E_2
\end{aligned}$$

$$\text{or, } G_2 = f_1 E_2 - f_1 R_{33}^{-1} R_{33} E_2 = \mathbf{0} \quad (\text{IV.8})$$

$$\begin{aligned}
G_3 &= f_1^3 \mathbf{M}(-R_{33} E_1)^T + f_1^2 \mathbf{M}_{n+1,n}^T (-R_{33} E_2)^T + f_1 \mathbf{M} R_{33} \\
&= -f_1^5 \mathbf{M} R_{33} + f_1^5 (1 - f_1^2)(\mathbf{M}_{n+1,n}^T Q_2 \mathbf{M}_{n+1,n}) R_{33} \\
&\quad - f_1^3 (1 - f_1^2) \mathbf{M}_{n+1,n}^T Q_2 \mathbf{M}_{n+1,n} R_{33} + f_1 \mathbf{M} R_{33} \\
&= f_1 (1 - f_1^4) \mathbf{M} R_{33} - f_1^3 (1 - f_1^2)^2 \mathbf{M}_{n+1,n}^T Q_2 \mathbf{M}_{n+1,n} R_{33} \\
&= f_1 [(1 - f_1^4) \mathbf{M} - f_1^2 (1 - f_1^2)^2 \mathbf{M}_{n+1,n}^T Q_2 \mathbf{M}_{n+1,n}] R_{33}
\end{aligned}$$

As before, the term between brackets is equal to the inverse of R_{33} . i.e.

$$G_3 = f_1 I \quad (\text{IV.9})$$

Substituting for G_1 , G_2 , and G_3 in (IV.3), we obtain

$$P_{22} = \frac{1}{1 - f_1^2} \mathbf{M}^{-1} = P, \quad (\text{IV.10})$$

which is identical with the original case as if no changes has happened to the observed satellites. Similarly, the lower left part of the inverse of the covariance matrix, P_{21} , can be obtained as

$$P_{21} = P_{22} [\mathbf{0} \quad \cdots \quad \mathbf{0} \quad G_1 \quad G_2 \quad G_3] \quad (\text{IV.11})$$

or,

$$P_{21} = [\mathbf{0} \quad \cdots \quad \mathbf{0} \quad \mathbf{0} \quad \mathbf{0} \quad P] \quad (\text{IV.12})$$

Using (4.9), the upper left part of the inverse of the covariance matrix, P_{11} , can be obtained as

$$P_{11} = \begin{bmatrix} P & -f_1 P & \cdots & \mathbf{0} & \mathbf{0} & \mathbf{0} & \mathbf{0} \\ -f_1 P & (1 + f_1^2) P & \cdots & \mathbf{0} & \mathbf{0} & \mathbf{0} & \mathbf{0} \\ \vdots & \vdots & \vdots & \vdots & \vdots & \vdots & \vdots \\ \mathbf{0} & \mathbf{0} & \cdots & (1 + f_1^2) P & -f_1 P & \mathbf{0} & \mathbf{0} \\ \mathbf{0} & \mathbf{0} & \cdots & -f_1 P & R_{11} & R_{21}^T & R_{31}^T \\ \mathbf{0} & \mathbf{0} & \cdots & \mathbf{0} & R_{21} & R_{22} & R_{32}^T \\ \mathbf{0} & \mathbf{0} & \cdots & \mathbf{0} & R_{31} & R_{32} & RR_{33} \end{bmatrix}, \quad (\text{IV.13})$$

where,

$$RR_{33} = R_{33} + f_1 P \quad (\text{IV.14})$$

VITA

- Candidate's Full Name** : Ahmed El-Sayed El-Rabbany.
- Place and Date of Birth** : Alexandria, Egypt; 11th September 1961.
- Permanent Address** : Dept. of Transportation
Faculty of Engineering, Alexandria University
Alexandria, EGYPT
- Schools Attended** : Abulabbas El-Azhareya Elementary School
Alexandria, 1967-1973.
- El-Gameia El-Khayreya Junior High School
Alexandria, 1973-1976.
- El-Anfoushy High School
Alexandria, 1976-1979.
- Universities Attended** : Faculty of Engineering, Alexandria University
1979-1984, B.Sc.Eng. (Hons).
- Faculty of Engineering, Alexandria University
1985-1988, M.Sc.Eng.
- Dept. of Geodesy and Geomatics Engineering
University of New Brunswick
1990-1994, Ph.D. candidate.

PUBLICATIONS :

- Georgiadou, Y, I. Webster, **A. El-Rabbany**, and A. Kleusberg (1990). "Analysis of the 1989 Vancouver Island GPS Survey Data." Final contract report prepared for Pacific Geoscience Centre of the Geological Survey of Canada. Geodetic Research Laboratory, University of New Brunswick, Fredericton, N.B., Canada.
- El-Rabbany**, A. and A. Kleusberg (1992). "Physical Correlation in GPS Differential Positioning." *Proceedings of the 6th International Geodetic Symposium on Satellite Positioning*, 17-20 March, Columbus, Ohio, USA.
- Kleusberg, A., **A. El-Rabbany**, and I. Webster (1992). "Some Recent Developments in Surveying with the Global Positioning System." Proc. 1st. International Conference and Exhibition on Surveying and Mapping, 25-27 May, Tehran.

El-Rabbany, A. and A. Kleusberg (1993). "Modeling Temporal Correlations in GPS Differential Positioning." Presented at the European Geophysical Society XVIII General Assembly, 3-7 May, Wiesbaden, Germany.

El-Rabbany, A. and A. Kleusberg (1993). "Efficient Algorithm for the Inverse of the Fully Populated Covariance Matrix in GPS Differential Positioning." Presented at the European Geophysical Society XVIII General Assembly, 3-7 May, Wiesbaden, Germany.

El-Rabbany, A. and A. Kleusberg (1993). "Improved Accuracy Estimation of Differential GPS: Theory and Results." Paper presented at the ION GPS-93, *Sixth International Technical Meeting of the Satellite Division of the Institute of Navigation*, Slat Lake City, Utah, 22-24 September.